

Geochronology and Provenance of the Late Devonian Canowindra Fish Bed, Lachlan Orogen

By

Lou-Andrea Gennatas

A thesis submitted to Macquarie University

For the degree of Master of Research

Department of Earth and Environmental Sciences

October 2019



MACQUARIE
University
SYDNEY · AUSTRALIA

Examiner's copy

Statement of originality:

Except where acknowledged in the customary manner, I certify that, to the best of my knowledge, the material presented in this thesis is original and has not been presented, accepted or been published, in whole or part, for the award or consideration of a higher degree or diploma at this or any other university.

Lou-Andrea Gennatas

25/10/2019

Abstract

Placoderms, armoured fish, are recognised as the most diverse group of fish in the Devonian period and were found throughout the world in marine and freshwater environments. Fossil records show placoderms occur from Early Silurian to the Late Devonian, and completely disappear from the fossil record at the Devonian to Carboniferous boundary. The Canowindra fish bed of the Mandagery Formation, is a remarkable Lagerstätte of placoderm fish, first discovered in 1956. The timing and cause of death, however, also remains uncertain.

This study suggests the Canowindra fish bed was deposited in a shallow marine environment, as opposed to the previously suggested fluviatile environment. Field observations suggest that the fish assemblage lies within the lower rather than the upper part of the Mandagery Formation. Zircon U/Pb radiometric dating presents a maximum depositional age of 363 ± 3.1 Ma for the Canowindra fish bed. Finally, using these new findings, a new timescale of the Hervey Group is introduced, as well as a new model for the cause of death of the Canowindra fish fauna. The new model suggests the timing and cause of death may be associated with the Frasnian-Famennian mass-extinction event.

Acknowledgements

I would like to acknowledge and thank everyone who provided me with guidance and support throughout this project, both scientifically and emotionally. I would like to acknowledge Dr Zheng-Xiang Li for initiating and allowing me to take on this project, as well as the Age of Fish Museum, Dr Alex Ritchie and Bruce Looms for providing amazing fish bed samples.

Firstly, I would like to thank my supervisors, Associate Professor Elena Belousova and Dr Richard Glen for taking on the role as my supervisors for this project. A big thank you to Elena for providing this opportunity and an extensive amount of time to guide me through this amazing project. I am very grateful for the patience you have showed as I laboured through the thesis, and the time you took to help me find a scholarship allowing me to finish my research. Thank you to Richard for also providing and sharing your time and extensive knowledge on the regional geology, I have learned so much through your knowledge. I am also very grateful to Dr Kate Selway for providing me with a scholarship, allowing me to continue and finish my research, thank you very much Kate.

Thank you to everyone at the Earth and Environmental Department who helped me for all types of difficulties and knowledge gaps I encountered. Including but not limited to Dr Kim Jessop, for always finding the right word I'm looking for; Dr John Adam, for providing valuable information on placoderm fish, and Dr Stefan Loehr, Dr Sean Murray, Dr Steve Craven, Dr Yi-Jen Lai, and Lauren Robinson for providing much needed help on instrument and analytical methods. Also, thank you to Rosa Didonna, Ananuer Halimulati and Hindol for checking up on me during late nights with extra food to boost my motivation.

Finally, I would like to thank my amazing friends and family for being there when I needed them the most. To my parents, for providing me with the possibility to study in Australia and helping me through tough times. To my grand-parents, Mimi, Jacques, Pierre and Elizabeth for always being available to talk when I need it the most, knowing that we have completely different time zones. To my younger sister, Camille, for giving me tips on image designing. To Kaycee, Enrico and Pierre for keeping me company and encouraging me during times of intense and late-night writing. And finally to Charlotte, Gonzague and Cassandre, you are like a second family to me here in Sydney and I am so grateful to have met and become very close, you have always made me feel at home when I miss my family the most.

Contents

| | |
|----------------------------------------------------------------------------|-----------|
| Statement of originality | i |
| Abstract..... | ii |
| Acknowledgment..... | iii |
| Contents..... | iv |
| 1. Introduction | 1 |
| 1.1. Project Aims..... | 2 |
| 1.2. Project Structure | 2 |
| 2. Previous work | 3 |
| 2.1. Lachlan Orogen | 3 |
| 2.1.1.Overview..... | 3 |
| 2.1.2.Eastern Lachlan Orogen (NSW) evolution throughout the Devonian | 4 |
| 2.2. Hervey Group..... | 5 |
| 2.2.1.Nomenclature..... | 5 |
| 2.2.2.Distribution | 5 |
| 2.2.3.Stratigraphy..... | 6 |
| 2.2.4.Age..... | 7 |
| 2.3. Mandagery Formation | 8 |
| 2.3.1.Distribution | 8 |
| 2.3.2.Petrography | 9 |
| 2.3.3.Depositional environment..... | 9 |
| 2.3.4.Age..... | 10 |
| 2.4. Canowindra Fish..... | 10 |
| 2.4.1.Discovery | 10 |
| 2.4.2.Paleoichthyology..... | 11 |
| 2.4.3.Putative age and cause of death..... | 11 |
| 3. Methods | 13 |
| 3.1. Field observations and sample collection | 13 |
| 3.2. Sample processing and preparation | 14 |
| 3.3. Scanning Electron Microscope (SEM) | 16 |
| 3.3.1.Cathodoluminescence (CL) zircon imaging..... | 16 |
| 3.3.2.Backscattered Electron (BSE) Imaging and NanoMin analyses..... | 16 |
| 3.4. Laser Ablation ICPMS analyses | 17 |
| 3.5. X-ray diffraction (XRD) | 19 |
| 4. Results..... | 20 |
| 4.1. Field observations | 21 |

| | |
|------------------------------------------------------------------------------------------------------------------------|-----------|
| 4.2. Thin sections – SEM | 23 |
| 4.2.1. Petrographical and BSE imaging analysis | 23 |
| 4.2.2. NanoMin analysis | 26 |
| 4.3. XRD analysis | 27 |
| 4.4. Zircon U-Pb and Hf-isotope analyses | 28 |
| 4.4.1. U-Pb age results | 28 |
| 4.4.2. Zircon trace-element analysis | 34 |
| 4.4.3. Hf-isotope composition | 37 |
| 5. Discussion | 38 |
| 5.1. Hervey Group | 38 |
| 5.1.1. Hervey Group stratigraphy and age constraints from previous studies | 38 |
| 5.1.2. Mandagery Formation and age constraints from previous studies | 38 |
| 5.1.3. Mandagery Formation depositional environment from new field and petrographic observations | 39 |
| 5.1.4. Possible depositional environment of the Canowindra fish bed | 39 |
| 5.2. Zircon ages and trace-element signatures of younger zircon populations within the Mandagery Formation | 40 |
| 5.2.1. Defining the younger populations | 40 |
| 5.2.2. Defining the maximum depositional age for the Canowindra fish bed | 43 |
| 5.2.3. Zircon trace-element signatures | 43 |
| 5.2.4. Zircon Hf-isotope composition | 43 |
| 5.3. Implications of the new geochronological data and maximum depositional ages for the Hervey Group timescale | 44 |
| 5.4. Models for the cause of the mass-kill event of the Canowindra fish | 45 |
| 5.4.1. Putative model from previous studies | 45 |
| 5.4.2. New model: Frasnian-Famennian mass-extinction event | 45 |
| 6. Conclusion | 48 |
| Reference | 50 |
| Supplementary material | 55 |

1 Introduction

Placoderms, a long extinct Devonian fish group found throughout all marine and freshwater environments, represent the most dominant and diverse vertebrate group of the middle Palaeozoic era (Long et al., 2008; Young, 2010). In 1956, a single sandstone slab containing 114 Late Devonian placoderm fish, from the Mandagery Formation of the Late Devonian Hervey Group, was found between Canowindra and Gooloogong during blasting operations about 10km south-west of Canowindra (New South Wales), which was later notified by Mr. W.A. Simpson to the Australian Museum (Fletcher, 1956; Johanson & Ahlberg, 1997; Young, 1999). This discovery was found to be one of the most significant and unique find of Devonian fish throughout Australia due to the remarkably well-preserved fossils. The exact location of the fish bed, however, had not been recorded and remained uncertain until 1993 when palaeontologist Dr Alex Ritchie (Australian Museum, Sydney) rediscovered the source of the fish slab and, with the Cabonne Shire Council and local community support, excavated 60 to 70 tonnes of thoroughly well-preserved fish slabs containing over 4000 specimens (Johanson, 1995, 1997; Johanson & Ahlberg, 1997). Most of the slabs are now kept in Canowindra, in a specially funded and built museum (Age of Fishes Museum), fully dedicated to their fossils. The sheer number and extraordinary preservation of the Canowindra fish community represents a unique event in Australia. Indeed, in July 2013, the museum welcomed Sir David Attenborough, for a tour of the museum and its fossils, who also described this finding as “world class” (Age of Fishes Museum, 2013).

Since the fish slab discovery, studies have thoroughly studied the morphology and biological correlations of the Late Devonian Canowindra placoderms (Johanson, 1995, 1997; Johanson & Ahlberg, 1997; Young, 1999). These studies have suggested a Late-Frasnian to Early-Famennian age for the Canowindra fossil fish assemblage (Johanson, 1995, 1997; Young, 1999, 2006a). However, none have provided any radiometric dating of the fish bed, nor a clear understanding of the mass-kill event, and its depositional environment, which provided such well-preserved fossils. Furthermore, while observing the fish slab at the Canowindra fish museum (Age of Fishes Museum), Prof. Zheng-Xiang Li (Curtin University) noticed the fish were lying in a thin (2 to 10cm) white fine-grained layer (personal communication), which has not been defined in previous studies of the Canowindra fish bed (Johanson, 1995, 1997; Johanson & Ahlberg, 1997).

Using field observations, zircon analysis and petrography, this study presents a detailed study of the Mandagery Formation age and depositional environment observed at the fish locality, including the stratigraphic locality of the fish assemblage within the unit, as well as interpretations on the possible cause and time of death of the fish fauna.

1.1 Project Aims

- I. Establish the time of death of the Canowindra fish community.
- II. Refine age, stratigraphy and depositional environment of the Canowindra fish fauna within the Mandagery Formation.
- III. Analyse and identify the presence of a thin tuffaceous layer within the Canowindra fish bed.
- IV. Test the putative death models of the fish community.

1.2 Project Structure

Chapter 2 provides a literature review of the Canowindra fish site extending to its regional geology. This section will be separated into sub-sections from the Lachlan Orogen to the Hervey Group, the Mandagery Formation and the Canowindra fish fauna.

Chapter 3 presents the methodology and techniques used for this study: sample selection and preparation, zircon cathodoluminescence imaging using scanning electron microscope, zircon U/Pb and trace elements analysis using Laser Ablation Inductively Coupled Plasma Mass Spectrometry, and mineral composition using X-ray Powder Diffraction.

Chapter 4 presents the results obtained from analyses described in chapter 3.

Chapter 5 discusses the results provided in chapter 4 and their outcome related to the aims of this project.

Chapter 6 Summarises the outcomes of this project and the significance of these findings.

2 Previous work

2.1 Lachlan Orogen

2.1.1 Overview

Throughout the Palaeozoic era, a subduction system was active along the eastern margin of Australia, with periods of compression and extension producing large-scale sedimentation interspersed with magmatic activity (Glen, 2013; Gray & Foster, 2004). The Late Devonian Canowindra fish assemblage is found within eastern New South Wales (NSW), in the eastern subprovince of the Lachlan Orogen (fig.2.1) (Glen, 2013; Young, 2006a). The Lachlan Orogen ranges in age from the Cambrian to the Carboniferous (Glen, 2005), and forms a central part of the Tasmanides of eastern Australia (Fergusson *et al.*, 2017; Forster & Gray, 2000; Gray & Foster, 2004; Glen, 2013). The Tasmanides extend throughout

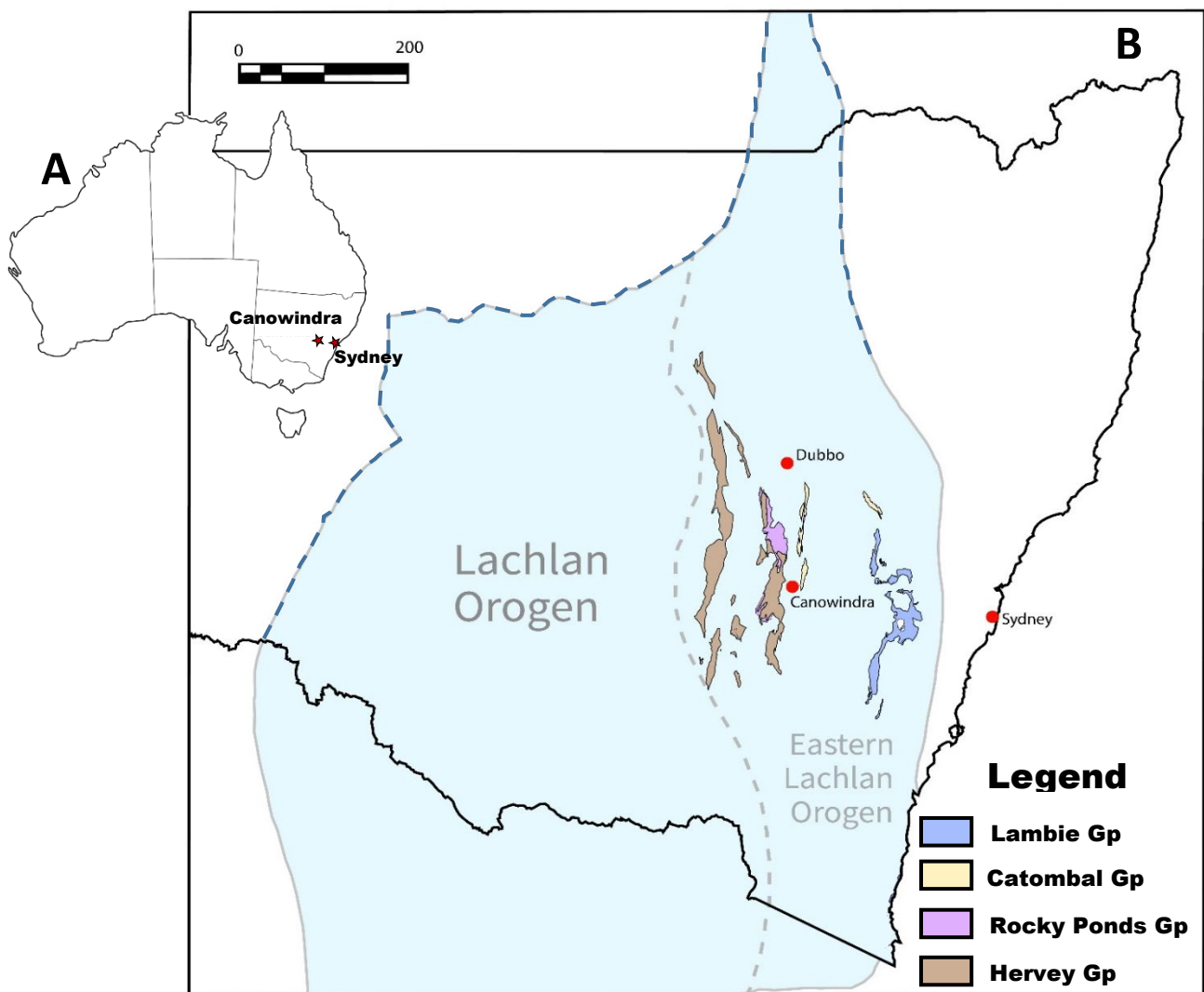


Figure 2.1: **A:** Map of Australia with the location of Canowindra and Sydney. **B:** Extent of the Lachlan Orogen (light blue) throughout NSW, including the Middle Devonian Rocky Ponds Group (purple) and the Late Devonian outcrops of the Lambie Shelf: Hervey Group (brown), Catombal Group (pale yellow) and the Lambie Group (blue), in the eastern subprovince of the Lachlan Orogen. Blue dashed lines represent uncertain orogen boundaries. (Glen, 2013; Dawson & Glen, 2006)

a third of the eastern Australian surface area. It comprises the Bowen, Gunnedah & Sydney basins as well as five orogens, which developed from the Neoproterozoic to early Mesozoic along the eastern margins of Gondwana: Delamerian Orogen, Thomson Orogen, New England Orogen, Mossman Orogen and the Lachlan Orogen (Fergusson *et al.*, 2017; Glen, 2013).

2.1.2 Eastern Lachlan Orogen (NSW) evolution throughout the Devonian

Located in the eastern subprovince of the Lachlan Orogen, the Canowindra fish bed is found within the Hervey Group of the Lambie Shelf (Glen, 1998), overlying the Dulladerry Volcanics (Rocky Ponds Group) and the Cowra Trough sediments (Pogson & Watkins, 1998).

The Cowra Trough formed in the Early Silurian following the cessation of volcanism in the Molong Volcanic Belt of the Macquarie Arc (Glen *et al.*, 2002; Pogson & Watkins, 1998). During the Late Silurian, felsic volcanic eruptions, such as the Canowindra Volcanics (previously known as Canowindra Porphyry; Powell, 1984; Pogson & Watkins, 1998), were common in the Cowra Trough initiated by an extensional phase, during which voluminous granitic plutons formed, such as the Cowra Granodiorite (Fergusson *et al.*, 2017; Lyons *et al.*, 2000). In the Early Devonian, the Cowra Trough transitioned to a shallow water environment, with predominant carbonate deposition. Due to tectonic activity, resulting in uplift and folding of the region, deposition in the Cowra Trough ceased by the early Middle Devonian (Pogson & Watkins, 1998). Uplift and folding throughout southeastern Australia, in the Middle Devonian resulted in the formation of the Tabberabberan Highlands (Powell, 1984). However, no outcrops of Eifelian age (early Middle Devonian) were preserved, with the exception of a shallow-water clastic outcrop in north-west Sydney, within the Mudgee district (Powell, 1984). By the end of the Middle Devonian, volcanic activity within the eastern Lachlan Orogen had ceased, with no further studies suggesting any younger volcanic eruptions throughout the region and NSW (Foster & Gray, 2000; Gray & Foster, 2004; Pogson & Watkins, 1998; Powell, 1984).

Following the Middle Devonian tectonism, Conolly (1965a), Pogson & Watkins (1998) and Fergusson *et al.* (2017) described a shallow marine transgression setting in the Eastern Lachlan Orogen, causing a widespread shallow marine environment in the very eastern region to fluvial in the western region of the Eastern Lachlan Orogen (Hervey Group), resulting in the deposition of the Lambie Shelf throughout the Late Devonian (fig.2.1; Powell, 1984; Webby, 1972).

The Late Devonian Lambie Shelf rocks of central Eastern Lachlan Orogen occur in three major groups as meridional belts (fig.2.1; Glen, 2005). The Lambie Shelf began as shallow marine sedimentation within two basins, the Hervey Basin, composed of the Hervey Group, and the Lambie Basin, composed of the Catombal Group and Lambie Group. The marine sedimentation in the Lambie Shelf was then shortly replaced by terrestrial sedimentation (Pogson & Watkins, 1998; Webby, 1972). In the most eastern region lies the Lambie Group with a maximum preserved thickness of 3000m, followed by the Catombal

Group with a maximum preserved thickness of 1650m, and to the west lies the Hervey Group with a maximum preserved thickness of 1600m (fig.2.1; Pogson & Watkins, 1998).

2.2 Hervey Group

2.2.1 Nomenclature

The major geological study of the Hervey Group has been published by Conolly in the 1960s (1963, 1965a, 1965b). Following Conolly's papers, minor updates on the Hervey Group stratigraphy have been presented (Lyons *et al.*, 2000; Young, 1999), with no further major studies having been published since. Subsequently, geological and biological studies within the Hervey Group (Johanson, 1995, 1997; Johanson & Ahlberg, 1997; Warren & Watkins, 1998; Young, 1999, 2006a), such as Devonian fish faunas found within the Cowra, Grenfell, Peak Hill and Jemalong Range (all within 100km from the Canowindra fish bed), have all proceeded to use the Hervey Group stratigraphy as defined by Conolly (1963, 1965a, 1965b).

2.2.2 Distribution

The Hervey Group is a major Late Devonian sedimentary rock unit which disconformably lies above the Dulladerry Volcanics from the Rocky Ponds Group, with outcrops found throughout NSW (fig.2.1).

In the Canowindra region, Conolly (1965a, 1965b) described three major Hervey Group outcrop locations, as elongate north-south synclinal belts (fig.2.2). As shown in figure 2.2 (Conolly, 1965a), the most eastern belt of the Hervey Group (fig.2.2) is the longest belt with a total length of about 225km and a maximum width of about 38km between Parkes and Manildra, otherwise averaging at 6 to 11km. The similar central belt (fig.2.2) lies parallel to the eastern belt about 32km west. The most western belt (fig.2.2) is found about 56km west of the central belt and represents the shortest belt (Conolly, 1965a). Conolly (1965a) describes the three synclinal structures as being the result of extensive erosion of a large Upper-Devonian sediment coat which experienced open folding and broad warping. In his papers, Conolly (1965a, 1965b) defines the Hervey Group stratigraphy at eight locations throughout the three synclinal structures. However, the boundaries presented by Conolly (1965a) in figure 2.2 have since been updated and modified (Pogson and Watkins, 1998).

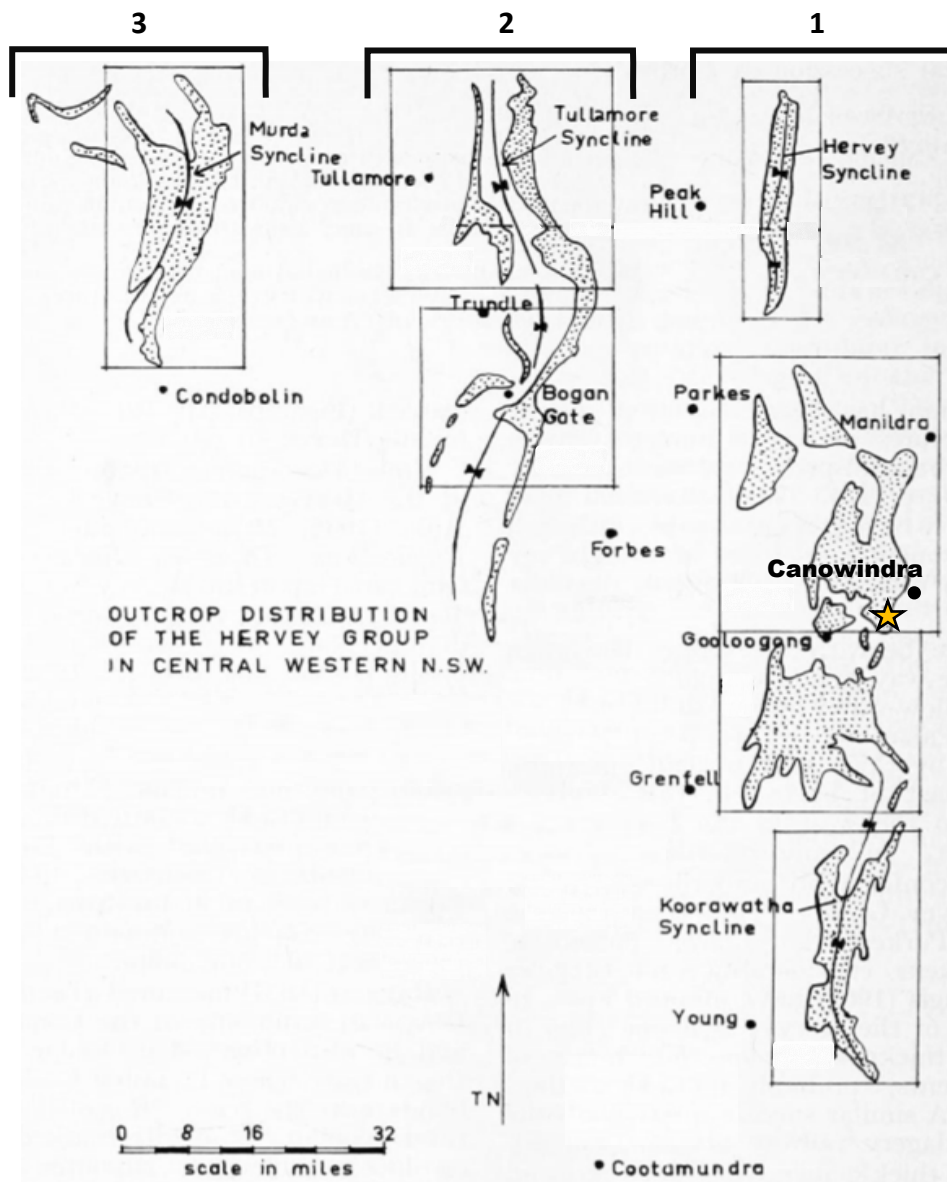


Figure 2.2: Map of the Canowindra Hervey Group outcrops as shown by Conolly (1965a) showing a pattern of 3 elongate north-south synclinal belts (1-3). Yellow star: Canowindra fish site. Adapted from Conolly (1965a).

2.2.3 Stratigraphy

The Canowindra fish site is found within the Manildra-Gooloogong region of the eastern belt (fig.2.3), where Conolly (1965a, 1965b) defined the stratigraphy of the Hervey Group from base to top as the Kadina Formation, Mandagery Sandstone, Pipe Formation, Bumberry Formation and the Eurow Formation. Where the basal sedimentary beds, Kadina Formation, are mainly composed of red lithic sandstone with finer layers of red mudstone and siltstone. The Kadina Formation is then overlain by a thicker assemblage, composed of the Mandagery Formation, Pipe Formation and Bumberry Formation, described as white quartz-rich sandstones, conglomerates, and similar red mudstone & siltstone beds. The final overlaying unit, Eurow Formation, is composed of red mudstone and siltstone beds, with the occasional minor red lithic and quartz-rich sandstone (Conolly, 1965a).

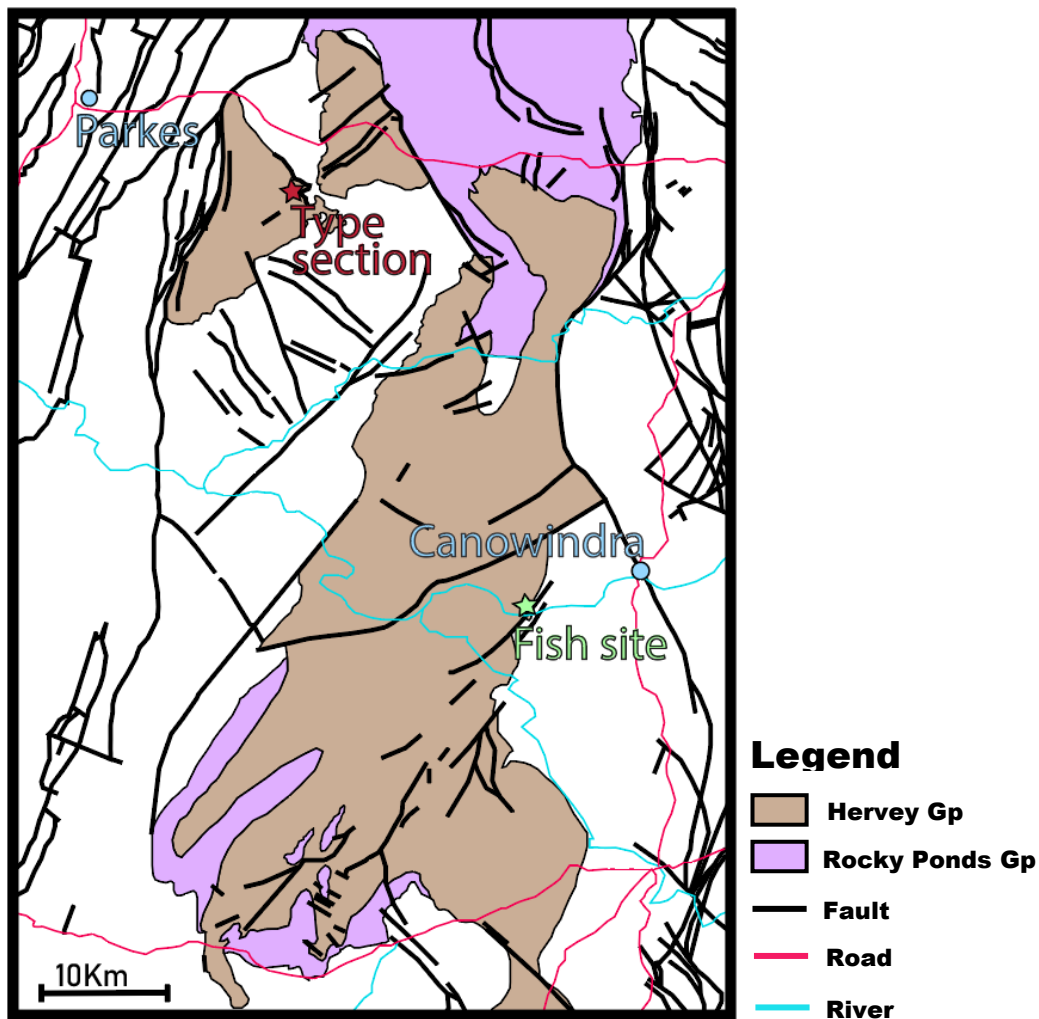


Figure 2.3: Map of the Manildra-Gooloogong region Hervey Group and Rocky Ponds outcrops, including faults. (Dawson and Glen, 2006)

However, Young (1999) describes Conolly's (1965a, 1965b) stratigraphy of the Hervey Group to be unreliable as the latter appears to have delineated each unit based on topography, that is, the author defined the limits using the dominant sandstone strike ridges which are separated by units composed of finer-grained sandstone. Yet, as Young (1999) clearly states, these structural features are highly dependent on the overall relief and may therefore not define the limits of a unit. Since Conolly (1965a, 1965b), however, several studies and regional geological map sheets have suggested refined stratigraphies of the Hervey Group (Lyons *et al.*, 2000; Raymond *et al.*, 1998; Raymond *et al.*, 2000a & b; Young, 1999).

2.2.4 Age

No dating of the Hervey Group has yet been published, with the closest radiometric date acquired for the underlying Curumbenya Ignimbrite of the mid-Dulladerry Volcanics (Rocky Ponds Group) at 376 ± 4 Ma (Black, 1996). However, this single Dulladerry Volcanics date has not been published and was provided by personal communication (Pogson & Watkins, 1998). This single date from the Dulladerry Volcanics was also used by Young (1999), who created a generalised stratigraphic framework of the

| Period | Epoch | Age | Group | Units |
|-------------------|--------|---------------------|----------------------------|---------------------------------|
| DEVONIAN | Late | Famennian | Hervey Group | Eurow Formation |
| | | | | Bumberry Formation |
| | | Pipe Formation | | |
| | | Mandagery Formation | | |
| | Middle | Frasnian | Rocky Ponds Group | Kadina Fm |
| | | Givetian | | Dulladerry Volcanics |
| | Early | Eifelian | Eugowra Suite | Granites |
| | | Emsian | | |
| | | Pragian | | |
| | | lochkovian | | |
| Cumbijowa Granite | | | | |
| SILURIAN | Late | Pridoli | Derriwong Group | Bindogandri Granite |
| | | Ludlow | | Coonigal Group |
| | Early | Wenlock | Douro Group & Forbes Group | Moura Formation |
| | | Llandovery | | Glenisla Volcanics |
| | | | | Mumbidgle Fm Bocobidgle Cgmt |

Figure 2.4: Stratigraphy of the Hervey Group at the Manildra-Gooloogong region, as defined by Lyons et al. (2000), Raymond et al. (1998), Raymond et al. (2000a & b) and Young (1999). Dashed lines represent uncertain unit boundaries.

Hervey Group based on Middle to Late Devonian macrovertebrate zones, without providing any other date. Figure 2.4 below presents a stratigraphy of the Hervey Group, and underlying units, at the Canowindra fish site, as defined by Lyons *et al.* (2000), Raymond *et al.* (1998), Raymond *et al.* (2000a & b) and Young (1999).

2.2.5 Depositional environment

The Hervey Group sediments, as described by Conolly (1965a, 1965b), suggest a lower-alluvial to delta plain depositional environment consisting of intervals of meandering and braided fluvial systems, with the presence of marine horizons near the basal section of the Hervey Group. However, Young (1999) suggest marine environments were also present within the mid-section of the Hervey Group. Finally, in his paper on the petrology and origin of the Hervey Group, Conolly (1965b) provides petrographic analyses of over 100 thin sections of the majority of the Hervey Group sandstones sequences and concludes that fragments of polycrystalline quartz and quartz-rich sandstone show a west to south-west landmass source due to an increase of these fragments south- and west-ward.

2.3 Mandagery Formation

2.3.1 Distribution

The Mandagery Formation (previously known as Mandagery Sandstone from Conolly (1965a)) conformably overlies the Kadina Formation and underlies the Pipe Formation at the Canowindra fish locality (Young, 1999). Conolly (1965a) defined the base of the unit as the first white sandstone above the Kadina Formation and its top bed by the last white sandstone bed overlain by a thick sequence of fine-grained red beds, belonging to the Pipe Formation. Its name originates from the Mandagery railway station, located on the western railway line to Parkes (Warren & Watkins, 1998). Within the Manildra-Gooloogong region, the unit is mainly composed of fine to medium-grained white and red sandstone with thin intervals of thin shale and red and green siltstone (Conolly, 1965a, 1965b). Conolly (1965a)

states that the thickness of the unit strongly varies from Mandagery, where the unit is observed to be the thickest, with a thinning towards the south, east and north. The unit also appears to be in fault contact with the Early-Silurian Canowindra Volcanics, located along the eastern region of the Mandagery Syncline as a 1km long outcrop (Pogson & Watkins, 1998).

2.3.2 Petrography

Conolly's (1965b) thin section analyses of the quartz-rich sandstone suggest a moderately-well sorted medium-sized quartz grains (0.16-0.33mm) in a silica cement matrix. He also described the presence of granular lithic sandstone with 50% sub-angular to sub-rounded quartz grains with about 20% red siltstone and 25% volcanic fragments in a ferruginous cement (Pogson & Watkins, 1998). The composition of the Mandagery Formation at different localities throughout the Hervey Group has been provided by Conolly (1965b), see table 2.1. Conolly's (1965b) table (table 2.1) shows a relatively consistent composition of the Mandagery Formation throughout the Hervey Group, with the exception of chert and feldspar which only appears at fewer locations. Finally, Conolly (1965b) also appears to suggest the presence of volcanic fragments throughout the Mandagery Formation.

| Sample Area | Number of Analyses | Mono-crystalline Quartz | Poly-crystalline Quartz | Chert | Volcanic Rocks | Quartzose Sediments | Shale | Clay Pellets | Feldspar | Iron Oxides | Secondary Quartz | Matrix | Modal grain size in mm. |
|----------------------------|--------------------|-------------------------|-------------------------|-------|----------------|---------------------|-------|--------------|----------|-------------|------------------|--------|-------------------------|
| MANDAGERY SANDSTONE | | | | | | | | | | | | | |
| Hervey Syncline, North | 4 | 77.2 | 2.2 | | 3.0 | 2.4 | 0.2 | 2.2 | | 0.8 | 1.8 | 12.0 | 0.2 |
| Hervey Syncline, Central | 5 | 81.0 | 2.0 | | 3.0 | 2.4 | 1.0 | 1.0 | 0.4 | 0.4 | 1.0 | 6.8 | 0.26 |
| Hervey Syncline, South | 4 | 78.4 | 3.2 | | 2.2 | 3.0 | 1.6 | 1.0 | | 0.8 | 0.5 | 9.3 | 0.22 |
| Parkes Syncline, North | 6 | 82.2 | 1.3 | 0.3 | 3.3 | 0.7 | 0.3 | 1.5 | 1.7 | 0.2 | 1.5 | 7.0 | 0.23 |
| Mandagery Railway | 8 | 78.9 | 1.3 | 0.1 | 1.0 | 0.9 | 0.4 | 8.7 | 0.1 | 0.6 | 1.5 | 7.5 | 0.16 |
| Parkes Syncline, South | 4 | 89.7 | 0.5 | 0.3 | 1.5 | 0.2 | 0.2 | 3.5 | | | 1.1 | 3.0 | 0.16 |
| Bumberry Syncline, East | 4 | 88.2 | 1.2 | | 0.8 | 0.5 | 0.2 | 2.2 | | 0.2 | 1.5 | 5.2 | 0.19 |
| Wangilla | 3 | 74.0 | 0.3 | | 0.5 | 0.5 | 0.5 | 10.5 | | 1.2 | 2.5 | 10.0 | 0.12 |
| Nangar Trig. | 0 | 83.3 | 0.2 | 0.6 | 1.4 | 0.3 | 0.4 | 3.0 | | 0.1 | 0.8 | 9.9 | 0.22 |
| Eugowra West | 7 | 78.2 | 1.3 | 0.8 | 3.2 | 0.5 | 0.5 | 3.7 | | 0.2 | 2.3 | 9.3 | 0.23 |
| Nyrang Creek | 3 | 78.3 | 0.6 | | 3.0 | 1.0 | | 6.7 | 0.1 | 0.3 | 3.0 | 7.0 | 0.17 |
| Gooloogong Anticline | 9 | 80.6 | 9.5 | 0.3 | 0.1 | 2.0 | 0.4 | 2.3 | | 0.7 | 1.5 | 5.8 | 0.33 |
| Conimbla Syncline | 3 | 82.7 | 2.7 | | 0.7 | 1.0 | 0.7 | 3.3 | | 0.2 | 1.7 | 7.0 | 0.22 |
| Koorawatha Syncline, North | 3 | 73.7 | 6.8 | 3.3 | 0.3 | 2.0 | 3.3 | 2.3 | | | 3.8 | 4.3 | 0.42 |
| " " Central | 3 | 72.0 | 6.0 | 2.0 | 0.1 | 4.0 | 4.0 | 3.0 | | 0.3 | 5.3 | 3.3 | 0.43 |
| " " South | 5 | 72.8 | 5.6 | 1.4 | 4.6 | 0.8 | 1.0 | 7.0 | | 0.1 | 0.2 | 6.3 | 0.28 |

Table 2.1: Composition of Mandagery Formation (Mandagery Sst) sandstones at different locations throughout the Hervey Group outcrops as measured by Conolly (1965b). (Conolly, 1965b)

2.3.3 Depositional environment

Conolly (1965a) describes the presence of ripple marks, bedding, flow and load casts, as well as scour, slump and fill structures, with the rare occurrences of lenticular beds, within the sandstone beds throughout the Mandagery Formation (Pogson & Watkins, 1998). Conolly (1965a) and Pogson & Watkins (1998) claim these features, along with the mineral composition of the unit, the progression of mudstone-dominated Kadina Formation to moderately well-sorted quartz-rich sandstone suggest a

marine regression progressing to a fluvial system. However, this suggestion was concluded based on the few observations stated previously with no further petrographic or analytical work.

2.3.4 Age

As previously stated, no radiometric dating of the Mandagery unit, or any of the Hervey Group units, have been previously published. However, with the presence of the Canowindra fish assemblage within the Mandagery unit, previous studies have suggested a Late-Frasnian to Early-Famennian age for the unit (Johanson, 1995, 1997; Johanson & Ahlberg, 1997; Young, 1999).

2.4 Canowindra Fish

2.4.1 Discovery

Since the discovery of the single fossil slab in 1956 and the rediscovery of its source in 1993, the Canowindra fish fossils, a remarkable fossil lagerstätte, have been well studied, including Dr Alex Ritchie's student Zerina Johanson who published detailed studies of the Canowindra placoderm fish morphology and biology (Johanson 1995, 1997; Johanson & Ahlberg, 1997; Young, 1999, 2006b). The 1956 slab measures 1 by 2m and contains 114 Late Devonian placoderm fish (fig.2.5). It is dominated by two types of antiarch placoderms, which are armoured fish only known from fossil records (Long, 2010), the *Bothriolepis* and the *Remigolepis* (Johanson & Ahlberg, 1997). Also present was the *Groenlandaspis*, a Late Devonian fish discovered in Greenland, and a unique long-bodied *Sarcopterygian*, an air-breathing, lobe-finned fish, named *Canowindra grossi* after the town and Dr Walter Gross by Thomson (1973) (Johanson & Ahlberg, 1997; Young, 1999). Among the 4000 fish from the 70-80 tonnes of uncovered slabs from the 1993 excavation, new specimens were identified, such as the *Mandageria fairfaxi*, and the *tristichopterid*, a lungfish similar to *Soedeberghia* as described by Campbell & Bel (1982), and a primitive member of the *Rhizodontida* (Johanson 1995, 1997; Johanson & Ahlberg, 1997; Young 1999).

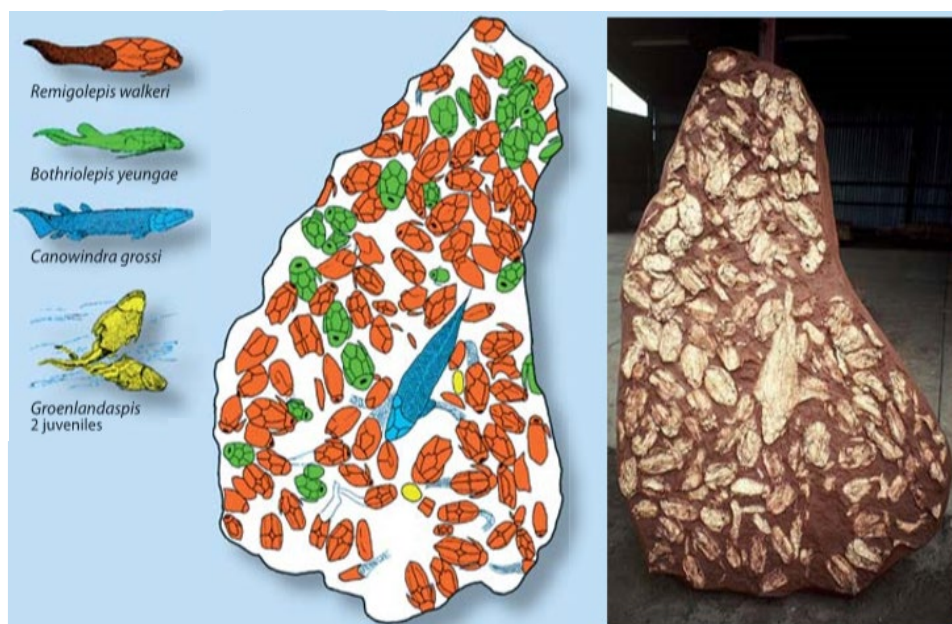


Figure 2.5: 1956 Canowindra fish sandstone slab with a colour-coded graphic reproduction of the slab showing type and position of each fish specimens. (Australian Age of Dinosaurs Inc., 2006).

2.4.2 Palaeoichthyology

Placoderm, also known as armoured fish, is a name which is derived from the Greek *plakos*, meaning plate, and *derma*, meaning skin. It refers to the interlocking bony plates armour which surrounds the front-end of the body (Young, 2010). The placoderm fish were present throughout the whole Devonian Period until the very last Famennian stage, with no fossil record of placoderms having crossed the Devonian-Carboniferous boundary (Young, 2010). The placoderms averaged at an approximate size of 20 to 30cm long but could reach a maximum length of 1m. The antiarchs are defined by the presence of pectoral appendages, i.e. the fish's pectoral fins are confined in bony tubes, recognised as "arms". Whereas most of these had segmented arms, some less advanced antiarchs, like the *Remigolepis* found in large quantity within the Canowindra fish fauna, had shorter oar-shaped arms (fig.2.6; Long, 1995, 2010).

In his book 'The Rise of Fishes', Long (1995, 2010) recognises the *Bothriolepis*, one of the two most dominant placoderms of the Canowindra fish fauna, as the most successful placoderm. Found in majority within freshwater deposits as well as few marine sites, this fish lived most of its life in marine environments and invaded river systems through shallow seaways and swimming upstream to breed and die (Long, 2010). Indeed, Long (1995, 2010) states that the *Bothriolepis* possessed both "lunglike" organs and a spiral intestine, giving them the ability to breathe, which he suggests allowed them to crawl out of the water, using its long pectoral appendages, to reach new, rotting vegetation-rich, pools away from predators (fig.2.6). Long (1995, 2010) states that the fish's intestine is usually comprised of organic sediments compositionally not related to the fossil's surrounding sediments, suggesting that the *Bothriolepis* was a "mud-grubber" which fed by pushing itself into the mud and ingesting organic-rich mud.

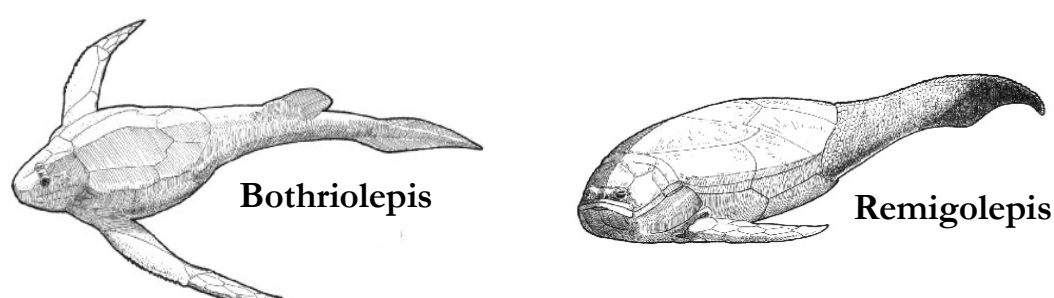


Figure 2.6: Schematic drawing of *Bothriolepis* and *Remigolepis*. (Age of Fishes Museum., 2019a, 2019b).

2.4.3 Putative age and cause of death

As previously stated, the Canowindra fish fauna has been extensively studied morphologically and biologically. Yet, no correlations with dating or geological features within the Mandagery Formation, or the Hervey Group, have been made with the morphology and biology of the Canowindra fish fauna (Johanson 1995, 1997; Johanson & Ahlberg, 1997; Young 1999). However, based on the fish fossils,

biology and morphology, previous studies suggest the fish date to the Late-Frasnian to Early-Famennian and a mass-kill event caused by the trapping of this fish community in a large water body which dried and shrunk due to strong drought events. This created a closed water body which trapped a large amount of fish, and as drought conditions continued, the water body dried, trapped and killed the present fish fauna (Johanson 1995, 1997; Johanson & Ahlberg, 1997; Young 1999). However, the environment in which the mass-kill event took place remains uncertain, as previous studies suggest either a marine (estuarine) or fluvial environment (Johanson 1995, 1997; Johanson & Ahlberg, 1997; Young 1999). Furthermore, the majority of the fish are fully preserved, with minor to no skeletal damage, in their living position, as well as being largely piled up against and on top of each other, suggesting a quick, yet gentle death (Johanson, 1997).

Understanding the origin of the Canowindra fish fauna could represent major geological and biological advancements. These findings could represent significant improvement to the Late Devonian stratigraphy and species connections and movements throughout Gondwana. Indeed, the Middle- to Late Devonian *sarcopterygian* fish to tetrapod, our putative ancestors, transition is recognised as one the most dramatic event within the vertebrates' evolution and has been extensively studied (Long & Gordon, 2004; Long *et al.*, 2006; Young, 2006a).

3 Methods

3.1 Field observations and sample collection

A fieldtrip undertaken for this project included a visit to the Age of Fishes Museum in Canowindra and a trip to the fish site, where field observations of the depositional environment were made. It is important to note that the fish site was reburied after the 1993 excavation to prevent any damage or vandalism, therefore limiting the possible in-situ observations for this project. Eight rock samples from the fish bed itself were provided by the Age of Fishes Museum from its storage facility. Six rock samples from the underlying and overlying beds were collected at the Age of Fishes site (see Appendix Table A1). A final rock sample, collected during the 1993 excavation but not recorded by the museum (Bruce Looms personal communication, 2019), was provided by Bruce Looms. The samples provided by the museum represent the top of the fish bed, turned over for display, where approximately 10cm thick sediments have been cleaned by Museum staff and volunteer students from local schools with the aim to provide a clear view of the fish specimen casts, see figure 3.1.

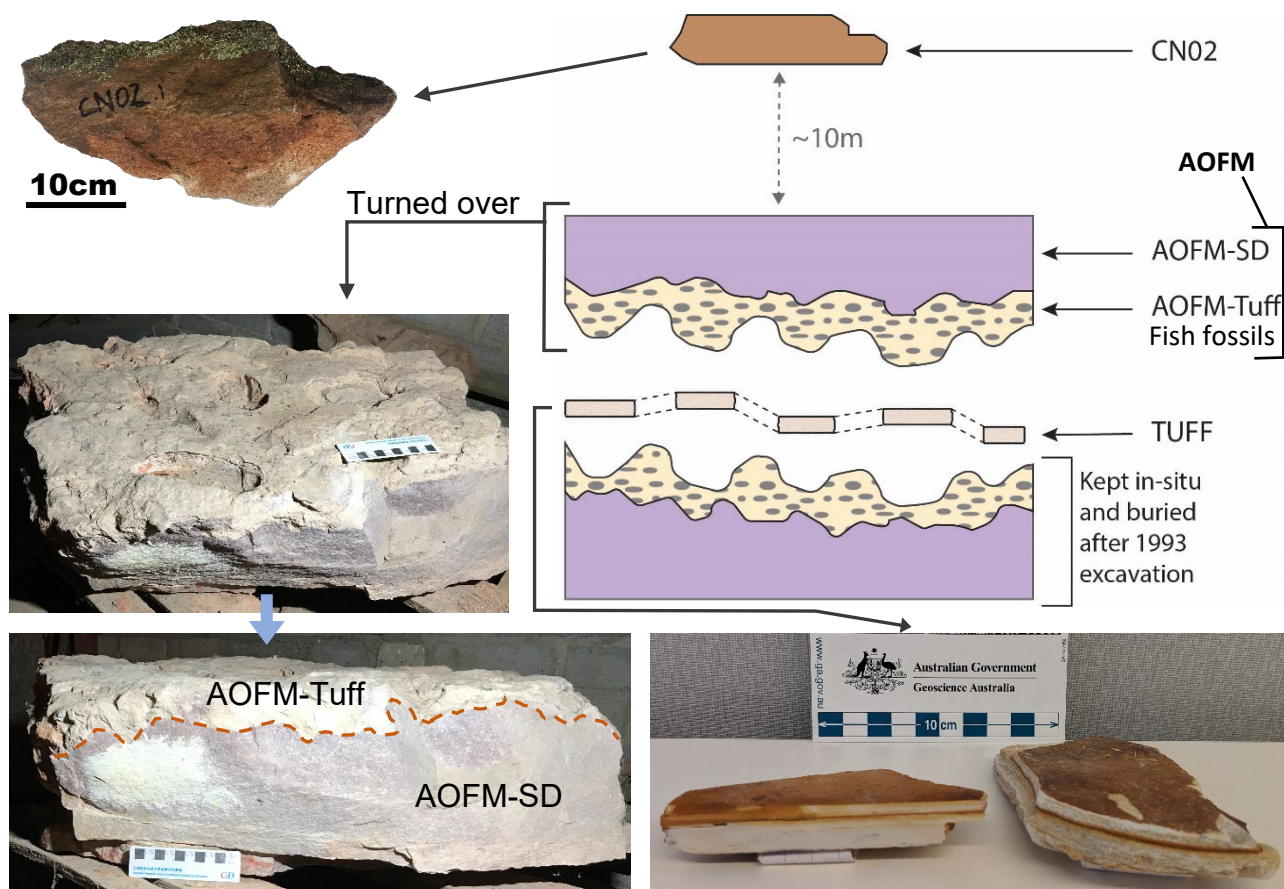


Figure 3.1: Schematic drawing of the Canowindra fish bed and photos of collected samples. Brown dashed line delineates the separation of the fish bed into sample AOFSM-SD and AOFSM-Tuff.

Five samples were analysed in this project (fig.3.1). Sample CN02 is a coarse-grained sandstone, from 10m above the fish layer (fig.2.3). Sample AOFM represents the fish bed sample provided by the Museum, in which the fish are embedded. AOFM has also been divided into 2 separate parts: AOFM-SD, is the top purple-like sandstone (8-12cm thick), and AOFM-Tuff is the underlying greyish-white finer grained sediment (1-5cm thick); relations between the two samples are shown in figure.3.1. The AOFM-Tuff sample was originally suspected to be a fine grained tuff (Zheng-Xiang Li personal communication, 2019), hence the name. It is important to note that the 2 samples AOFM-SD and AOFM-tuff show great thickness irregularities and are thus not planar, as shown by the sketch in figure 3.1. TUFF is a 1.5cm thick, very fine-grained white layer, found originally associated with the fish fossils (Bruce Looms, personal communication, 2019), but was removed from the fish slabs during the excavation, preserved and supplied by Bruce Looms.

The fish site locality itself occurs on the Fish Fossil Drive road, about 11km southwest of Canowindra. Its location is E148°33.986'/S33°35.940'. The site lies at the southern end of a 6km long, north-trending ridge and occurs within the Mandagery Formation of the Hervey Group (Young, 1999).

Field observations were made in the Mandagery Formation on this ridge as well as in the underlying unit (Kadina Formation) at and around the fish site, with coordinates of each stop recorded and provided in the results section. Sedimentary structures, bedding dip and strike and rock composition were observed and recorded along the ridge from the fish site (see chapter 4).

3.2 Sample processing and preparation

Thin sections, with a 30µm thickness, of samples AOFM and TUFF were made for petrographic observations, compositional analysis with a particular focus on possible volcanic components. The AOFM thin section was cut across the boundary between the AOFM-SD and AOFM-Tuff bed to allow detection of any possible petrographic variations (fig.3.2). Plane polarized (PPL) and cross polarized (XPL) images were then obtained and used for petrographic analysis and as a visual reference for the following-up Scanning Electron Microscope (SEM) imaging.

For further analysis, sample CN02, AOFM-SD and AOFM-Tuff were processed at the Geochemical Analysis Unit of Macquarie University to separate zircons from each sample. The samples were disaggregated using the SelFrag instrument (Griffin *et al.*, 2006), which separates minerals along grain boundaries by inducing high-voltage pulses through the rock placed in water, at a frequency of 3 Hz and a voltage ranging from 120 to 155 kV. Following disaggregation, individual samples were then sieved through a 600 and 300µm filter to obtain grain fraction smaller than 300µm. The samples were then panned to eliminate the majority of their light-mineral fractions (e.g. quartz, feldspar). The heavy mineral fractions of the samples were then processed through the Frantz Isodynamic Separator instrument to

remove any magnetic, paramagnetic minerals and non-magnetic residue. Finally, a heavy liquid separation using a sodium polytungstate solution was undertaken to separate zircon grains from the rest of the sample. The solution is denser than water (2.9 g/mL) and allows for the light minerals, such as clay and quartz, to float while the heavier minerals, such as zircon and rutile, sink and allows us to separate the majority of zircons and rutile grains. Once dry, zircon grains were hand-picked and mounted onto a double sticky tape mount under a binocular microscope. The CN02 sample is represented by 88 zircon grains, while 166 zircons were mounted from the AOFM-SD sample. Two zircon mounts AOFM-Tuff1 and AOFM-Tuff2 were produced for AOFM-Tuff sample, where AOFM-Tuff1 consisting of 108 grains zircons, mounted with TEMORA zircon standard grains, and AOFM-Tuff2 consisting of 217 zircon grains. The mounts were then set with epoxy resin and left to cure in a 25 mm diameter mould. The samples were ground, polished and carbon coated (20 nm) for Scanning Electron Microscope (SEM) imaging. Zircon U-Pb age, trace-element and Hf-isotope analyses were then performed using Laser Ablation-Inductively coupled Plasma Mass Spectrometry (LA-ICPMS) and laser-ablation multi-collector inductively-coupled plasma mass spectrometry (LA-MC-ICPMS) techniques.

Two rock samples AOFM-Tuff and TUFF were also disaggregated using a tungsten carbide mill for X-ray Powder Diffraction (XRD) analysis, to obtain the average bulk composition of both samples and allow for the detection in bulk composition differences.

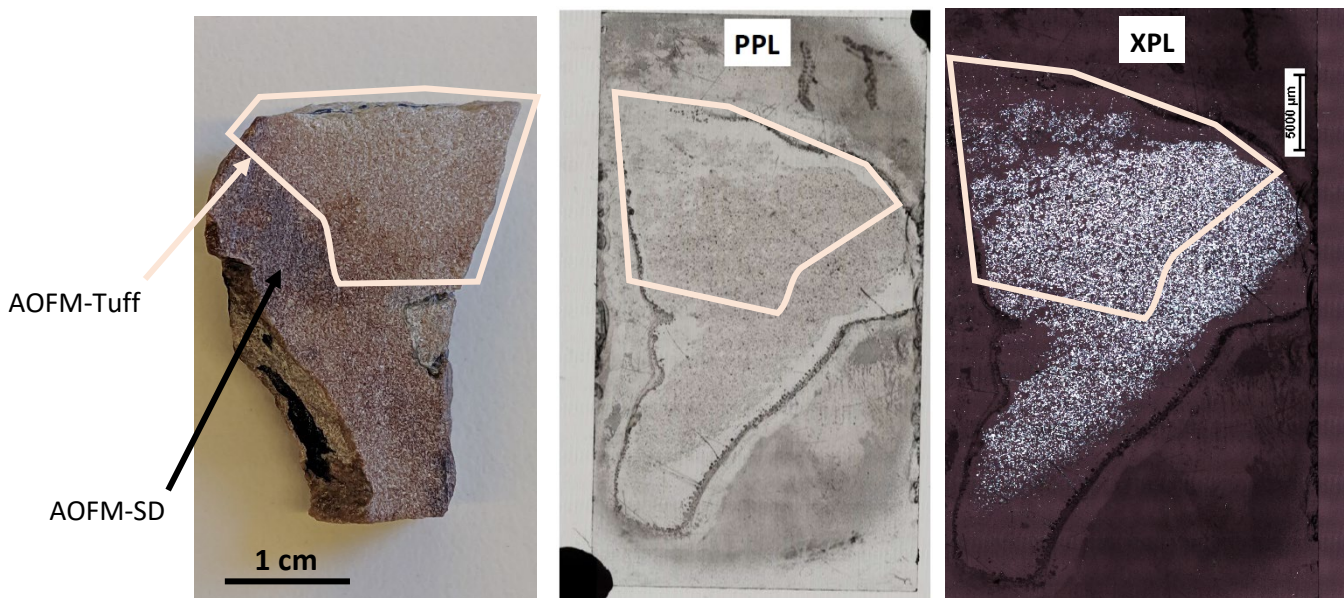


Figure 3.2: Left: Photo of small fish bed sample, AOFM, used for thin section analysis. PPL: Plane polarized image of AOFM. XPL: Cross polarized image of AOFM. Beige line delineates AOFM-Tuff from AOFM-SD.

3.3 Scanning Electron Microscope (SEM)

3.3.1 Cathodoluminescence (CL) zircon imaging

Zeiss EVO MA15 Scanning Electron Microscope (SEM) images of internal structure of all zircon grains in each sample (CN02, AOFM-SD and AOFM-Tuff 1 & 2) were collected with cathodoluminescence (CL) (Belousova *et al.*, 2002), acquired using an Oxford X-max 20 mm² silicon drift detector (SDD) using the Aztec acquisition software. The CL images were then used to visually evaluate and identify the best parts of homogeneous domains or rim regions of zoned zircons and avoid damaged (cracks or inclusions) zircon grains for LA-ICPMS and LA-MC-ICPMS analysis as shown in figure 3.3.

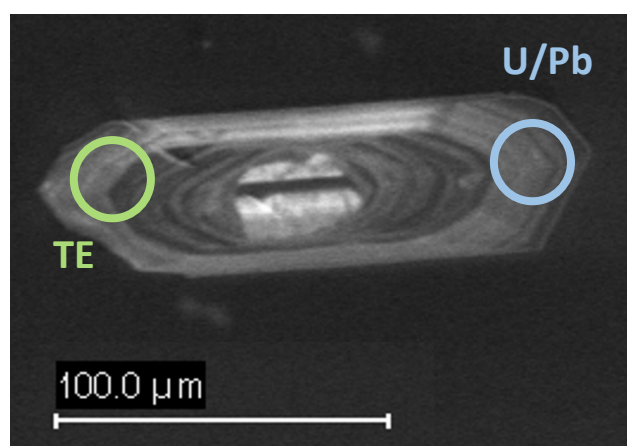


Figure 3.3: CL image of grain AOFM-Tuff1-30, showing targeted location for U/Pb dating (blue) and trace elements (green, TE).

3.3.2 Backscattered Electron (BSE) Imaging and NanoMin analyses

Backscattered Electron (BSE) imaging of the AOFM and TUFF thin sections were obtained for further analysis, of mineral phases and grain shape. BSE images were obtained on an FEI Teneo scanning electron microscope (SEM) using energy dispersive X-ray analysis (EDX) from a Bruker XFlash 6|30 detector, calibrated against a pure Cu standard. Sample AOFM was imaged with a dwell time of 5μs, a working distance (WD) of 9.7mm, a beam voltage of 15kV and an X-ray spacing of 2μm. Sample TUFF was imaged with a dwell time of 5μs, a working distance (WD) of 9.9mm, a beam voltage of 15kV and an X-ray spacing of 2μm.

The mineralogy of the TUFF sample was interpreted using the FEI NanoMin software. The software interprets EDX data by comparing sample spectra to a mineral reference library producing a micron-scale map of the mineralogy across the sample area. The NanoMin map was collected following the methods described in Fialips *et al.* (2018) using the FEI automated imaging software Maps 3.1 with a dwell time of 2μs, a WD of 10mm, a beam voltage of 15kV and a pixel spacing of ~0.049μm. The EDX

data was compared to a mineral reference library, available on the FEI NanoMin software, containing the most common minerals found in siliciclastic based rocks.

3.4 Laser Ablation ICPMS analyses

Zircon U-Pb geochronology

In situ U-Pb dating was performed on sample CN02, AOFM-SD, AOFM-Tuff1 and AOFM-Tuff2, using a Photon Machined Excite Excimer laser ablation system with a 193nm wavelength connected to an Agilent 7700cx ICPMS. The analytical procedures were performed following methods described by Jackson *et al.* (2004). U-Pb dating was measured separately from trace elements to allow higher precision dating of zircons. During U-Pb dating, isotopes ^{206}Pb , ^{207}Pb , ^{208}Pb , ^{235}U , ^{238}U and ^{232}Th were measured. A beam size of 40 μm , laser-energy density of approximately 7.59 J/cm² and frequency of 5Hz were used for all samples. Analytical points for U-Pb dating were placed avoiding both cracks and inclusions in each zircon grain, as defined by CL images (fig.3.3). Data acquisition was processed to minimise signal noise with a 60 seconds background shot and 120 seconds on signal. Samples were analysed in runs of 9-15 unknown points using two GJ-1 zircon standard analysis (Elhlou *et al.*, 2006) at the beginning and end as bracketing standard for instrument calibration. Three other internal zircon standards, 91500, Mud Tank and TEMORA, were measured in each run, as independent measures of instrument stability and data reproducibility. Their ages were within a $\pm 2\sigma$ standard deviation of published values (table 3.1). The raw signal data reduction and selection for U-Pb ages calculation were processed using the GLITTER software package (www.mq.edu.au/GEMOC). Common-Pb corrections were performed following Andersen's (2002) method. $^{206}\text{Pb}/^{238}\text{U}$ ages were measured and processed with a 2σ standard deviation, a 95.4% confidence interval and a discordance based on $^{206}\text{Pb}/^{238}\text{U}$ and $^{207}\text{Pb}/^{235}\text{U}$ variations. Finally, concordia diagrams, weighted average and relative probability plots were generated using the Isoplot software 4.15 (Ludwig, 2008).

Table 3.1: U/Pb ages, precision and accuracy obtained on zircon standards for LA-ICPMS analysis

| Sample | Age ^a (Ma) | | ²⁰⁷ Pb/ ²³⁵ U | | ²⁰⁶ Pb/ ²³⁸ U | | ²⁰⁸ Pb/ ²³² Th | |
|-----------------------------------|--------------------------------------|------------|-------------------------------------|------|-------------------------------------|-------------|--------------------------------------|-------|
| | ²⁰⁷ Pb/ ²⁰⁶ Pb | 2SD | | 2SD | | 2SD | | 2SD |
| GJ-1 | | | | | | | | |
| TIMS^b Long term | 608.5 | 0.4 | | | | | | |
| This project (n = 72) | 609.4 | 66.4 | 593.7 | 34.3 | 589.7 | 41.7 | 604.2 | 72.5 |
| TEMORA | | | | | | | | |
| TIMS^c | | | | | 416.8 | 0.24 | | |
| This project (n = 32) | 464.4 | 153.6 | 421.3 | 26.7 | 413.3 | 12.5 | 422.8 | 83.8 |
| 91500 | | | | | | | | |
| TIMS^d | 1065.4 | 0.3 | | | | | | |
| This project (n = 40) | 1075.4 | 42.9 | 1065.3 | 22.3 | 1060.4 | 20.7 | 1032.3 | 281.4 |
| Mud Tank | | | | | | | | |
| TIMS^e | | | | | 732 | 5 | | |
| This project (n = 31) | 741.2 | 40.7 | 724.8 | 13.0 | 719.7 | 12.5 | 706.0 | 110.5 |

^a Weighted mean age (Ma) \pm 2 sigma errors (at 95% confidence) using Isoplot (Ludwig, 2008).

^b Long term ages from LAM-ICPMS analyses at GEMOC (Jackson et al., 2004).

^c Black *et al.* (2003b)

^d Wiedenbeck *et al.* (1995)

^e Black and Gulson (1978)

Zircon trace-element analysis

In situ trace-element analysis was performed on the youngest zircon grains from each sample, 3 zircon grains from sample CN02, 6 from sample AOFM-SD, 3 from sample AOFM-Tuff1 and 8 zircon grains from sample AOFM-Tuff2. Trace elements, including P, Y, Zr, Nb, La, Ce, Pr, Nd, Sm, Eu, Gd, Tb, Dy, Ho, Er, Tm, Yb, Lu, Hf, Ta, Th and U, were measured in each samples using the equipment and operating conditions used for the U-Pb dating as described above, with two NIST610 standard glass used for instrument calibration and measured at the beginning and end of each run. Two other well-characterised standards, BCR-2G and GJ-1 zircon, were measured in each run, as an independent measure of instrument stability and data reproducibility. The data for BCR-2G and GJ-1 zircon standards obtained during this work are within a $\pm 2\sigma$ standard deviation of published values (table 3.2). Analytical points for trace-element analysis were placed close to U-Pb dating pits within the same region type of each zircon grains as defined by CL images, also avoiding both cracks and inclusions (fig.3.3). The same GLITTER software package was used for processing trace-element data.

Zircon Hf-isotope analysis

In situ Hf-isotope analysis was obtained on 10 unknown points, including 3 zircon grains from CN02, 3 zircon grains from AOFM-SD and 4 grains from AOFM-Tuff. ¹⁷⁶Hf/¹⁷⁷Hf values were measured using a Photon Analyte G2 Excimer laser ablation system with a 193nm wave length connected to Nu Plasma II multi-collector ICPMS. The analytical procedures followed methods described by Griffin et al. (2000)

and Belousova et al. (2009). The analyses were carried out with a spot size of 50 μ m for standards, zircon grain CN02-53 and all 3 grains from the AOFM-Tuff samples. All other grains from CN02 and AOFM-SD were measured with a 40 μ m spot size. Point locations were placed close to both U-Pb dating and trace elements points, within the same domain of each zircon grains as defined by CL images. A Helex II sample holder with He as carrier gas, a laser-energy density of approximately 7.59 J/cm² and a frequency of 5Hz were used for all samples. Data acquisition was processed with a 30 seconds background shot and 60 seconds on signal (if sufficient material was present). All samples were analysed in a single run together with three Mud Tank and two TEMORA zircon standards analysed as a check for instrument stability and accuracy control. ¹⁷⁶Hf/¹⁷⁷Hf values for the Mud Tank and TEMORA zircon standards are within a 1 SE error of published values (table 3.3).

Table 3.3: Hf-isotope analyses obtained on zircon standards using LA-MC-ICPMS technique

| Standard | ¹⁷⁶Hf/¹⁷⁷Hf (laser)^a | This project | n |
|-----------------|--------------------------------------------------------------|---------------------|----------|
| TEMORA | 0.282680 \pm 15 | 0.282672 \pm 4 | 2 |
| Mud Tank | 0.282487 \pm 9 | 0.282503 \pm 3 | 4 |

^a (Kemp *et al.*, 2005)

3.5 X-ray diffraction (XRD)

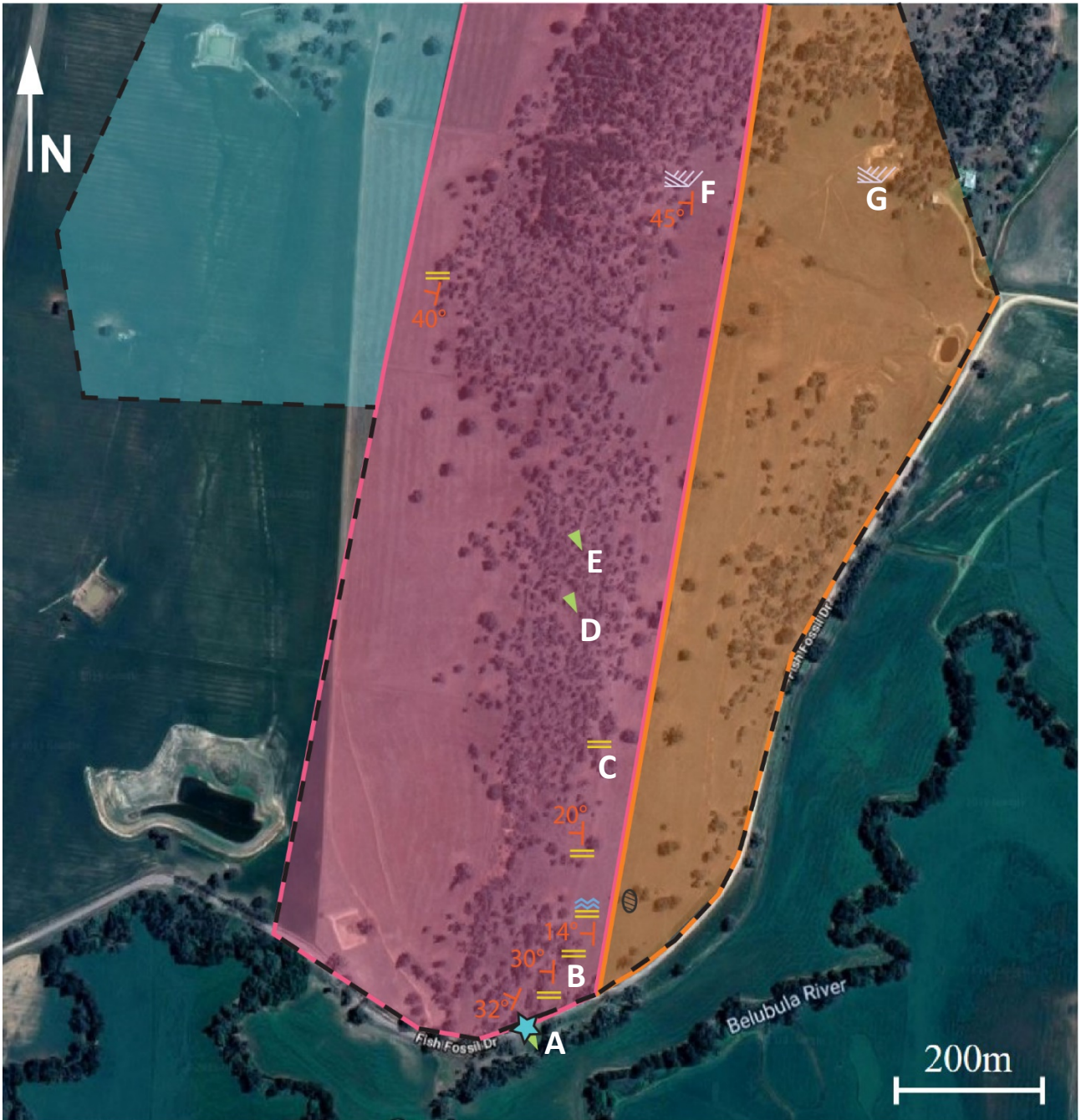
The bulk mineralogy of sample AOFM-Tuff and TUFF (fig.3.1) was determined by X-ray diffraction (XRD) of the powdered samples. Both samples were milled for ~15s in a tungsten carbide mill for XRD analysis. The analytical procedures followed methods described by Abbott *et al.* (2019), where diffraction patterns were collected from 5 to 90° 2 θ using a PANalytical Aeris XRD instrument. Instrument conditions were as follows: Co-radiation source with 40kV generator voltage and 15mA tube current, 0.5° fixed divergence slit, 0.022 2 θ step size, 0.1s per step dwell time, 23mm beam mask, and beam knife in high position. Finally, phase identification was determined using Panalytical HighscorePlus software, with the ICSD database, to interpret the diffraction patterns.

4 Results

4.1 Field observations

Field observations on the Canowindra fish site were recorded during a fieldtrip in May 2019 and summarised in the map shown in Figure 4.1. Field studies have been done for the sedimentary structures that are outcropped along the ridge northward from the fish site. Three units from the Hervey Group, the Kadina, Mandagery and Pipe Formations, were observed along the ridge, dipping and younging west, with an average strike of 352 and average dip of 31° (fig. 4.1). The units' boundaries observed in the field have been outlined by continuous lines, however not all boundaries outcropped (or exposed) and thus shown as dashed lines for each unit. The Mandagery Formation, as observed at the fish site and along the ridge (fig. 4.1, pink region), is represented by a medium to fine-grained planar-bedded salmon-coloured sandstone (fig. 4.1B). Some bioturbations have been observed within the Mandagery Formation locality, however none were found in-situ, but on loose slabs and rock blocks along the ridge (fig. 4.1A, D & E). A large cross-bed (1-2m thick) structure showing a westward younging were recorded about 1km north of the fish site, however no prominent cross bedding was found near the fish site (fig. 4.1F). Small ripples were noted about 170m north from the fish site (fig. 4.1C), but none were observed anywhere else. Conolly (1965a & b) described thin, red and green, siltstone and shale beds within the Mandagery Formation, however, these were not found during our fieldwork.

The boundaries of the overlying (Pipe Fm) and underlying (Kadina Fm) units of the Mandagery Formation were not found due to the lack of outcrops throughout the study area. However, two outcrops within the Kadina Formation as described by Pogson and Watkins (1998) have been observed. These are located east of the Mandagery Formation and represented by grits-sized feldspar- and quartz-rich white-coloured sandstone (fig. 4.1G & H).



LEGEND

- | | | |
|-------------------|----------------------|---------------------|
| Fish fossils site | Estimated limits | Pipe Formation |
| Cross bedding | Dip and strike | Mandagery Formation |
| Planar bedding | Coarse grain outcrop | Kadina Formation |
| Small ripples | | |
| Burrows | | |



Figure 4.1: Map of the of the Canowindra fish site and ridge. Letters represent the location at which each photo, A to H, were taken. **A:** A slab with bioturbation sedimentary structures. **B:** Medium to fine-grained purple sandstone. **C:** Ripple marks. **D:** Loose rock with bioturbations. **E:** Loose rock with bioturbations. **F:** 1-2m cross-bed. **G:** Grits-sized feldspar- & quartz-rich white-coloured sandstone. **H:** Grits-sized feldspar- & quartz-rich white-coloured sandstone, loose rock.

Figure 4.2 shows a traverse, undertaken within the Mandagery Formation, starting about 25m north from the fish site. Observations indicated a consistent composition of fine-grained planar-bedded and purple-coloured sandstone throughout the section, with the exception of a grits-sized (1-3mm) quartz- and feldspar-rich sandstone outcropping at the very end of the traverse (fig. 4.2 ‘end’).

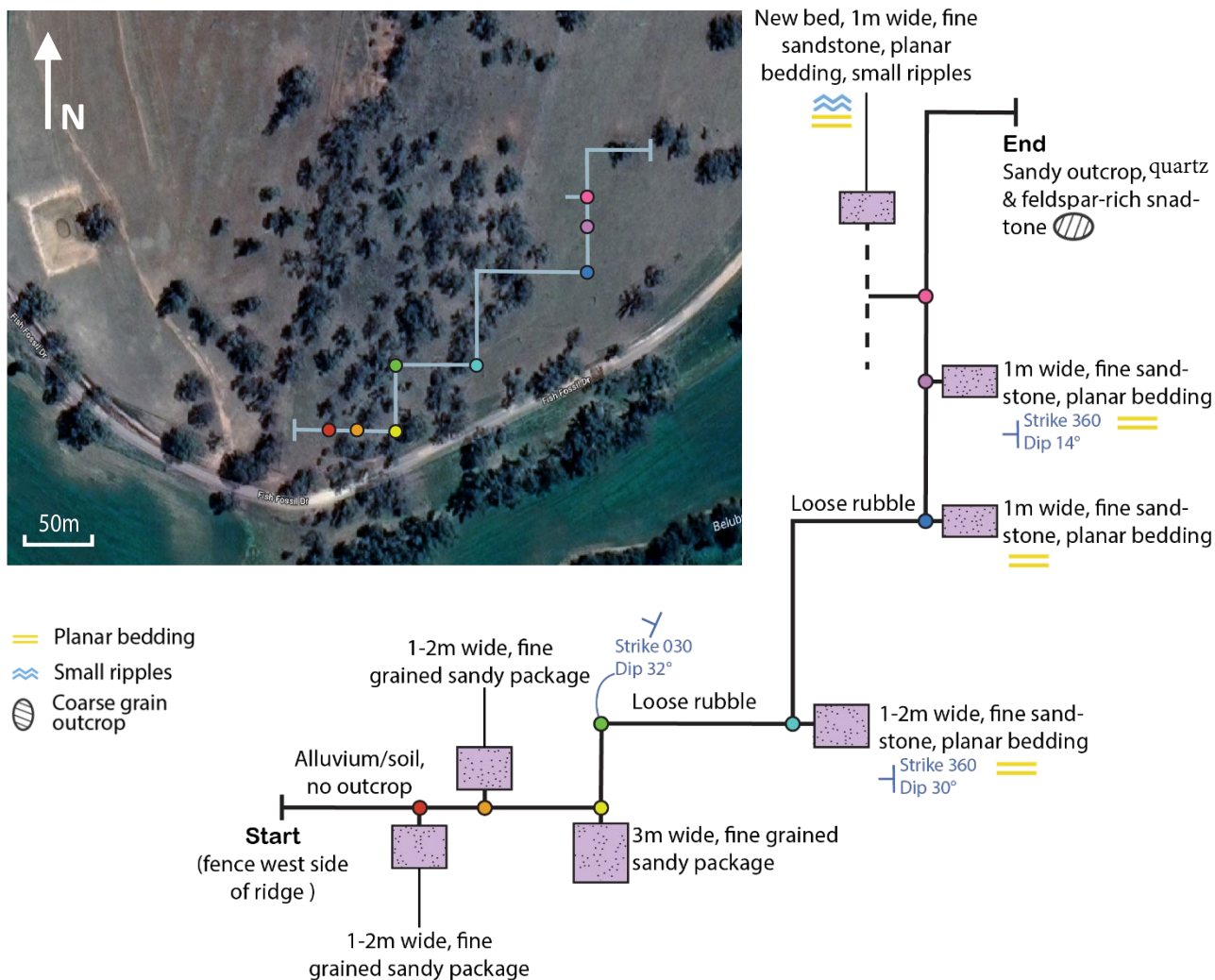


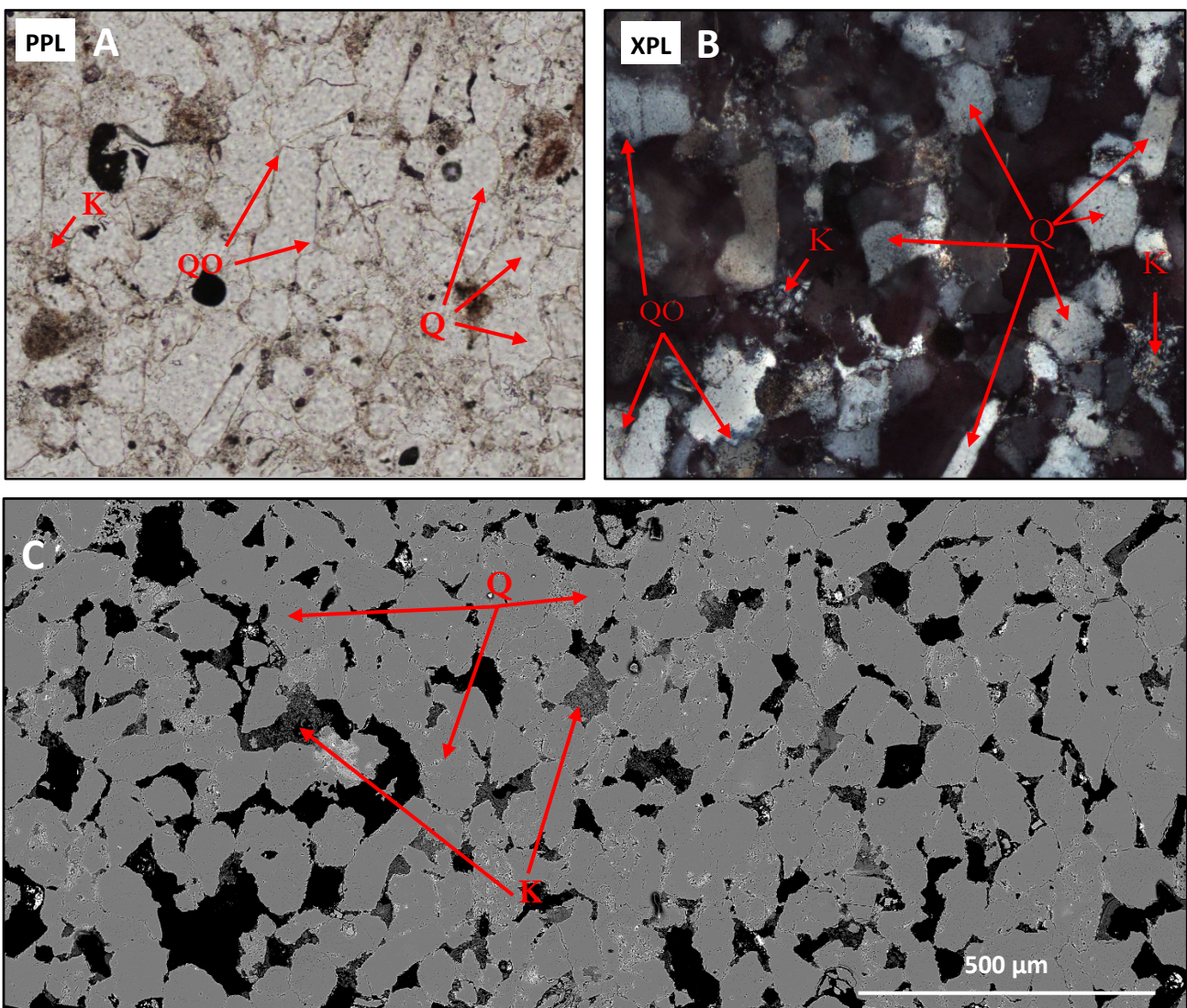
Figure 4.2: Right: Traverse starting about 25m north from the fish site. **Left:** Location of the traverse shown on aerial photo of the Canowindra fish site and ridge.

4.2 Thin sections – SEM

4.2.1 Petrographical and BSE imaging analysis

Petrographical description and backscattered electrons (BSE) analysis of the AOFM (fish bed sample) and TUFF thin sections were made to identify major mineral phases and rock composition of each samples. All thin sections were cut perpendicular to bedding and all images obtained from AOFM and TUFF also shown perpendicular to bedding. Petrographical and BSE images of the AOFM sample are shown in figure 4.3, and those for the TUFF sample are shown in figure 4.4.

As revealed by the images shown in figure 4.3, the AOFM sample is dominated by 100-250 μm quartz grains (Q) with uniform (pale to dark grey) interference colours (fig.3A, B & C). The quartz grains are sub-angular to sub-rounded, moderately sorted and cemented with quartz (labelled as QO on the images). Some quartz grains appear to be coated by a thin layer of iron oxide, which shows a faint orange colour at the edges of these grains in cross polarized light (XPL) (fig. 4.3A). Some chequerboard-like kaolinite cement (K) is also present throughout the sample (fig. 4.3C & D). Pore-spaces are found throughout the sample, appearing as brownish and speckled in plane polarized light (PPL) and black in XPL. Finally, few mica grains, <5%, as elongated, 30-80 μm , flakes which appear to be weathering to kaolinite, can be observed in BSE images, see figure 4.3d & e.



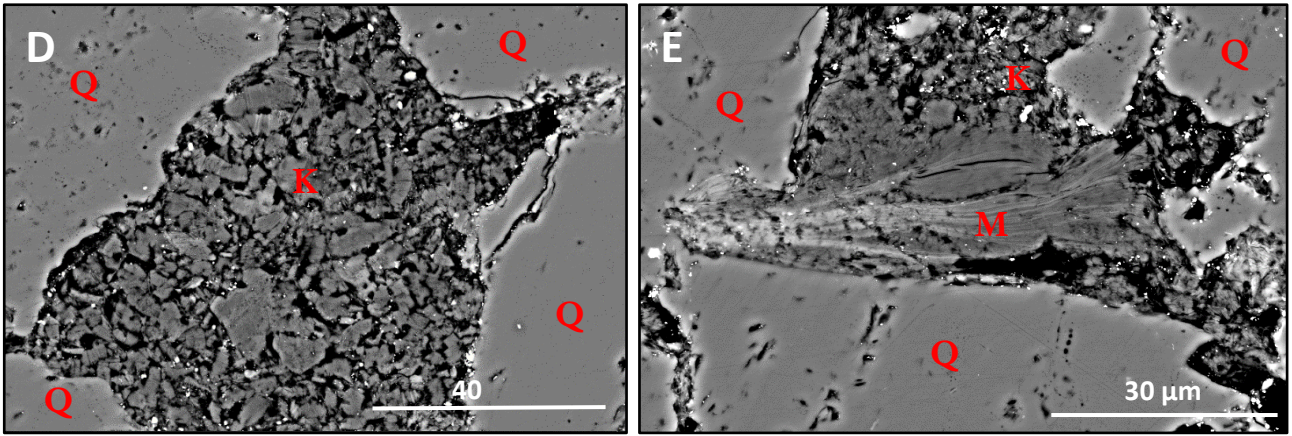
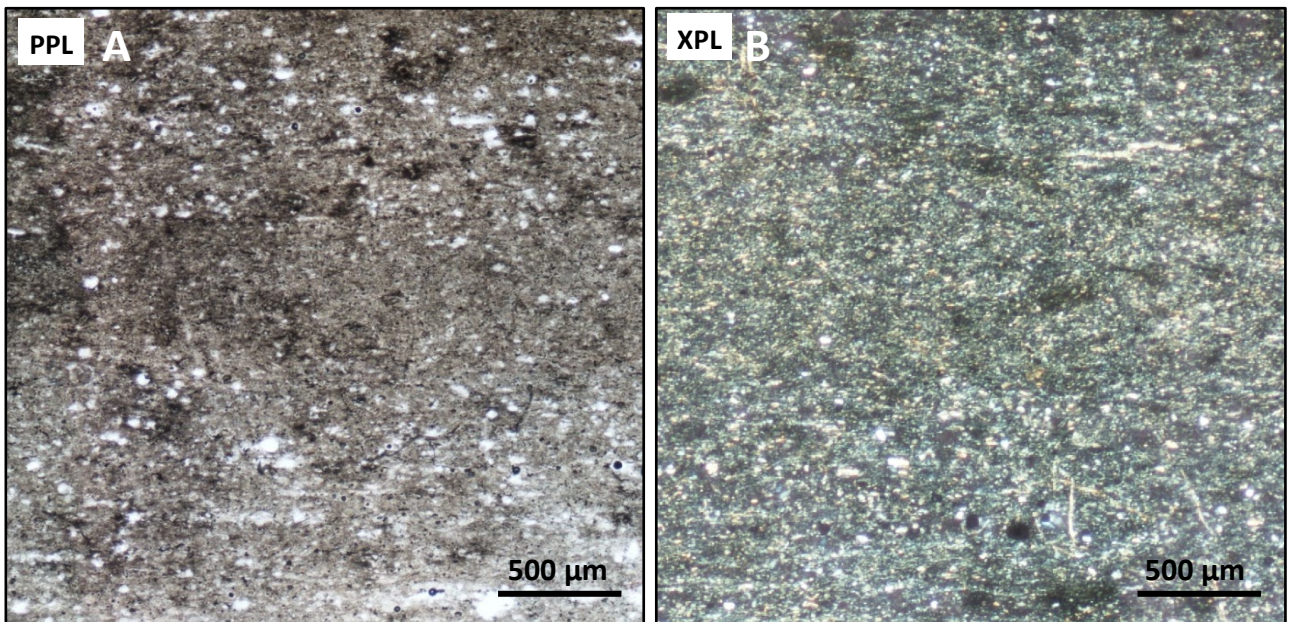


Figure 4.3: Images for sample AOFM, where minerals are defined as: Q: Quartz, QO: Quartz overgrowth, K: Kaolinite. **A:** Under plane polarized light. **B:** Under crossed polarized light. **C:** BSE image. **D:** BSE image of kaolinite cement. **E:** BSE image of mica weathering to kaolinite.

The images for sample TUFF, provided in figure 4.4, show fine-grained, porous, shale-like, textures (fig. 4.4A, B & C). The majority of this sample is very fine grained, $<10\mu\text{m}$, lacks any prominent grain shape and makes identification of mineral type difficult. A few elongated, $10\text{-}60\mu\text{m}$, grains of mica (M) are present throughout the sample and appear to be mostly parallel to bedding, as well as being weathered to kaolinite (K) (fig. 4.4C, D & E). Up to $10\text{-}50\mu\text{m}$, sub-angular, single rutile (R) grains are also present and clearly visible in BSE images (fig. 4.4C). Finally, larger, $20\text{-}50\mu\text{m}$, sub-rounded to rounded quartz grains appear sporadically throughout the sample; these are surrounded by the very fine grained and unidentified minerals as well as a higher volume of pore spaces.



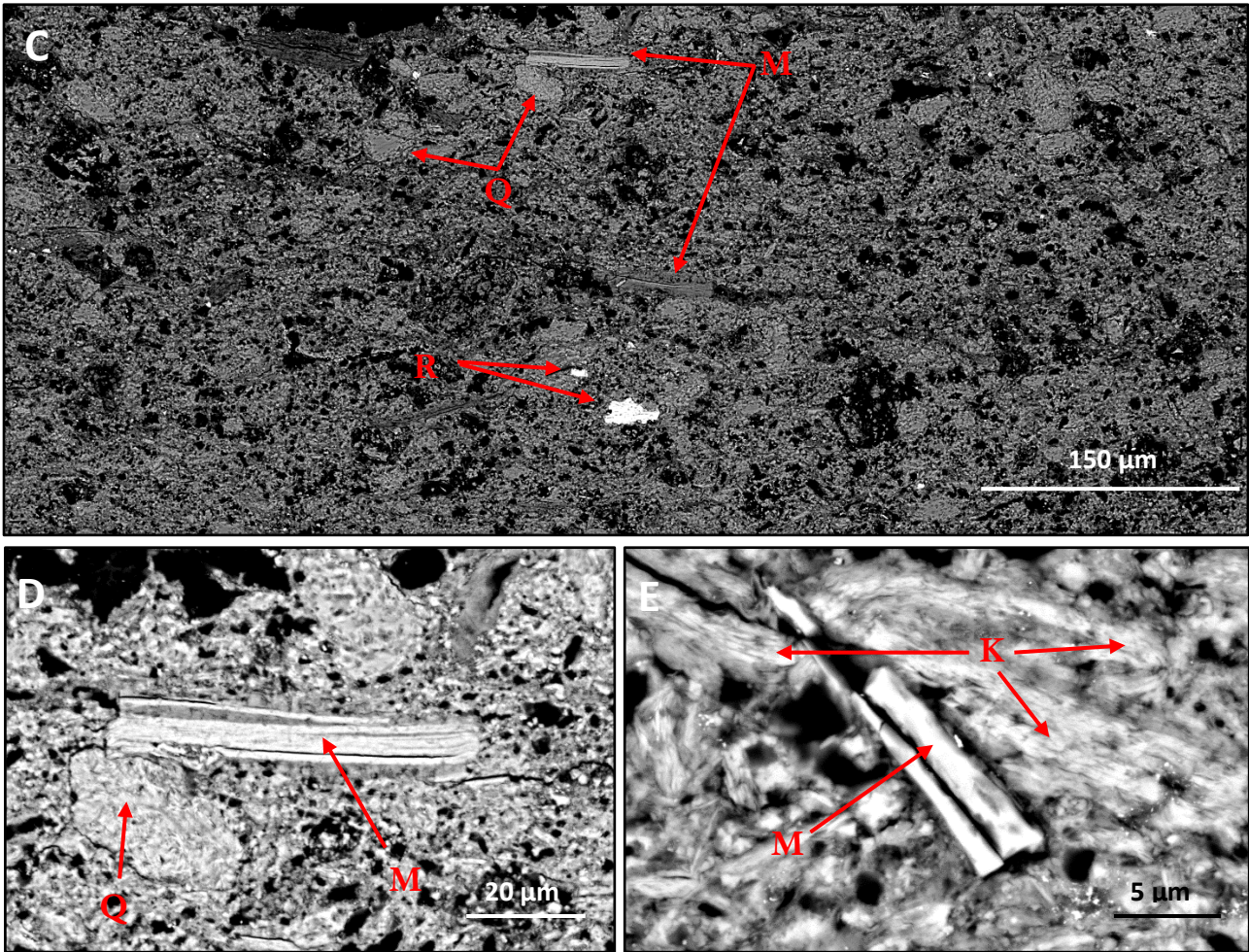


Figure 4.4: Images for sample TUFF, where minerals are defined as: Q: Quartz, M: Mica, K: Kaolinite & R: Rutile. **A:** Plane polarized image. **B:** Crossed polarized image. **C:** BSE image. **D:** BSE image of mica and quartz grain. **E:** BSE image of mica weathering to kaolinite.

4.2.2 NanoMin analysis

Additional NanoMin images, with and without BSE shown in figure 4.5A & B were accordingly collected for the TUFF sample with the aim to identify its mineral phases and structures. The NanoMin imaging revealed that the majority of the sample is dominated by quartz (80-90%), with minor kaolinite (10-15%) and illite (~5%). The quartz grains, shown in grey-blue in BSE (fig. 4.5A) and dark blue without BSE (fig. 4.5B), appear to be present in two different crystal structures: very fine, 1-5 μm , rounded quartz grains representing the majority of the quartz population, and larger, 20-50 μm , sub-angular to rounded quartz grains. Kaolinite occurs throughout the imaged sample, on weathered muscovite as elongated, 10-60 μm grains, located mainly around pore spaces and also represented as a single large, 100 μm sub-angular grain found at the top of the NanoMin images. The kaolinite distribution also appears to show a laminated pattern throughout the sample, parallel to bedding. Minor amounts of K-feldspar, and accessory minerals albite and anorthite occur sporadically throughout the NanoMin image. These show no clear crystal

structure, with a stronger concentration of K-feldspar located within a single 100 μm grain. A few very fine, 1-3 μm , zircon and rutile grains are present and visible as bright pink and red spots respectively, visibly clearer without the BSE (fig. 4.5B).

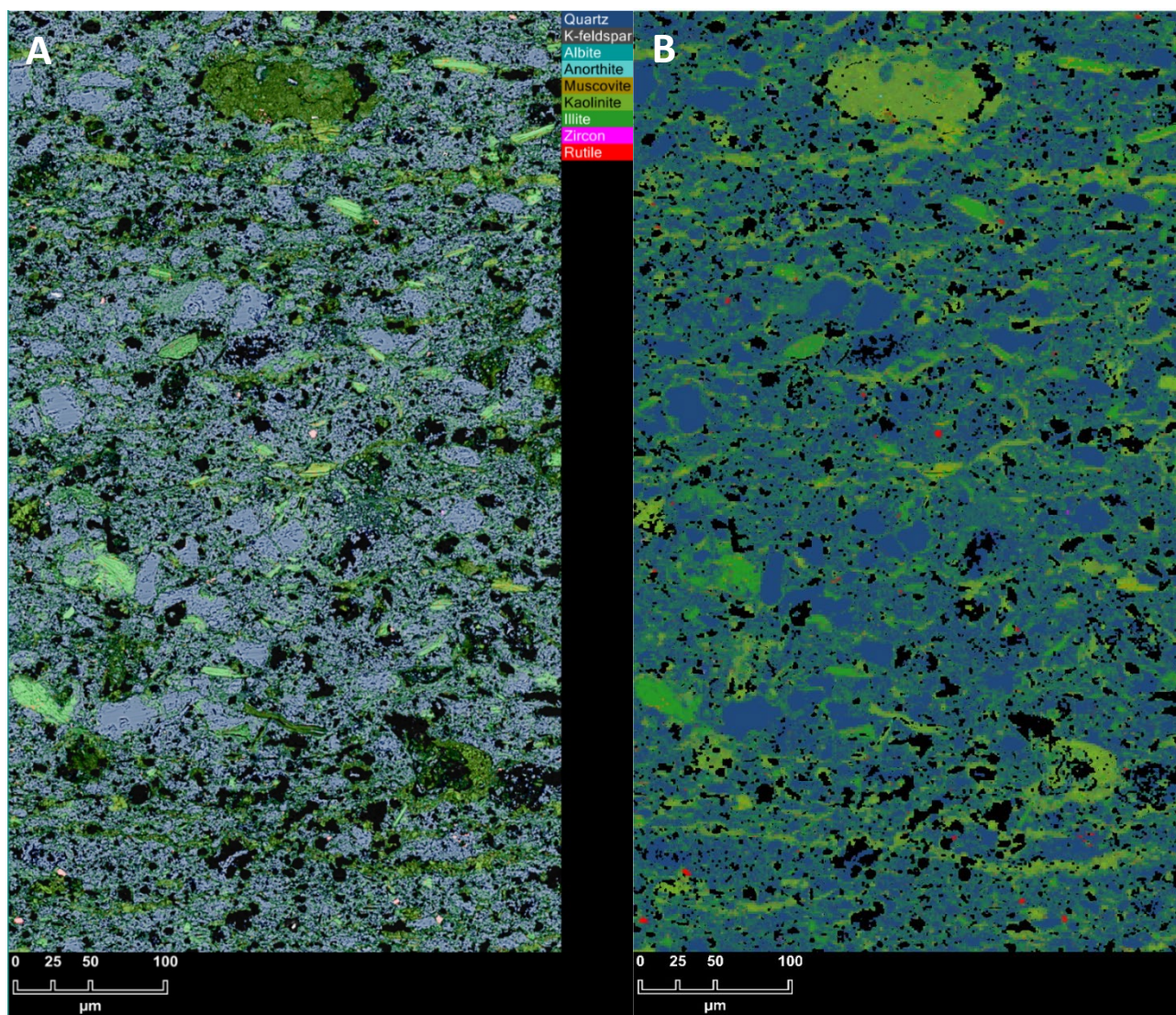


Figure 4.5: NanoMin images of sample TUFF. Minerals are defined by the colours provided in the legend showed on the image. **A:** With BSE. **B:** Without BSE.

4.3 XRD analysis

X-ray powder diffraction (XRD) analysis of AOFM-Tuff and TUFF was undertaken to determine the average bulk composition of both samples and identify, if present, any compositional differences. Figure 4.6 provides the XRD results of the AOFM-Tuff sample and figure 4.7 provides the TUFF sample XRD results. Both samples have very similar average bulk composition, and are composed mostly of quartz (peaks defined by blue lines), with relatively minor quantities of micas (green lines).

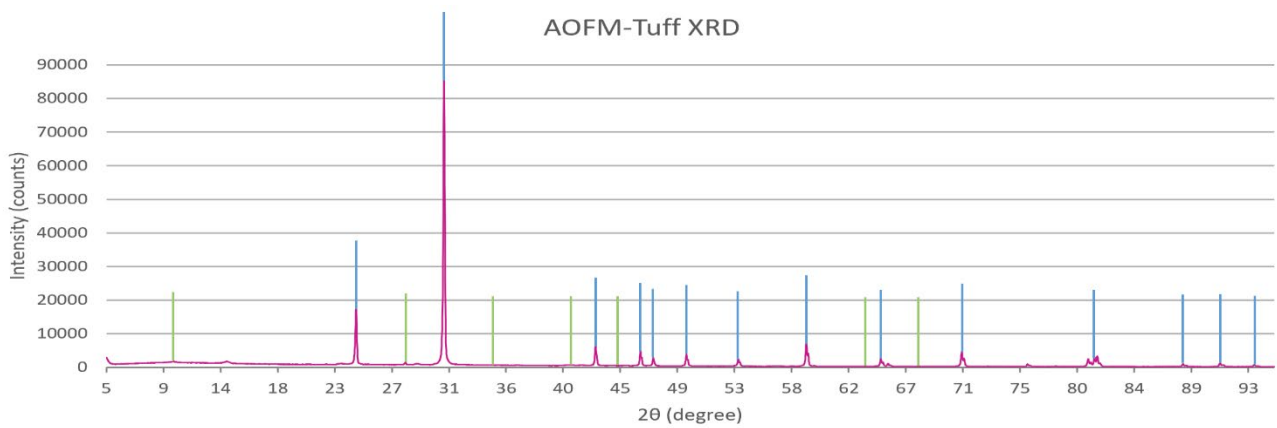


Figure 4.6: Representative bulk X-ray diffractogram of the sample AOFM-Tuff. **Blue lines:** Quartz. **Green lines:** Micas

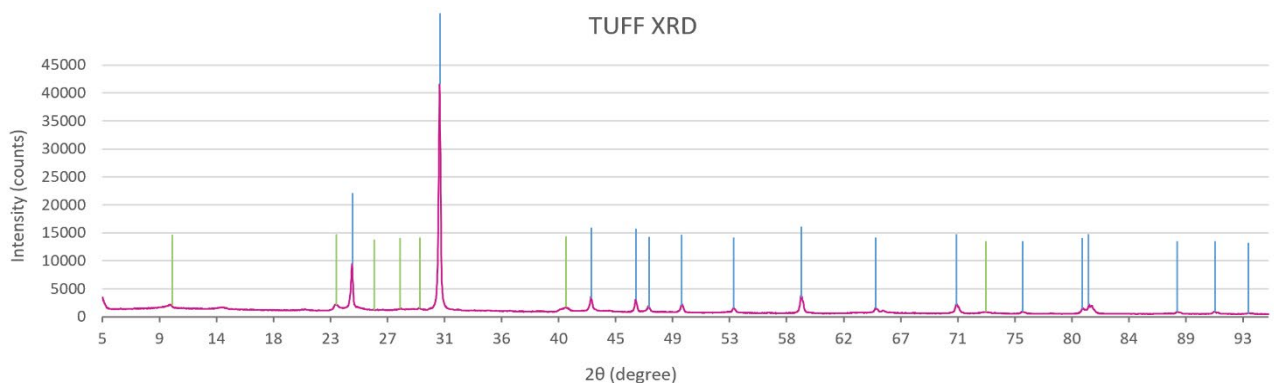


Figure 4.7: Representative bulk X-ray diffractogram of the sample TUFF. **Blue lines:** Quartz. **Green lines:** Micas

4.4 Zircon U-Pb and Hf-isotope analyses

4.4.1 U-Pb age results

U-Pb isotope analysis were obtained on detrital zircons recovered from samples CN02, AOFM-SD and AOFM-Tuff (Appendix tables A2-A5) to determine the maximum depositional ages of these three structurally distinct beds within the Mandagery Formation. The stratigraphic locations of those beds, such as 10 metres above the fish bed (represented by sample CN02), immediately above (represented by sample AOFM-SD) and within the fish bed (sample AOFM-Tuff) will hopefully allow the best estimate for the age of the Canowindra fish (fig.3.1).

CN02 – 10 metres above fish site

90 zircons from CN02 were picked out and mounted. The mounted grains range in size from 60 to 140µm with euhedral and subhedral shapes, some elongate and zoned, with colours ranging from colourless, light pink, to light yellow. 61 zircon grains from the CN02 zircon mount were selected for U-Pb dating, based on their crystal structure. These grains include elongate and prism-like grains, with minimal cracks and inclusions, while also avoiding zoned grains with very narrow rims to prevent getting mixed and thus inaccurate U/Pb ages. Figure 4.8A presents a concordia diagram of all the data acquired

for this sample, with rejected analyses highlighted in red. Figure 4.9 shows a relative probability plot of all of CN02's data without the rejected analysis, as defined in figure 4.8. There are two major age populations identified in figure 4.9, with a scatter of single older grains. The older scattered minor peaks are represented by an Archean grain with an age of 2884 ± 36 Ma, a Mesoproterozoic grain with an age of 1209 ± 14 Ma and a Neoproterozoic grain of 673 ± 12 Ma. A secondary age peak, defined by 8 grains, provides a Cambrian age of 531 ± 6 Ma. The major and youngest age population, defined by 49 grains, shows the highest peak in the sample at 431 ± 6 Ma (Silurian). For better visualisation, the youngest 58 zircon grains, younger than 650Ma, are presented in figure 4.8B, including a single rejected grain shown in red, due to its discordant age of $>20\%$ (defined by rim discordance). The three youngest grains, shown in box "C" of figure 4.8B, appear clearly grouped and much younger than the rest of the analysed grains, forming the youngest population in the sample (fig. 4.8D). These three concordant or near-concordant grains were used to produce a weighted average and concordia diagrams, figure 4.8C & D, and suggest a $^{206}\text{Pb}/^{238}\text{U}$ concordia age of 372 ± 1.8 Ma (MSWD = 1.7), with 95% of confidence level and 2σ error, which provides the best estimate of the maximum deposition age for the CN02 sample.

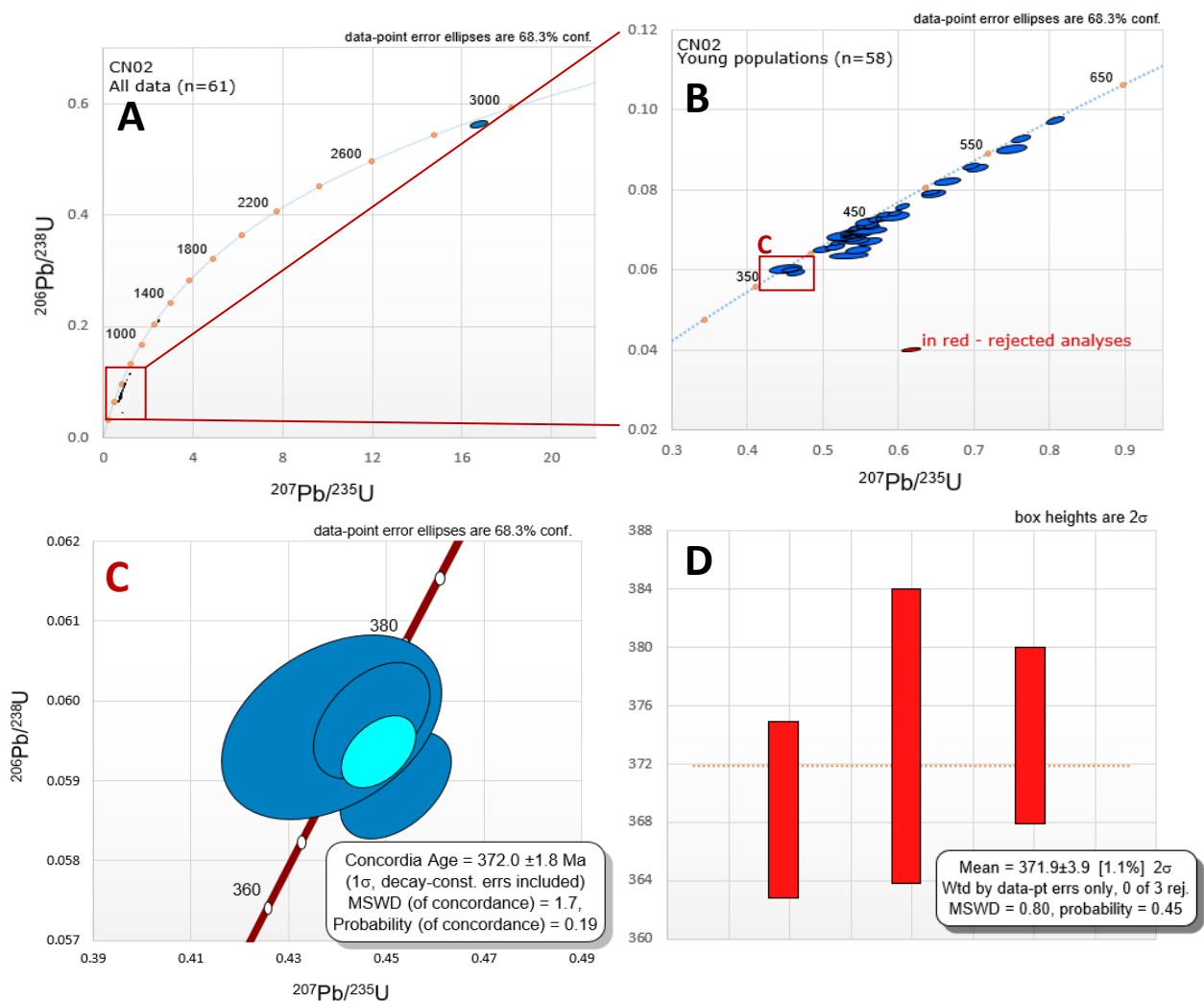


Figure 4.8: Sample CN02. **A:** Concordia of all U/Pb age analyses. **B:** Concordia of the major younger population, box "C" shows the youngest population. **C:** Concordia of the youngest 3 grains. **D:** Weighted average of the youngest 3 grains, defined by box "C".

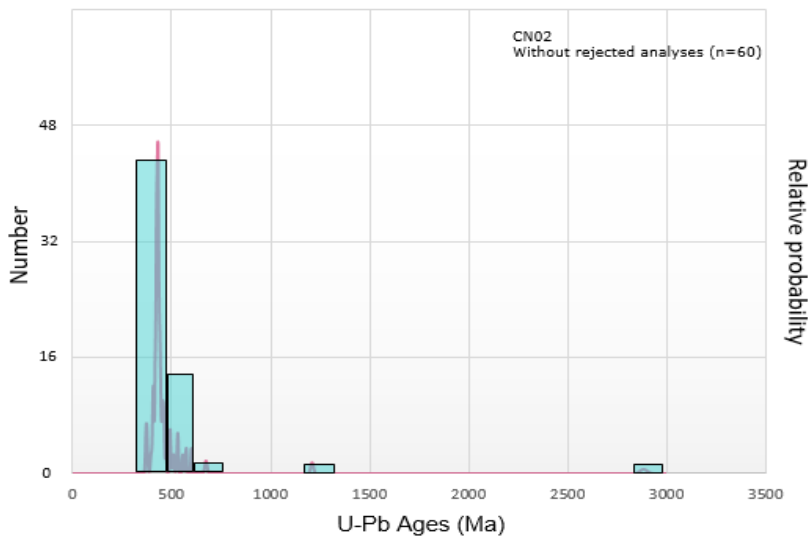


Figure 4.9: Relative probability graph of U/Pb ages (without the rejected analyses) of sample CN02. Histograms indicate the number of grains in each major peaks.

AOFM-SD – Purple sandstone overlying the fish fossils

234 zircons from AOFSM-SD were picked and mounted. The targeted and mounted grains ranged in size from 60 to 150 μ m and limited to euhedral and subhedral shapes, sometimes elongate and zoned, with colours ranging from colourless, lightly opaque white, to light pink. 72 zircon grains were selected, based on their CL images, as defined previously, and used to determine their U-Pb ages. Figure 4.10A presents a concordia diagram of all measured ages acquired. The youngest 67 zircon grains, younger than 600Ma, are presented in figure 4.10B, including 17 rejected grains shown in red. Figure 4.11 shows a relative probability plot of AOFSM-SD, without the rejected analysis, as defined in figure 4.10. There is one major age population identified in figure 4.11, with a scatter of single older grains. The older scattered minor peaks are represented by two Palaeoproterozoic grains with an age of 1808 ± 22 Ma and 1643 ± 20 Ma, a Mesoproterozoic grain with an age of 1025 ± 12 Ma, and two Neoproterozoic grains with an age of 888 ± 16 Ma and 575 ± 6 Ma. Two secondary age peaks, provide a Cambrian age of 521 ± 8 Ma, defined by 2 grains, and Ordovician age of 484 ± 6 Ma defined by 6 grains. The major age population, defined by 22 grains, shows the highest peak in the sample at 428 ± 6 Ma (Silurian). It is followed by two major secondary peaks providing a Devonian age of 408 ± 6 Ma and 360 ± 4 Ma. The three youngest grains, shown in box “C” of figure 4.10B, appear to be the youngest population in the sample (fig. 4.10D). These three grains were used to define weighted average and concordia plots, shown in figure 4.10C & D. The concordia age however, was not obtainable due to a lack of concordance from those zircons (probability of 0.00 as shown in fig. 4.10C). The population age was therefore obtained using the weighted mean approach, shown in figure 4.10D, which suggests a $^{206}\text{Pb}/^{238}\text{U}$ weighted mean age of 361.2 ± 2.9 Ma (MSWD = 0.62), with 95% of confidence level and 1σ error, for the best estimate of the maximum deposition age of the AOFSM-SD sample.

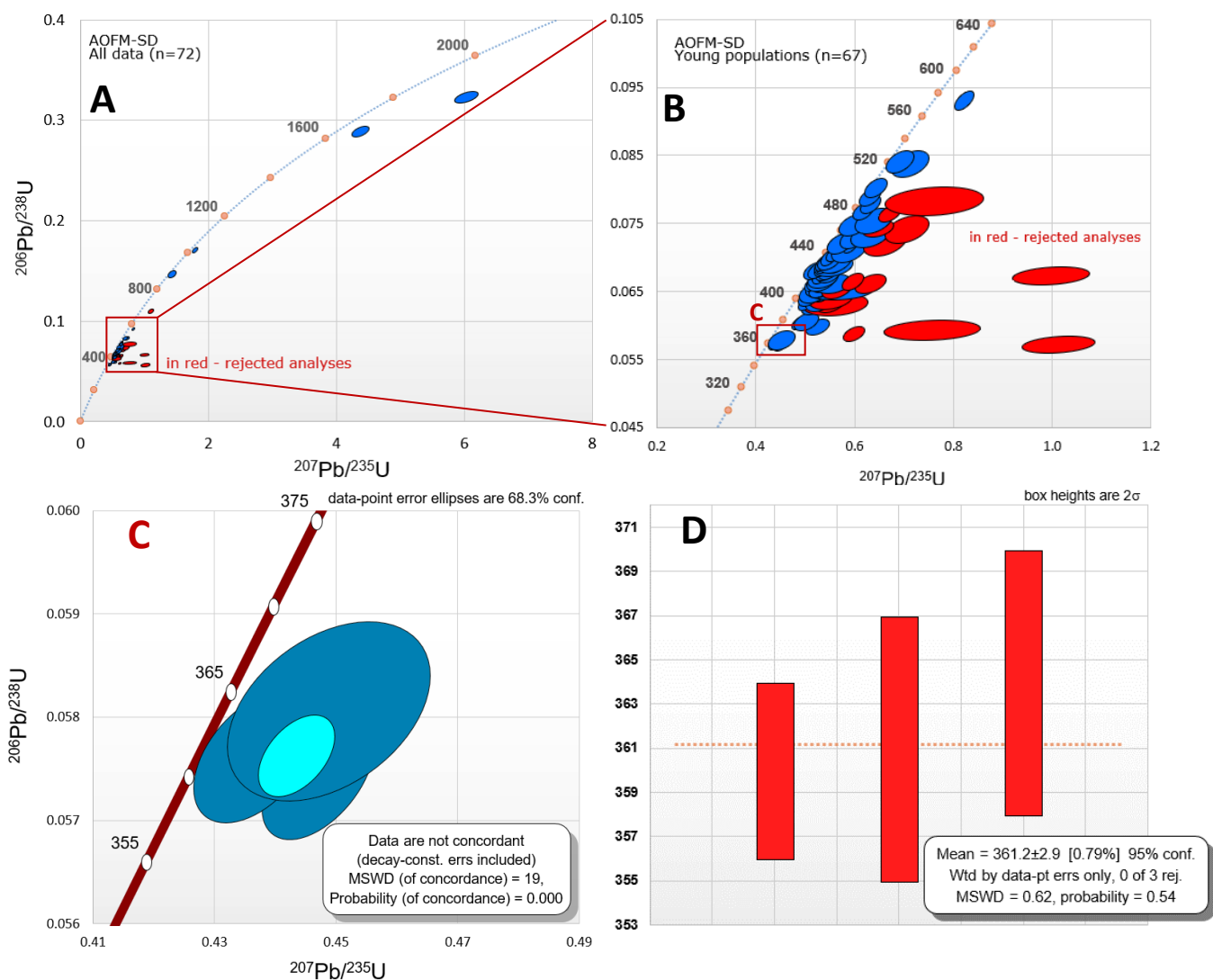


Figure 4.10: Sample AOFSM-SD. **A:** Concordia of all U/Pb age analyses. **B:** Concordia of the major younger population, box "C" shows the youngest population. **C:** Concordia of the youngest 3 grains. **D:** Weighted average of the youngest 3 grains, defined by box "C".

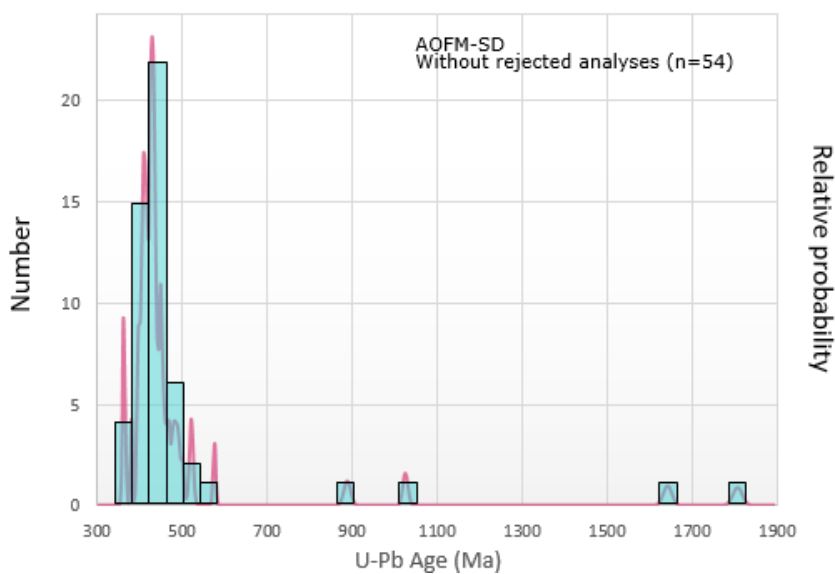
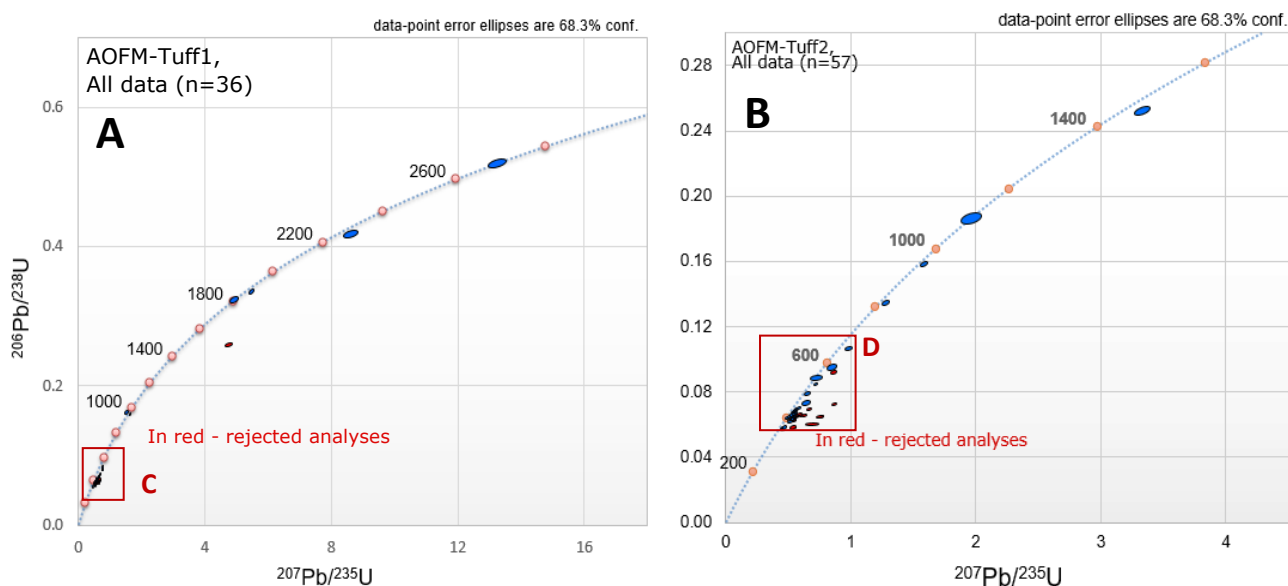


Figure 4.11: Relative probability graph of U/Pb ages for zircons (<20% discordant) from the sample CN02. Histograms indicate the number of grains in each major peaks.

AOFM-Tuff – White tuffaceous-like sandstone containing fish fossils

36 zircon grains from the AOFM-Tuff1 and 57 grains from the AOFM-Tuff2 zircon mounts were selected, based on crystal structure revealed on CL images, as defined previously, and used to determine U-Pb ages. Figure 4.12A & B presents concordia plots for zircons from AOFM-Tuff1 and AOFM-Tuff2 samples accordingly, wherein the younger populations (younger than 700Ma), 30 zircon grains for AOFM-Tuff1 and 53 for AOFM-Tuff2, are presented in figure 4.12C & D, including a total of 17 rejected grains, shown in red. Figure 4.13 shows a relative probability plot of AOFM-Tuff1 & AOFM-Tuff2 without the rejected analysis, as defined in figure 4.12. There is one major age population identified in figure 4.13, with a scatter of single older grains. The older zircons are represented by an Archean grain with an age of 2703 ± 34 Ma, 3 Palaeoproterozoic grains with ages of 2257 ± 32 Ma, 1878 ± 20 Ma and 1822 ± 30 Ma, a Mesoproterozoic grain with an age of 1456 ± 18 Ma, a Neoproterozoic grain at 673 ± 12 Ma. There are two minor Neoproterozoic age peaks at 822 ± 12 Ma (4 grains) and 661 ± 10 (2 grains). The major age population, defined by 58 grains, shows the highest peak in the sample at 415 ± 6 Ma (Devonian), and is followed by a secondary and youngest peak, defined by 5 grains, providing a Devonian age of 364 ± 6 Ma. The four youngest grains, shown in boxes “E” of figure 4.12C & D, presents the youngest population in the sample (fig. 4.12F). These four grains are used for a weighted average and concordia graph, figures 4.12E & F, where the weighted average graph’s mean age (fig. 4.12F) will be favoured as it provides a better value of MSWD = 0.52 compared to a MSWD of 3.9 obtained from the concordia approach (fig. 4.12E). Therefore, the best estimate of the maximum depositional age for the AOFM-Tuff sample is the $^{206}\text{Pb}/^{238}\text{U}$ weighted mean age of 363.0 ± 3.1 Ma (MSWD = 0.52), with a 95% confidence level.



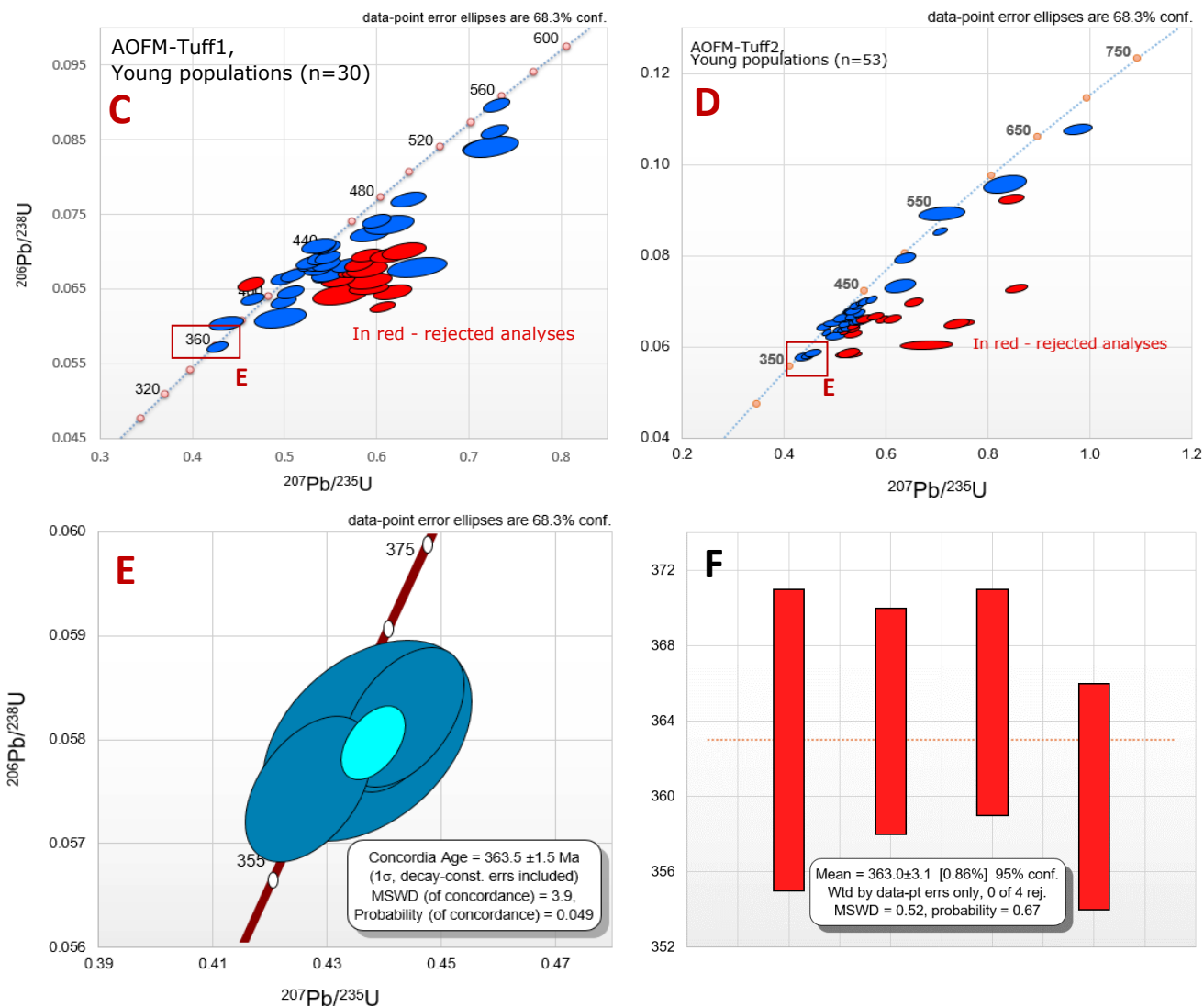


Figure 4.12: Sample AOFM-Tuff 1 & 2. **A:** Concordia of U/Pb age analyses of zircons from AOFM-Tuff 1 and **B:** AOFM-Tuff2. **C:** Concordia of the major younger population, box “C” shows the youngest population in AOFM-Tuff1 and box “D” in **D:** AOFM-Tuff2. **E:** Concordia of the youngest 4 grains, defined by box “E” in AOFM-Tuff 1 & 2. **D:** Weighted average of the youngest 4 grains, defined by box “E” in AOFM-Tuff 1 & 2.

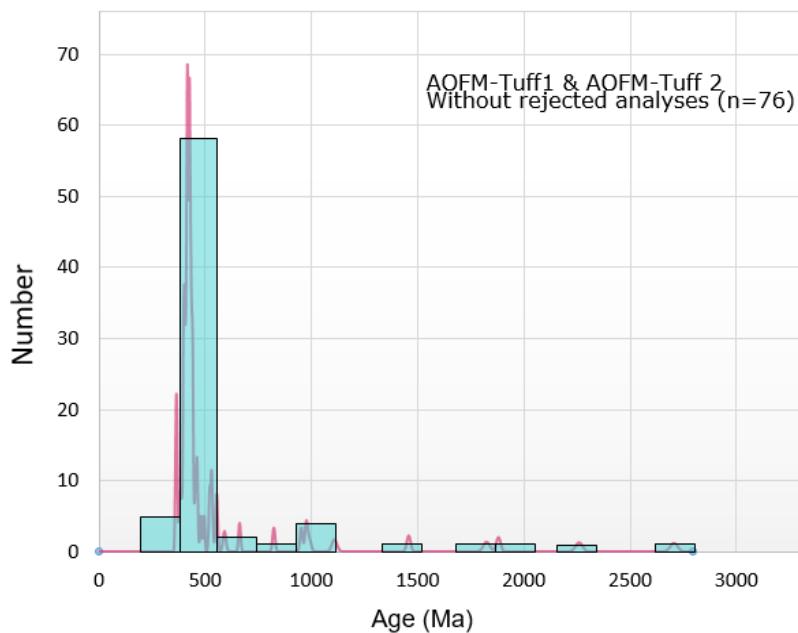


Figure 4.13: Relative probability graph of U/Pb age analyses, that are less than 20% discordant, of sample AOFM-Tuff 1 & 2. Histograms indicate the number of grains in each major peaks.

4.4.2 Zircon trace-element analysis

A total of 80 zircon grains were analysed for trace elements (Appendix table A6) to help define the provenance of each sample, including CN02 (19 grains), AOFM-SD (23 grains) and AOFM-Tuff1 & 2 (defined as AOFM-Tuff, 38 grains). Representative zircons of all age populations as defined by U/Pb dating (from 360 to 1780Ma) from each sample were selected for trace-element analysis. Figure 4.14 provides the chondrite-normalized rare earth element (REE) graph of all grains, with the exception of one rejected AOFM-tuff grain. As shown in figure 4.14, all three samples show a very similar pattern typical of this mineral (Belousova *et al.*, 2002). CN02 (shown in blue) however, shows a slightly more noticeable depletion in REE than AOFM-SD (shown in red) and AOFM-Tuff (shown in brown).

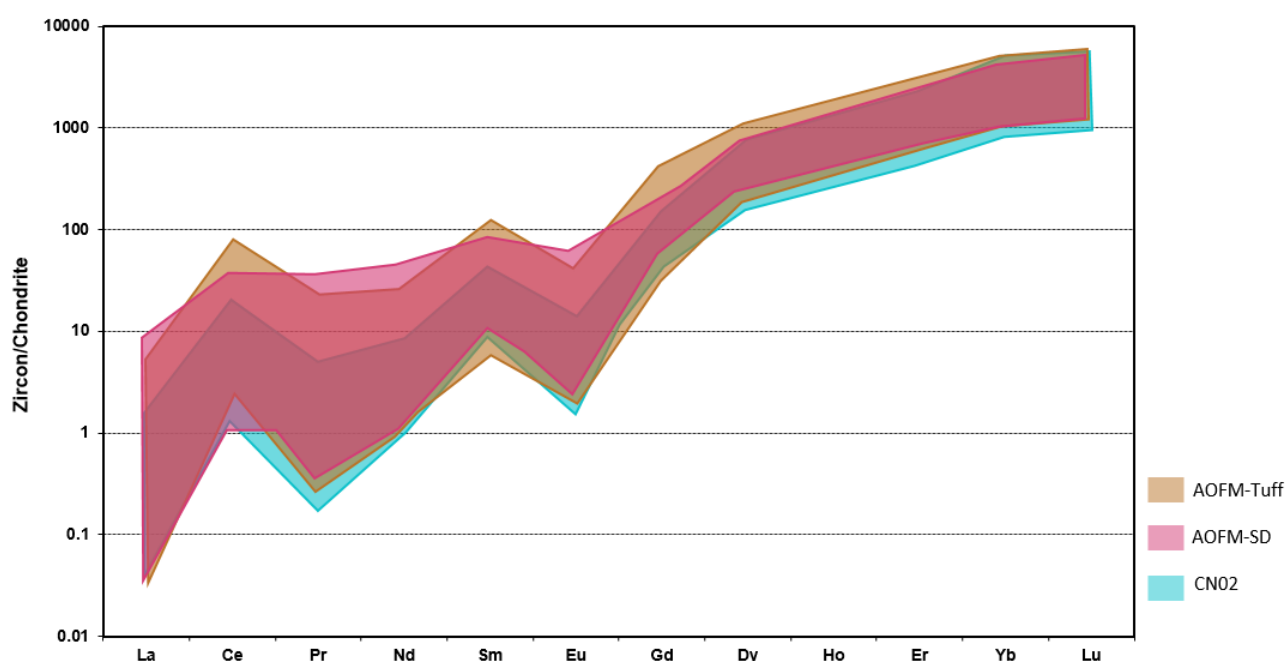


Figure 4.14: Chondrite-normalized rare earth element (REE) graph for zircons of all age populations from samples CN02 (19 grains), AOFM-SD (23 grains) and AOFM-Tuff1 & 2 (defined as AOFM-Tuff, 38 grains).

Figure 4.15 provides a U/Yb ratio vs Y (ppm) graph of all the 79 grains representative of all age populations in all studied samples. Using a discriminant diagram provided by Grimes *et al.* (2007), figure 4.15 differentiates continental crust from oceanic crust zircons. Where AOFM-SD and AOFM-Tuff spans throughout the continental and oceanic crust field, while CN02 appears to be relatively more concentrated within the continental crust field.

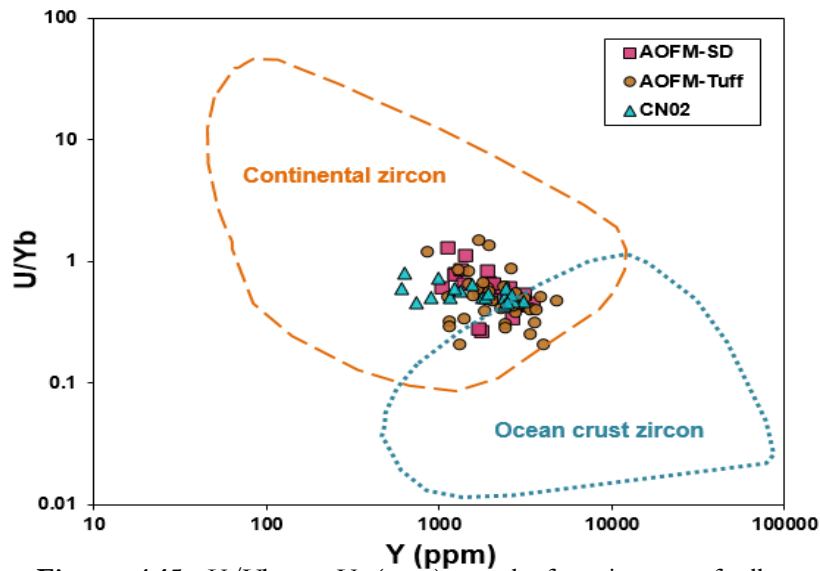


Figure 4.15: U/Yb vs Y (ppm) graph for zircons of all age populations from samples CN02 (19 grains), AOFM-SD (23 grains) and AOFM-Tuff1 & 2 (defined as AOFM-Tuff. 38 grains). Fields are

Figure 4.16 provides a chondrite-normalized REE graph of the youngest zircon grains, as defined by the youngest age population (360-394Ma), of all studied samples CN02 (4 grains), AOFM-SD (6 grains) and AOFM-Tuff (11 grains). All zircon grains in this figure show a HREEs enrichment and depletion in LREEs, with distinct positive Ce and negative Eu values, which is a typical signature of most of magmatic zircons. Each sample has been assigned a colour to allow for differences in their REE values to be distinguished on this diagram: CN02 zircons are shown in blue, AOFM-SD in red and AOFM-Tuff1 & 2 in grey. REEs of the youngest grains of all three samples present a very similar pattern, however, grains from the CN02 sample show a slightly more depleted pattern compared to AOFM-SD and AOFM-Tuff.

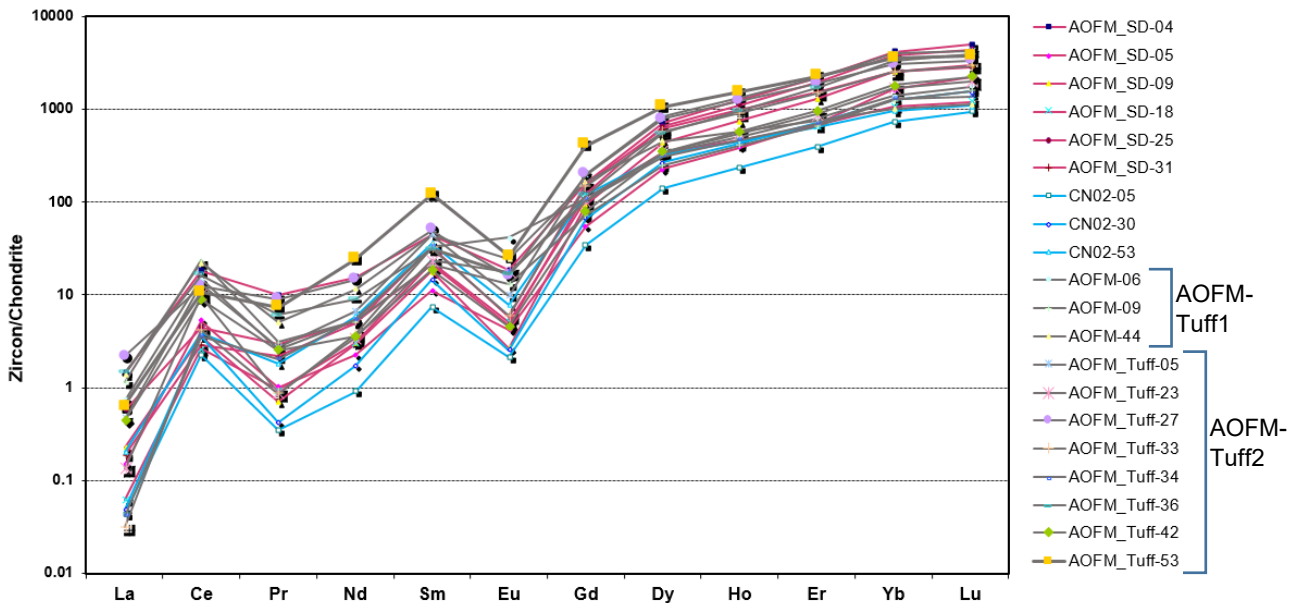


Figure 4.16: Chondrite-normalized rare earth element (REE) graph of the youngest zircon grains, as defined by the youngest age population (360-394Ma), of sample CN02 (4 grains), AOFM-SD (6 grains) and AOFM-Tuff1 & 2 (defined as AOFM-Tuff, 11 grains).

Y (ppm) vs Yb/Sm and Hf (wt%) vs Y (ppm) graphs of the youngest zircon population of CN02, AOFM-SD and AOFM-Tuff have also been provided in figures 4.17A & B. Discriminant diagrams as provided by Belousova *et al.* (2002), are used to determine possible trace-element differences between all three samples. Figure 4.17A shows all three samples are of felsic/intermediate composition. Samples AOFM-SD and AOFM-Tuff have similar Y values while sample CN02 is slightly lower. AOFM-SD also shows a higher Yb/Sm ratio in comparison to CN02 and AOFM-Tuff. Figure 4.17B indicates that zircons from AOFM-Tuff are derived from magma(s) of more felsic composition than CN02 and AOFM-SD. CN02 also shows a slight decrease in Y, while AOFM-SD has the highest Hf. However, for all zircon elements shown, there is no clear distinction between the samples.

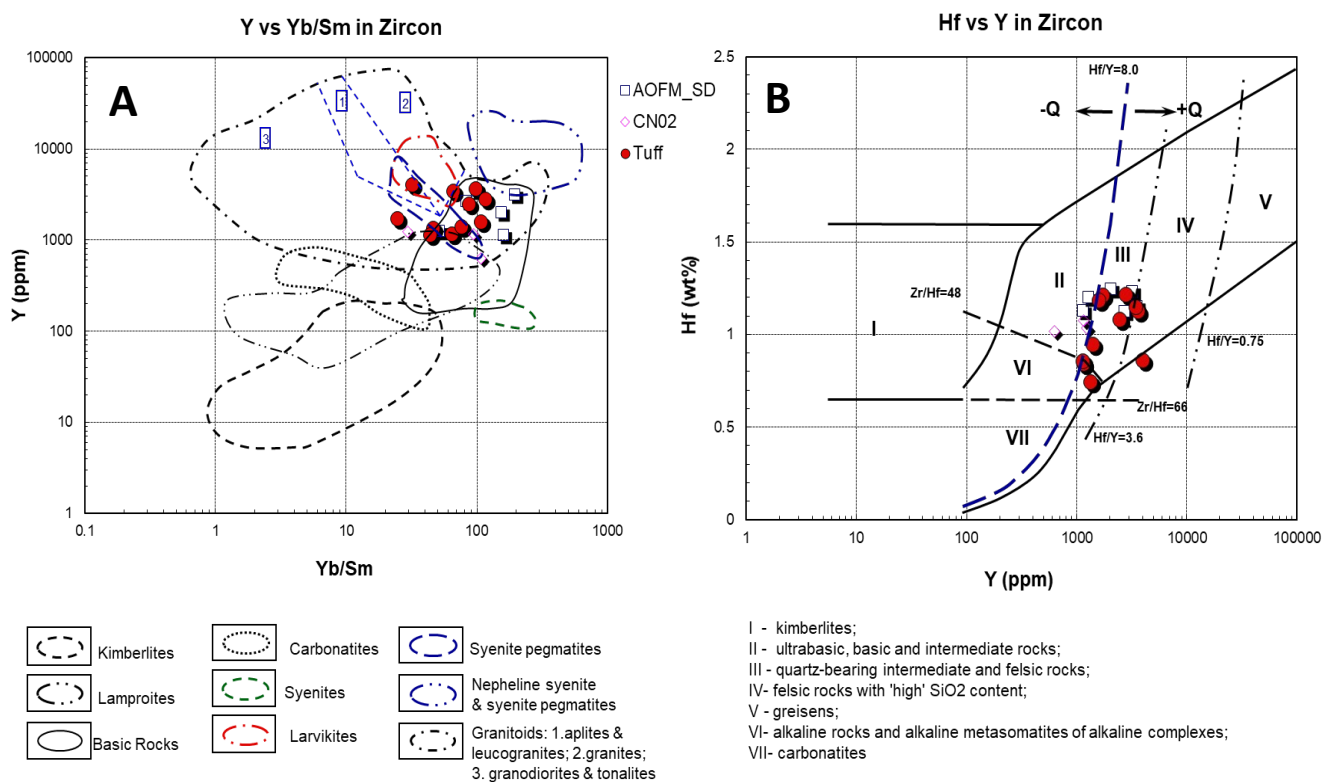


Figure 4.17: **A:** Y (ppm) vs Yb/Sm (ppm) graph and **B:** Hf (wt%) vs Y (ppm) for zircons of youngest age populations from sample CN02 (4 grains), AOFM-SD (6 grains) and AOFM-Tuff1 & 2 (defined as AOFM-Tuff, 11 grains). After Belousova *et al.* (2002).

4.4.3 Hf-isotope composition

Hf-isotope data was acquired only on the youngest zircons in each studied sample (Appendix table A7), as shown by figures 4.8C, 4.10D & 4.12E. This is to provide a deeper understanding of the magmatic provenance of each sample, i.e. the isotopic differentiation of mantle and crustal reservoirs, contributing to the zircons' parental magmas. The $^{176}\text{Hf}/^{177}\text{Hf}$ values of the youngest grains of samples CN02, AOFM-SD and AOFM-Tuff, are provided in figure 4.18. Four zircon grains from AOFM-Tuff sample are shown in blue, three zircons from AOFM-SD in orange and three zircons from CN02 in grey. A trend-line was also calculated using the Excel function (purple line), and defined by all zircons presented in the graph, with an R^2 (coefficient of determination) value of 0.3442. AOFM-Tuff $^{176}\text{Hf}/^{177}\text{Hf}$ values range from 0.282479 to 0.282662, AOFM-SD values range from 0.282376 to 0.282605 and CN02 values range from 0.282315 to 0.282451. The negative and positive ϵHf state of each point is also provided and defined by a plus (green "+") or minus (red "-") symbol. Sample AOFM-Tuff presents 3 negative ϵHf grains ranging from -2.8 to -0.2 and one positive ϵHf grain at 3.7, representing the highest value of all samples studied. Sample AOFM-SD presents 2 negative ϵHf grains at -6.5 and -4.2, and one positive ϵHf grain at 3.7. However, only negative ϵHf grains have been measured in CN02, ranging from -8.6 to -3.8.

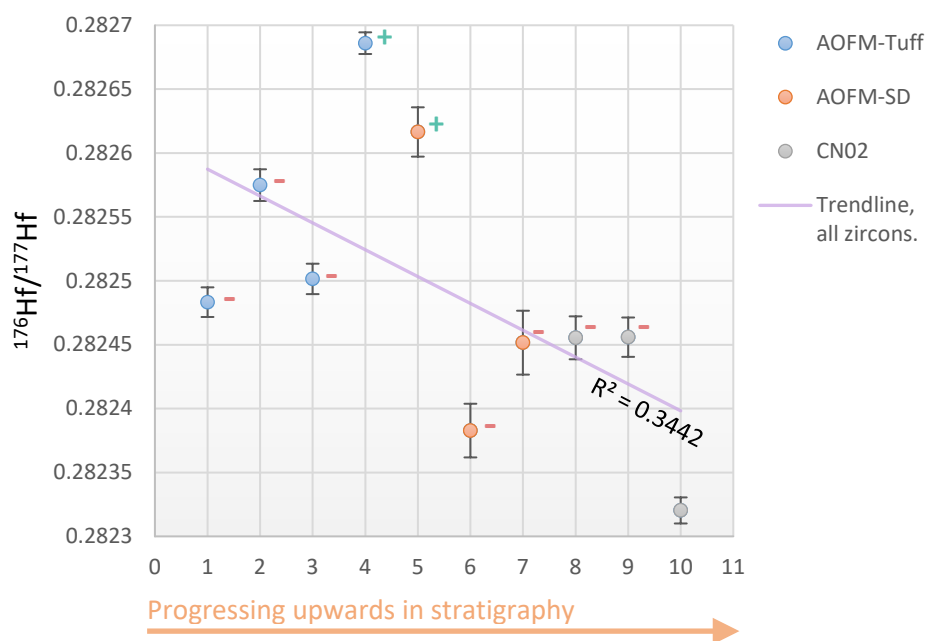


Figure 4.17: $^{176}\text{Hf}/^{177}\text{Hf}$ of youngest zircons of sample CN02 (3 grains), AOFM-SD (3 grains) and AOFM-Tuff1 & 2 (defined as AOFM-Tuff, 4 grains). Trendline with $R^2 = 0.3442$ (coefficient of determination) is shown in purple. Green "+" indicates positive ϵHf values and red "-" indicates negative ϵHf values.

5 Discussion

5.1 Hervey Group

This section provides a recapitulation of the stratigraphy of the Hervey Group based on field and petrographic observations.

5.1.1 Hervey Group stratigraphy and age constraints from previous studies

As previously stated, the Hervey Group is a Late Devonian sedimentary rock unit which lies disconformably above the Rocky Ponds Group in central New South Wales (fig. 2.4; Warren & Watkins, 1998). The Hervey Group is composed of five formations, from base to top as the Kadina, Mandagery, Pipe, Bumberry and Eurow formations. Its age has been assigned entirely to the Late Devonian period (Conolly, 1965a, 1965b; Warren & Watkins, 1998). Formation boundaries within the Hervey Group have been previously defined largely on incoming or outgoing of sandstone-rich packages, which are reflected in changes in topography (Young, 1999; 2000). The positions of these boundaries on the time scale are not well defined, with the main constraints being fish plates and scales, with no published radiometric data. As previously stated, the closest radiogenic date provided in the region is from the Curumbenya Ignimbrite of the mid-Dulladerry Volcanics (Rocky Ponds Group), providing an age of 376 ± 4 Ma (Black, 1996). This suggests the base of the Hervey Group is Frasnian. However, this age is only a personal communication, and was established using the standard SL13 (Warren & Watkins, 1998), which has since been found non-homogeneous and may therefore result in an age 1% too young (Black et al, 2003a). Therefore, the age of the Curumbenya Ignimbrite may be as old as $380 \text{ Ma} \pm 4 \text{ Ma}$ and thus early Frasnian.

5.1.2 Mandagery Formation and age constraints from previous studies

The Canowindra fish site, located in the Manildra-Gooloogong region, lies within the Mandagery Formation (Johanson, 1997). The Mandagery Formation overlies the Kadina Formation and underlies the Pipe Formation near the Canowindra fish locality (Conolly, 1965a & b; Young, 1999). As previously stated, it is a fine to medium-grained white and red sandstone with thin intervals of shale and red and green siltstone (Conolly, 1965a, 1965B). Conolly (1965a) and Pogson & Watkins (1998) recorded the presence of ripple marks, bedding, flow and load casts, as well as scour, slump and fill structures, with the rare occurrences of lenticular beds. Based on those sedimentary structures, Conolly (1965a) and Pogson & Watkins (1998) inferred a depositional environment of a marine regression progressing upwards into a fluvial system.

Consistent with the previous section, the age constraints for the Mandagery Formation, and all other formations of the Hervey Group, are poorly defined. Young (1999, 2000) suggested a Frasnian to Famennian age for the Mandagery Formation based on correlations of fish fauna with other parts of the world, but these age constraints are poor with a lack of radiometric ages.

5.1.3 Mandagery Formation depositional environment from new field and petrographic observations

Sandstones of the Mandagery Formation below and above the fossil fish site crop out for approximately 6km along a ridge north of the fish site (fig.4.1). The consistent presence of fine-grained planar-bedded sandstone on this ridge suggests a low energy system within a shallow water environment, where the sediments were deposited on planar surfaces (based on Reineck and Singh, 1980). The limited presence of bioturbation, observed as irregular ‘bubble-like’ and ‘worm-like’ cavities (fig.4.1A, C, D & E), is consistent with shallow and low energy environment. The lingoid nature of ripples (figure 4.1C), general absence of planar ridge crests, and presence of discontinuous and broken crests, are all similar to what Reineck and Singh (1980) suggested formed in beach or shallow water environments. Only one outcrop of cross beds (planar beds with coset height of 1-2 m) was found on the ridge, about 1km north of the fish site (fig.4.1F). This general absence of cross beds argues against an oft-cited fluvial depositional environment for the Mandagery Formation, either in meandering or braided streams.

5.1.4 Possible depositional environment of the Canowindra fish bed

Samples AOFM-SD and AOFM-Tuff were analysed to observe differences in age and composition, thin sections were made targeting the transition zone between those two samples as shown in figures 4.3 and 4.4. However, as previously stated, no clear differences appear between the two lithologies, both showing similar grain shapes, grain-sizes and distribution of minerals in thin section. Their mineralogy, based on petrographic, XRD (fig.4.6) and BSE (fig.4.3) analyses, is approximately 90-95% quartz plus “floating” mica in a silica and kaolinite cement. A nearshore shallow water environment is consistent with the kaolinitic quartz arenite composition of the fish bed (AOFM-SD & AOFM-Tuff), following the ideas of Khalifa (2017), whose work in Africa suggested the kaolinitic quartz arenite composition (kaolinite cement with primary quartz grains) formed in such an environment.

Petrographic observations and analyses of sample TUFF were made on the thin white layer associated with the fish fossils, shown in figures 4.4 and 4.5. As observed in PPL and XPL (figure 4.4A & B), “TUFF” appears to be a very fine-grained layer (<2 μ m) with no distinct mineral phases observable under a petrological microscope. In BSE images (figure 4.4C, D, & E), rutile and mica grains can be distinguished, but these only represent a small fraction of the thin section (~5-10%), with the exception of a few larger and distinct quartz grains (up to 30 μ m, ~10%). The remainder of the grains appear too

fined-grained ($<2\mu\text{m}$) to distinguish. However, XRD analysis of “TUFF” (figure 4.7) determined a composition with a majority of quartz ($>85\%$), and minor quantities of micas ($<15\%$). This is very similar to the average bulk composition of AOFM-Tuff, with a majority of quartz ($>85\%$) and minor quantities of micas ($<15\%$). However, when compared with NanoMin analysis, TUFF (fig.4.4 & 4.5) shows a very different texture to the fish bed, AOFM fig.4.3), wherein the quartz grains appear to be very fine-grained ($<2\mu\text{m}$), yet micas show similar elongate, grain size and shapes. Kaolinite cement is present throughout TUFF, with a minor presence of K-feldspars ($<2\mu\text{m}$). A short interval of wind-blown material may explain why this thin layer (TUFF, $\sim 1.5\text{cm}$ thick) has a very different texture and grain size (Reineck and Singh, 1980).

Finally, previous studies have suggested the Canowindra fish site stratigraphically lies in the upper part of the Mandagery Formation (e.g. Young, 1999). However, my field work suggests the fish site is in fact located within the lower part of the Mandagery Formation. Using the map in figure 4.1, the fish site lies approximately 60m along the ground west of the lower boundary of the Mandagery Formation. Similarly, the fish site is found at the surface approximately 300m east of the upper boundary, extrapolated through cover from $\sim 1\text{km}$ to the north, in a region of consistent planar strike of 352 and dip of 31° degrees west. Using trigonometry, a total thickness of approximately 180m is determined for the Mandagery Formation at the ridge, with the fish site lying approximately 30m above the base and 150m below the upper boundary.

5.2 Zircon ages and trace-element signatures of younger zircon populations within the Mandagery Formation

5.2.1 Defining the younger populations

In this section, field and laboratory observations are discussed. First, the younger populations and the maximum depositional ages of samples CN02, AOFM-SD and AOFM-Tuff are provided. Then the stratigraphic implications on the Hervey Group, as a result of the maximum depositional ages found within the Mandagery sedimentary sequences, are discussed. Finally, the synthesis of all collected analytical data, as well as the petrographic observations and analyses, of all studied samples, are put into context of the cause for the mass-kill event of the Canowindra fish.

Zircon U/Pb ages obtained from samples CN02 (fig.8a), AOFM-SD (fig.9a) and AOFM-Tuff (fig.10a & b) show a large distribution of ages, ranging from Late Devonian to Late Archean. Given the Hervey Group is younger than 380 Ma (see earlier) all older ages are thought to be reworked from older units or represent a range of supplying provinces (e.g., Glen *et al.*, 2016). The relative probability plots of samples CN02 (fig.4.9), AOFM-SD (fig.4.11) and AOFM-Tuff1 & 2 (fig.4.13) all show similar zircon age distributions, with a distinct Silurian population and a very broad maximum peak at 415-431Ma. The

Lachlan Orogen, in the 415-431Ma time interval, was characterized by major lithospheric extension, resulting in formation of rift basins, rift volcanics and formation of S- and I-type granitic batholiths, (e.g., Glen, 2005; Rosenbaum, 2018). The close similarity in the age distributions between these samples suggests a common source for the three samples of the Mandagery Formation. This project and further discussion, however, will focus on the youngest population to determine the maximum depositional age of the Canowindra fish bed from the Mandagery Formation.

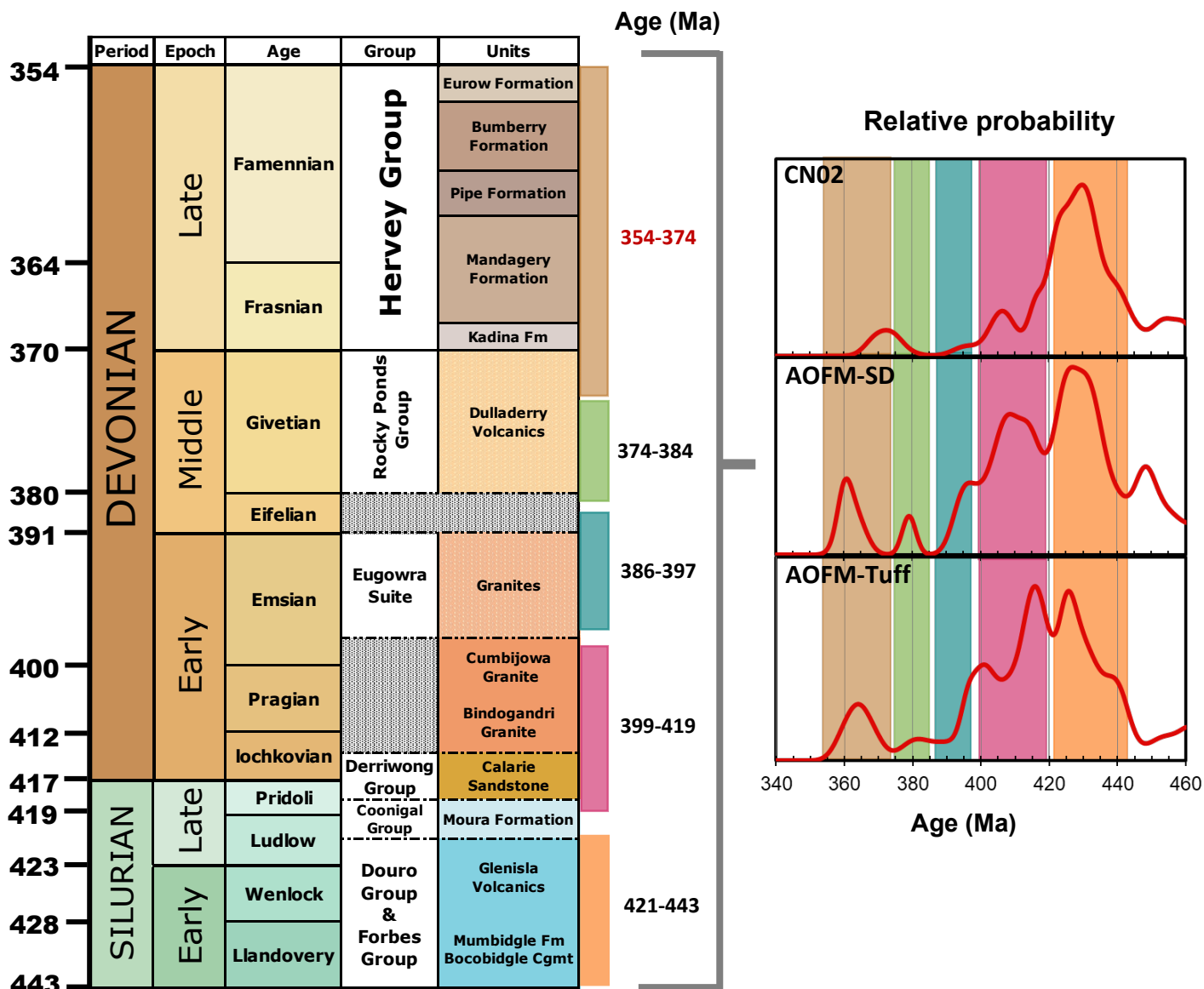


Figure 5.1: Right: Relative probability graph of 340-460Ma U/Pb ages (without the rejected analyses) of sample CN02 (top), AOFM-SD (middle) and AOFM-Tuff (bottom). Coloured bands: Distinct age populations defined by major peaks and compared with the stratigraphy chart (left). Left: Stratigraphy of the Hervey Group at the Manildra-Gooloogong region, as defined by Lyons et al. (2000), Raymond et al. (1998), Raymond et al. (2000a & b) and Young (1999), using the 1999 GSA timescale (GSA, 1999). Dashed lines represent uncertain unit boundaries.

The younger populations of samples CN02, AOFM-SD and AOFM-Tuff, are restricted to 354-444Ma age range (fig.5.1). Within this age range five major age populations have been recognised according to the major peaks on the relative probability plots. Each age population in figure 5.1 are assigned a coloured band, shown across all relative probability plots and also along the stratigraphy chart. The most prominent, and oldest, peak, observable in all three samples, occurs at 425-430Ma (late Wenlock to early Ludlow) and occurs within the orange band. During the late Wenlock to early Ludlow, the closest volcanic activity to Canowindra are the Glenisla Volcanics (figure 5.1), which crops out sporadically from Grenfell and north along the Coolac-Narromine fault (Wallace & Raymond, 2000). As well as the Canowindra Volcanics, which crops out from 18km south of Cowra, through Canowindra, and all the way to Cudal (Powell, 1984; Krynen *et al.*, 1998), and granites (Glen *et al.*, 2016). With reference solely to the age, the Glenisla and Canowindra Volcanics could provide possible local sources for these zircons. The following peak, defined by the pink band, occurs at 407-414Ma, which is particularly distinct in AOFM-SD and AOFM-Tuff, with a much smaller, yet clear, peak in the CN02 sample. Around 407-414Ma, the Cowra region was characterized by major granitic intrusions, with the closest ones being the S-type Bindogandri and the I-type Cumbijowa Granites. These have been suggested to be of Early to Middle Devonian age (Raymond *et al.*, 2000a & b). The next population, defined by the blue band shows a variable peak at 396Ma, clear in AOFM-SD and AOFM-Tuff, and weak in CN02, which could have also originated from the Eugowra Suite and the Dulladerry Volcanics. The next peak, defined by the green band, is distinct in AOFM-SD, weak in AOFM-Tuff and ambiguous in CN02 at 380Ma, with a close age to the suggested 376 ± 4 Ma obtained from the middle flow band of the Dulladerry Volcanics (Black, 1996).

The last and youngest zircon population, 354-374Ma, defined by the brown band, shows our best estimates for the maximum deposition ages for each of the three samples: 372 ± 1.8 Ma (MSWD = 1.7; fig.8C) for CN02, 361.2 ± 2.9 Ma (mean with MSDW = 0.62; fig.9D) for AOFM-SD and 363.0 ± 3.1 Ma (MSDW = 0.52) for AOFM-Tuff. No felsic volcanic activity, however, has been recorded within this age interval in NSW (Lyons *et al.*, 2000; Pogson & Watkins, 1998, Powell, 1984). However, ~360 Ma granites have been recorded in Victoria (VandenBerg *et al.*, 2000), and could provide a possible source for these 354-374Ma zircons.

As previously stated, CN02 comes from a bed about 10m above the Canowindra fish site (AOFM-SD and AOFM-Tuff), yet the maximum depositional age obtained from CN02 is the oldest age found in all three samples. However, this age defined for CN02 may be due to statistical reasons such as a lack of youngest zircon grains mounted or selected for analysis, as well as the possible unfortunate circumstance of not having picked and mounted youngest grains. Nevertheless, the maximum deposition ages obtained from AOFM-SD and AOFM-Tuff correlate stratigraphically, where AOFM-SD (361.2 ± 2.9 Ma) and

AOFM-Tuff ($363.0 \pm 3.1\text{Ma}$), which have been separated from the same fish bed sample, provide equivalent radiogenic ages within analytical uncertainty.

5.2.2 Defining the maximum depositional age for the Canowindra fish bed

Having been collected directly from the sedimentary sequence in which the Canowindra fossil fish were embedded, the maximum depositional age of AOFM-Tuff provides the best estimate for the maximum age of the mass-kill event of the Canowindra fish. Therefore, the oldest timing of the mass-kill event of the Canowindra fish bed would be $363.5 \pm 1.5\text{Ma}$, suggesting a mid-Famennian (Late Devonian) age for the Canowindra fish fauna.

5.2.3 Zircon trace-element signatures

REE distribution of studied grains (fig.4.14) are typical of zircons of both continental and oceanic origin (Belousova *et al.*, 2002; Grimes *et al.*, 2007). For CN02 trace elements, a more continental crust provenance is suggested, whereas AOFM-SD and AOFM-Tuff appear to span throughout the continental and oceanic crust fields (fig.4.14 & 4.15) according to Grimes *et al.* (2007). The same pattern appears in the chondrite-normalized REE graph of the youngest population of each sample, shown in figure 4.16. However, according to Belousova *et al.* (2002) the youngest population of each sample (CN02, AOFM-SD and AOFM-Tuff) suggests a granitic and/or intermediate parental rock composition with no distinct separation between samples (fig.4.17).

5.2.4 Zircon Hf-isotope composition

The $^{176}\text{Hf}/^{177}\text{Hf}$ ratios of zircons from the youngest populations of studied samples, presented in figure 4.18, shows a decrease in $^{176}\text{Hf}/^{177}\text{Hf}$ values while progressing upwards in stratigraphy from AOFM-Tuff to AOFM-SD to CN02, which according to Griffin *et al.* (2004), suggests an increase in crustal reworking. While only two positive ϵHf are present, with the highest value of 3.7 from AOFM-Tuff ($363 \pm 8\text{Ma}$) and the second point of 1.6 from AOFM-SD ($364 \pm 6\text{Ma}$), reflecting a possible contribution of more mantle derived zircons (Griffin *et al.*, 2004), which may be more related to rifting magmatism at the time ($\sim 360\text{Ma}$). A wide range in zircon Hf-isotope composition can reflect a range of sources varying from S-type magmas or contractional/collisional related magmatism to I-type magmas or magmatism related to extensional tectonic episodes (Kemp *et al.*, 2009).

5.3 Implications of the new geochronological data and maximum depositional ages for the Hervey Group timescale

The Formation boundaries in the Hervey Group are not well defined by radiometric ages (Conolly, 1963; 1965a; 1965b; Lyons *et al.*, 2000; Pogson & Watkins, 1998; Raymond *et al.*, 1998; Young, 1999). The 2019 International Commission on Stratigraphy time scale (Cohen *et al.*, 2013 updated, Appendix fig.A2) shows very different radiometric ages in the Middle to Late Devonian than the 1999 geological timescale (GSA, 1999, Appendix fig.A1) existent when the mapping was carried out in the Forbes and Bathurst

regions (Lyons *et al.*, 2000; Pogson & Watkins, 1998). For example, the range of the Middle Devonian had changed from 370-391Ma to 382-393Ma, and the range of Late Devonian changed from 354-370Ma to 359-382Ma (GSA, 1999; Cohen *et al.*, 2013 updated). On the 1999 time scale the Mandagery Formation was inferred to range from Frasnian to Famennian, ~ 360 to 368Ma (Conolly, 1965a; 1965b; Lyons *et al.*, 2000; Pogson & Watkins, 1998; Raymond *et al.*, 1998; Young, 1999). My new age data suggest a maximum depositional age of 363 ± 3.1 Ma for the Canowindra fish site, located in the lower part of the Mandagery Formation. This now puts this Formation in the Middle to Upper part of the Famennian. Figure 5.2 presents a new Hervey Group timescale according to the current geological timescale (ICS, 2019) and the maximum depositional age obtained for the Canowindra fish bed (363 ± 3.1 Ma).

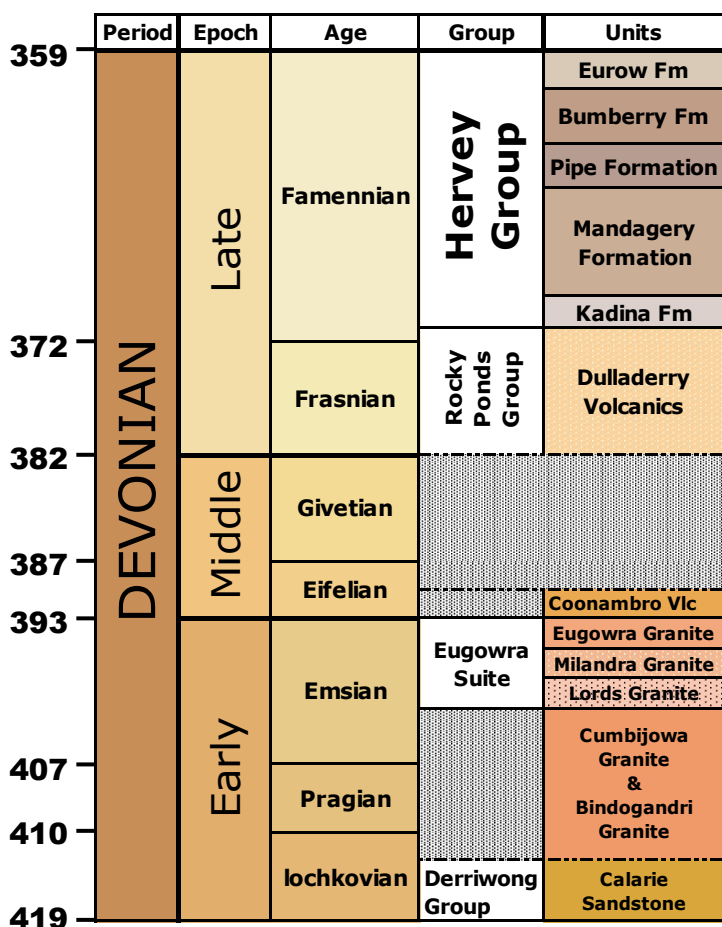


Figure 5.2: New geological timescale of the Hervey Group at the Manildra-Gooloogong region, according to the current geological timescale (ICS, 2019) and the maximum depositional age obtained for the Canowindra fish bed (363 ± 3.1 Ma). Units below the Mandagery Formation defined by Lyons *et al.* (2000), Raymond *et al.* (1998), Raymond *et al.* (2000a & b) and Young (1999). Dashed lines represent uncertain unit boundaries.

5.4 Models for the cause of the mass-kill event of the Canowindra fish

5.4.1 Putative model from previous studies

A current general consensus from previous studies on the cause of the mass-kill event of the Canowindra fish fauna suggests a mass-kill event caused by the trapping of this fish community in a large water body, which dried and shrunk due to strong drought events. This model suggested a fluvial environment where in the event of drought, a billabong was formed, trapping a large quantity of placoderm fish, which eventually died due to the continuing drought (Johanson 1995, 1997; Johanson & Ahlberg, 1997; Young 1999). The presence of cross-beds in the fish site area were suggested in previous studies (Conolly, 1965a; Pogson & Watkins, 1998), however, our new field observations indicate a general lack of cross-beds in the area, thus questioning a fluvial environment. This, combined with petrographic observations and the kaolinitic quartz arenite composition of the fish bed, may suggest a marine-regression depositional environment (Khalifa, 2017).

Furthermore, as suggested by Long (2010), *Remigolepis* and *Bothreolepis* fish, representing the majority of the Canowindra fish fauna, have lived in shallow marine environment. However, these type of fish is mostly found fossilised in freshwater deposits, where they would feed and possibly come to die. Another remarkable Lagerstätte of placoderm fossils located in Western Australia, known as the Gogo fish from the Gogo Formation, was also extensively studied by Long (2010; Long *et al.*, 2006). In his study of the Gogo fish fauna, Long (2010) found the fish fossils also lie within a marine deposit, with a similar suggested time of death at ~360Ma. Yet, the cause of death of the Gogo fish also remains uncertain (Long, 2010). This study suggests a new model for the cause of death of the Canowindra fish fauna, wherein the age and the depositional environment of the Canowindra fish fauna could be associated to a global mass-extinction in the Frasnian-Famennian stages.

5.4.2 New model: Frasnian-Famennian mass-extinction event

In this section, a new model is proposed for the timing and indirect cause of the mass-kill event of the Canowindra fish fauna. Due to a lack of palaeontological description on the biology of the fish and its possible habitats, our new model is purely constrained by geological information. This new model suggests the Canowindra fish mass-kill event is associated with a world-wide Frasnian-Famennian mass-extinction, a succession of short time mass-extinction episodes also known as the Kellwasser events, when 70-82% of organisms became extinct (George *et al.*, 2014; Barash, 2016; Long & Gordon, 2004; Percival *et al.*, 2018, Ricci *et al.*, 2013). Among these organisms, up to about 90% of phytoplankton, as we know of today in the oceans, were lost, the surface area of reefs was reduced by a factor of about 5000, which may be an indication in an increase in temperature (Sallan & Coates, 2010). A major decline in placoderms was also observed (Long & Gordon, 2004). This Late Devonian extinction is recognised as

one of the Phanerozoic “Big Five” mass-extinction event, and its cause has long been debated (George *et al.*, 2014; Percival *et al.*, 2018). However, recent studies are suggesting a set of interrelated factors, with the major factors including volcanism, sea-level change, widespread marine anoxia, tectonism, climatic and/or temperature changes, as well as impact craters, could be external triggers to the Frasnian-Famennian mass-extinction (George *et al.*, 2014; Barash, 2016; Percival *et al.*, 2018).

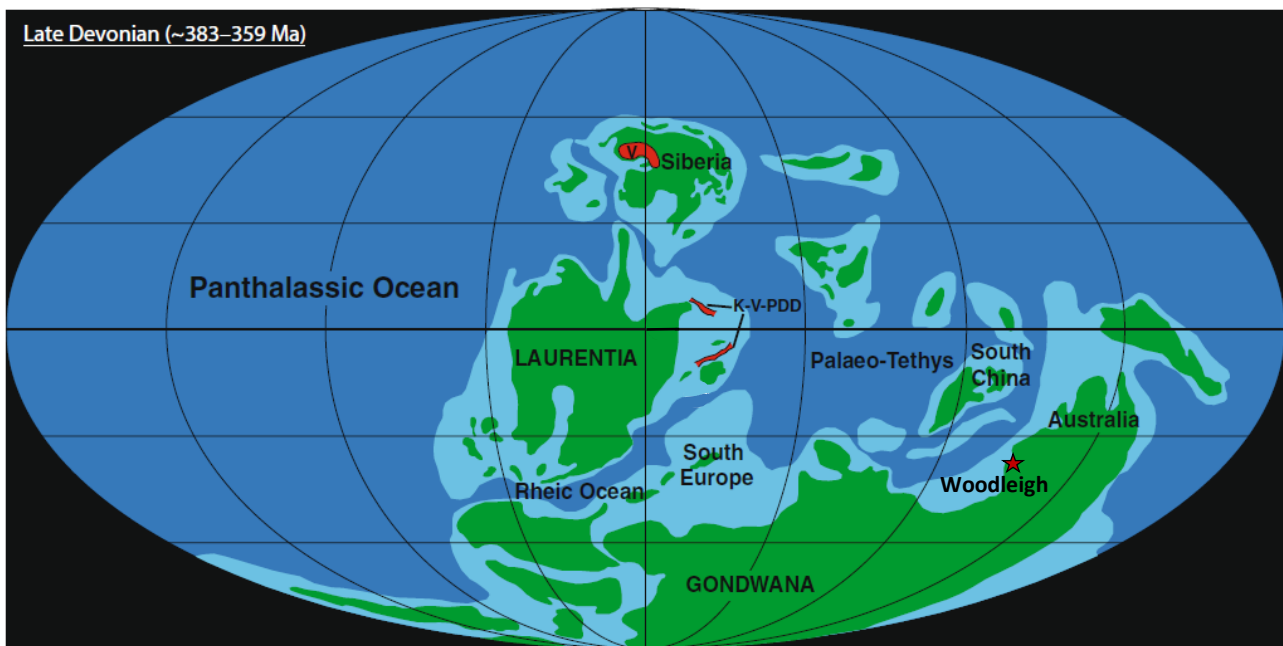


Figure 5.3: Palaeo-reconstructions and location of the Viluy Traps (V), rift systems Kola, Vyatka, and Pripyat-Dniepr-Donets (K-V-PDD) and the Woodleigh crater (red star), in the Late Devonian. Adapted from Percival *et al.* (2018).

Most studies have suggested the Frasnian-Famennian mass-extinction is best associated with large-scale volcanic activity, impact craters and oceanic anoxia (Barash, 2016; Percival *et al.*, 2018). Indeed, the Frasnian-Famennian stages coincide with a large volcanic emplacement in eastern Serbia, known as the Viluy Traps (fig.5.3), a Large Igneous Province (LIP), which is suggested to have produced over 1Mkm³ of basalts (Barash, 2016; Percival *et al.*, 2018). At the same time, Percival *et al.* (2018) also suggest a possible additional emplacement of 1Mkm³ basalts from rift systems Kola, Vyatka, and Pripyat-Dniepr-Donets (K-V-PDD), located in Eastern Europe. Figure 5.3 shows the palaeo-reconstructions and location of those areas in the Late Devonian. Two major pulses from the Viluy Traps have been found, with the first pulse dated at 376.7 ± 1.7 Ma and a second major pulse at 364.4 ± 1.7 Ma (Barash, 2016; Percival *et al.*, 2018; Ricci *et al.*, 2013).

Here, the timing of the second pulse coincides with maximum depositional ages defined for samples AOFM-SD ($361.2 \pm 2.9\text{Ma}$) and AOFM-Tuff ($363.0 \pm 3.1\text{Ma}$) from the Canowindra fish bed with analytical uncertainty. In addition, some global studies have suggested the Late Devonian was also characterised by a sudden succession of impact craters, such as the Woodleigh crater (fig.5.3), a 120km impact in the western coast of Australia, with an estimated age of $364 \pm 8\text{ Ma}$ (Barash, 2016). This event could have largely affected biodiversity as well as contributed to a climatic and/or temperature change due to ejected material. Studies have also observed sea-level rise and falls throughout the Frasnian-Famennian extinction. In particular, George *et al.* (2014) suggested a major sea-level fall in the mid-Famennian ($\sim 365\text{Ma}$) in their work on the Virgin Hills Formation, overlying the Gogo Formation (Western Australia). This agrees well with the petrographic and field observations provided in this study, suggesting a marine regression and thus shallow marine environment.

However, no anoxic event has yet been found or suggested in Australia, with one study having been published on oxic facies from the Canning Basin in Western Australia, suggesting anoxia was not the main cause for the mass-extinction event but instead the correlated timing of large-scale volcanism, tectonism, impact craters, sea-level changes and anoxia could have resulted in major changes of temperature, climate and oxygen levels throughout the Earth, affecting all types of biodiversities (George *et al.*, 2014).

With reference to the Canowindra fish bed maximum depositional age ($363.0 \pm 3.1\text{Ma}$), petrographic and field observations presented in this study, and its correlation with the timing of volcanism, impact crater and sea-level change presented above, this study suggests the mass-kill event of the Canowindra fish fauna may be associated with the Frasnian-Famennian extinction events. Wherein a lack of food, oxygen, and/or UV radiation, and/or an increase in gas emission, greenhouse effect and/or anoxia could have been the cause of death of the Canowindra fish fauna. Figure 5.4, created by Barash (2016), presents a summary diagram of all the suggested interrelated factors which could have led to the extinction of different faunas during the Frasnian-Famennian mass extinction.

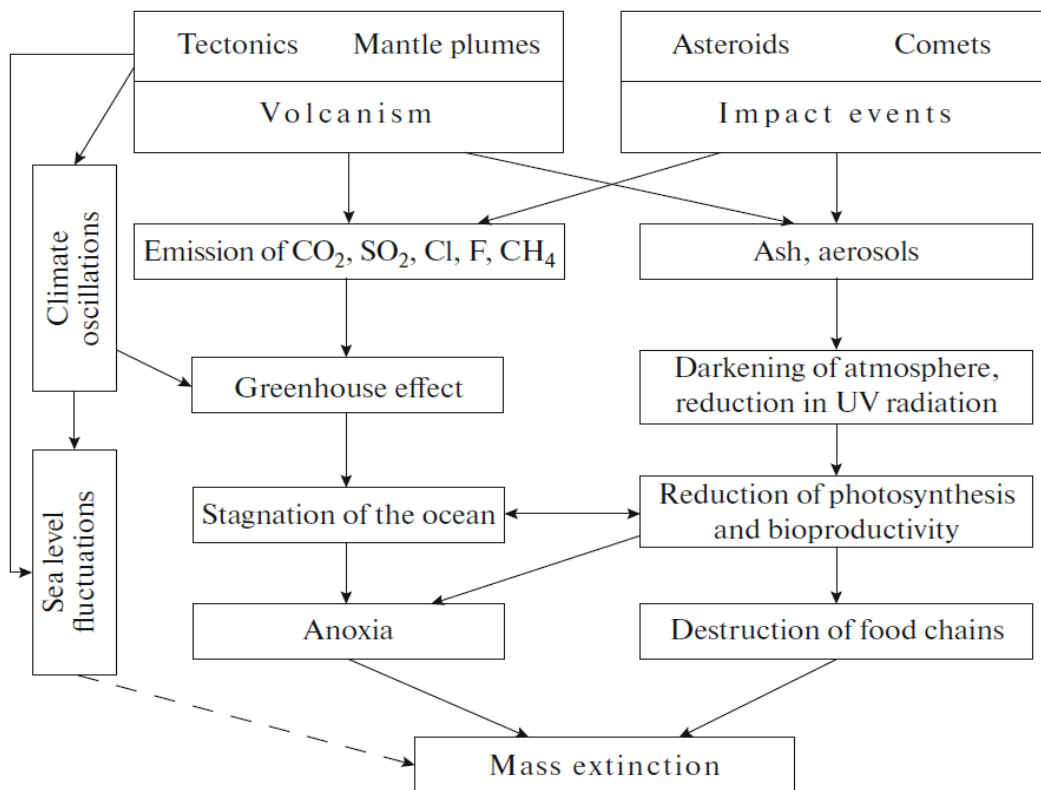


Figure 5.4: Summary diagram of all suggested interrelated factors which could have led to the extinction of different faunas during the Frasnian-Famennian mass-extinction. From Barash (2016).

6 Conclusion

Placoderms, armoured fish, are recognised as the most diverse group of fish in the Devonian period and were found throughout the world in both marine and freshwater environments. Fossil records show placoderms occur from Early Silurian to the Late Devonian, yet completely disappear from the fossil record at the Devonian-Carboniferous boundary. However, the cause of the sudden extinction remains uncertain. The Canowindra fish bed of the Mandagery Formation, is a remarkable Lagerstätte of placoderm fish, first discovered in 1956 and excavated in 1993. The timing and cause of death, however, also remained uncertain.

Using field observations, petrography and zircon analysis, this work presented a detailed study of the depositional environment of the Mandagery Formation at and around the fish locality, including the stratigraphic position of the fish assemblage within the unit, and new evidence for the cause and time of death of the Canowindra fish fauna.

Firstly, this study suggests the Canowindra fish bed was deposited in a shallow marine environment, as opposed to a generally, previously suggested fluvial environment. Secondly, field observations suggest that the fish assemblage lies within the lower rather than the upper part of the Mandagery Formation. Thirdly, zircon U/Pb radiometric dating presents a maximum depositional age of 363 ± 3.1 Ma for the Canowindra fish bed. Using the ICS (Cohen *et al.*, 2013 updated) time scale, this study suggests that the Mandagery Formation is Famennian rather than lower Famennian to Frasnian, thereby modifying inferred ages for the lower part of Mandagery Formation.

This thesis also tentatively proposes a new model for the cause of death of the Canowindra fish fauna. New age data suggest that the timing and cause of fish death at Canowindra may be associated with the world-wide Frasnian-Famennian mass-extinction event. However, despite this, the specific cause of death can only be guessed at and this thesis tentatively suggests that one possible cause might have been the introduction of possibly windblown fine-grained muddy unit (TUFF, fig.4.4 & 4.5) that quickly asphyxiated the fish.

However, further work on the palaeontology and biology of the Canowindra fish fauna, along with more detailed geological data, may be required to this and any other theory. As such, this project may act as a pilot study for further work in understanding the cause of the global extinction of placoderms towards the Devonian-Carboniferous boundary.

References

- Abbott, A.N., Löhr, S., & Trethewey, M., 2019. Are clay minerals the primary control on the oceanic rare earth element budget? *Frontiers in Marine Science*, 6:19.
- Age of Fishes Museum, 2019a. *Bothriolepis yeungae*. Visited: 10/08/2019: <http://www.ageoffishes.org.au/bothriolepis-yeungae.html>
- Age of Fishes Museum, 2019b. *Remigolepis walker*. Visited: 10/08/2019: <http://www.ageoffishes.org.au/remigolepis-walkeri.html>
- Age of Fishes Museum, 2013. David Attenborough visits Canowindra's fish fossils. Visited: 10/01/2019: <http://www.ageoffishes.org.au/index.html>.
- Andersen, T., 2002. Correction of common Pb in U–Pb analyses that do not report ^{204}Pb . *Chemical Geology*, 192:59–79.
- Australian Age of Dinosaurs Inc. 2006. Australian age of dinosaurs: the annual publication of Australian Age of Dinosaurs Inc., Winton, Queensland, Australia. *Australian Age of Dinosaurs Inc, Winton, Qld*.
- Belousova, E.A., Griffin, W.L., Shee, S.R., Jackson, S.E., O'Reilly, S.Y., 2002. Two age populations of zircons from the Timber Creek kimberlites, Northern Territory, as determined by laser-ablation ICP-MS analysis. *Australian Journal of Earth Sciences*, 48:757–765.
- Belousova, E., Reid, A., Griffin, W., & O'reilly, S., 2009. Rejuvenation vs. recycling of Archean crust in the Gawler Craton, South Australia: Evidence from U–Pb and Hf isotopes in detrital zircon. *LITHOS*, 113(3-4):570-582.
- Barash, M.S., 2016. Causes of the great mass extinction of marine organisms in the Late Devonian. *Oceanology*, 56(6):863-875.
- Black L.P. 1996. SHRIMP zircon U/Pb dating of samples from the Bathurst 1:250 000 map sheet area. Geological Survey of New South Wales, File GS1996/527 (unpublished).
- Black, L.P., Gulson, B.L., 1978. The age of the Mud Tank carbonatite, Strangways Range, Northern Territory. *Bureau of Mineral Resources. Journal of Australian Geology and Geophysics*, 3:227–232.
- Black, L., Kamo, S., Williams, I., Mundil, R., Davis, D., Korsch, R., & Foudoulis, C., 2003a. The application of SHRIMP to Phanerozoic geochronology; a critical appraisal of four zircon standards. *Chemical Geology*, 200(1), 171-188.
- Black, L., Kamo, S., Allen, C., Aleinikoff, J., Davis, D., Korsch, R., & Foudoulis, C. 2003b. TEMORA 1: A new zircon standard for Phanerozoic U–Pb geochronology. *Chemical Geology*, 200(1):155-170.
- Campbel, K.S.W., and Bell, M.W., 1982. *Soederberghia* (Dipnoi) from the Late Devonian of New South Wales. *Alcheringa* 6:143-149.
- Cohen, K.M., Finney, S.C., Gibbards, P.L. & Fan, J.X., 2013, updated. *The ICS International Chronostratigraphic Chart*. 36:199-204.

- Conolly, J., 1963. Upper Devonian Stratigraphy and Sedimentation in the Wellington-Molong District, N.S.W. *Royal Society of New South Wales, Journal and Proceedings*, 96(2):73–106.
- Conolly, J., 1965a. The stratigraphy of the Hervey Group in central New South Wales. *Journal and Proceedings, Royal Society of New South Wales* 98:37-83.
- Connolly, J.R., 1965b. Petrology and origin of the Hervey group, upper Devonian, central New South Wales. *Journal of the Geological Society of Australia*, 12:123–164.
- Conolly, J., Hall L.R. and Rose G. 1969. Upper Devonian Series. Packham GH (ed.), *The Geology of New South Wales. Journal of the Geological Society of Australia* 16:150-178.
- Dawson, M.W. & Glen, R.A., 2006. Eastern Subprovince of the Lachlan Orogen – Solid geology and mineral deposits, 1:500 000 map. *New South Wales Department of Primary Industries*.
- Elhlou, S., Belousova, E.A., Griffin, W.L., Pearson, N.J., O'Reilly, S.Y., 2006. Trace element and isotopic composition of GJ red zircon standard by laser ablation. Conference Abstract. *Geochimica et Cosmochimica Acta*, 70(18): A158.
- Fergusson, C.L., Henderson, R.A. & Offler, R., 2017. Late Neoproterozoic to early Mesozoic sedimentary rocks of the Tasmanides, eastern Australia: provenance switching associated with development of the East Gondwana active margin. In: R. Mazumder (Ed.), *Sediment Provenance: Influences on Compositional Change from Source to Sink* (pp.325-369). *Netherlands: Elsevier*.
- Fialips, C.I., Labeyrie, B., Burg, V., Mazière, V., Munerel, Y., Haurie, H., Jolivet, I., Lasnel, R., Laurent, J., Lambert, L. & Jacquelin-Vallée, L., 2018. Quantitative Mineralogy of Vaca Muerta and Alum Shales from Core Chips and Drill Cuttings by Calibrated SEM-EDS Mineralogical Mapping. *Unconventional Resources Technology Conference*.
- Fletcher, H.O., 1956. Ancient armoured fishes discovered at Canowindra, NSW. *Australian Museum Magazine* 12:87-105.
- Foster, D.A. & Gray, D.R., 2000. Evolution and Structure of the Lachlan Fold Belt (Orogen) of Eastern Australia. *Annual Review of Earth and Planetary Sciences*, 28(1): 47–80.
- Geological Society of America, 1999. 1999 Geologic Time Scale. *Geological Society of America*.
- George, A.D., Chow, N. & Trinajstić, K.M., 2014. Oxic facies and the Late Devonian mass extinction, Canning Basin, Australia. *Geology*, 42(4):327–330.
- Glen, R.A., 1998. 'Structural Geology'. In: Pogson D.J. & Watkins J.J., 1998. Bathurst 1:250 000 Geological Sheet SI/55-8: Explanatory Notes. Geological Survey of New South Wales, Sydney, xiv + 430 pp.
- Glen, R.A., 2005. The Tasmanides of eastern Australia. *Geological Society Special Publication* 246(1):23-96.
- Glen, R.A., 2013. Refining accretionary orogen models for the Tasmanides of eastern Australia. *Australian Journal of Earth Sciences: An International Geoscience Journal of the Geological Society of Australia* 60(3):315-370.
- Glen, R.A., Belousova, E. & Griffin, W. L., 2016. Department of Earth Planetary Sciences. Different styles of modern and ancient non-collisional orogens and implications for crustal growth : A Gondwanaland perspective. *Canadian Journal of Earth Sciences*, 53(11):1372-1415.

- Glen, R.A., Korsch, R.J., Direen, N., Jones, L.E.A., Johnstone, D., Lawrie, K.C., Finlayson, D.M., Shaw, R., 2002. Crustal structure of the Ordovician Macquarie Arc, Eastern Lachlan Orogen, based on seismic-reflection profiling. *Australian Journal of Earth Sciences* 49(2):323-348.
- Gray, D.R. & Foster, D.A., 2004. Tectonic evolution of the Lachlan Orogen, southeast Australia; historical review, data synthesis and modern perspectives. *Australian Journal of Earth Sciences* 51(6):773-817.
- Griffin, W.L., Pearson, N.J., Belousova, E.A., Jackson, S.R., van Achtebergh, E., O'Reilly, S.Y. & Shee, S.R., 2000. The Hf isotope composition of cratonic mantle: LAM-MC-ICPMS analysis of zircon megacrysts in kimberlites. *Geochimica et Cosmochimica Acta*, 64:133–147.
- Griffin, W.L., Belousova, E.A., Shee, S.R., Pearson, N.J., O'Reilly, S.Y., 2004. Archean crustal evolution in the northern Yilgarn Craton: U–Pb and Hf-isotope evidence from detrital zircons. *Precambrian Research*, 131:231–282.
- Griffin, W.L., Belousova, E.A., Walters, S.G. and O'Reilly, S.Y., 2006. Archaean and Proterozoic crustal evolution in the Eastern Succession of the Mt Isa district, Australia: U – Pb and Hf-isotope studies of detrital zircons. *Australian Journal of Earth Sciences* 53:125-149.
- Grimes, C.B., John, B.E., Kelemen, P.B., Mazdab, F.K., Wooden, J.L., Cheadle, M.J., Hanghoj, K., and Schwartz, J.J., 2007. Trace element chemistry of zircons from oceanic crust: A method for distinguishing detrital zircon provenance. *Geology*, 35(7):643-646.
- Jackson, S.E., Pearson, N.J., Griffin, W.L., Belousova, E.A., 2004. The application of laser ablation-inductively coupled plasma-mass spectrometry to in situ U–Pb zircon geochronology. *Chemical Geology*, 211: 47–69.
- Johanson, Z., 1995. New informations on jaw elements of *Remigolepis* (Placodermi; Antiarchi) from Canowindra, NSW, Australia (Upper Devonian). *Geobios* 28:103-107.
- Johanson, Z., 1997. New *Remigolepis* (Placodermi; Antiarchi) from Canowindra, New South Wales, Australia. *Geological Magazine* 134(6):813-846.
- Johanson, Z. & Ahlberg, P., 1997. A new tristichopterid (Osteolepiformes: Sarcopterygii) from the Mandagery Sandstone (Late Devonian, Famennian) near Canowindra, NSW, Australia. *Transactions Of The Royal Society Of Edinburgh-Earth Sciences* 88:39–68.
- Kemp, A.I.S., Wormald, R.J., Whitehouse, M.J. & Price, R.C., 2005. Hf isotopes in zircon reveal contrasting sources and crystallization histories for alkaline to peralkaline granites of Temora, southeastern Australia. *Geology*, 33(10):797-800.
- Kemp, A., Hawkesworth, C., Collins, W., Gray, C., & Blevin, P., 2009. Isotopic evidence for rapid continental growth in an extensional accretionary orogen: The Tasmanides, eastern Australia. *Earth and Planetary Science Letters*, 284(3):455-466.
- Khalifa, M.A., 2017. General characteristics of quartz arenite types and their role in the recognition of sequence stratigraphic boundaries in ancient coastal and near shore sediments. A case study from Egypt and Saudi Arabia. *Journal of African Earth Sciences*, 130:274-292.

- Krynen, J., Pogson, D.J. and Watkins, J.J. 1998. 'Canowindra Volcanics'. In: Pogson D.J. & Watkins J.J., 1998. Bathurst 1:250 000 Geological Sheet SI/55-8: Explanatory Notes. *Geological Survey of New South Wales*, Sydney, xiv + 430 pp.
- Long, J., 1995. The rise of fishes: 500 million years of evolution, *New South Wales University Press*, Kensington, N.S.W.
- Long, J., 2010. The rise of fishes: 500 million years of evolution, 2nd ed, *University of New South Wales Press Pty Ltd*, Sydney, N.S.W.
- Long, J., & Gordon, M., 2004. The Greatest Step in Vertebrate History: A Paleobiological Review of the Fish-Tetrapod Transition *. *Physiological and Biochemical Zoology: Ecological and Evolutionary Approaches*, 77(5):700–719.
- Long, J., Young, G.C., Holland, T., Senden, T.J., & Fitzgerald, E.M.G., 2006. An exceptional Devonian fish from Australia sheds light on tetrapod origins. *Nature*, 444(7116):203–207.
- Long, J., Trinajstić K., Young, G.C. & Senden, T., 2008. Live birth in the Devonian period. *Nature*, 453(7195):650-653.
- Ludwig, K.R., 2008. Isoplot 3.70 —A Geochronological Toolkit for Microsoft Excel, Berkeley Geochronology Centre Special Publication No. 4, Berkeley, California.
- Lyons, P., Raymond, O.L. & Duggan, M.B., 2000. Forbes 1:250 000 Geological Sheet S155-7 (2nd edition) Explanatory Notes. *Australian Geological Survey Organisation Record*, 20:80-82.
- Percival, L., Davies, J., Schaltegger, U., De Vleeschouwer, D., Da Silva, A., & Föllmi, K., 2018. Precisely dating the Frasnian-Famennian boundary: Implications for the cause of the Late Devonian mass extinction. *Scientific Reports*, 8(1):9578.
- Pogson, D.J. & Watkins, J.J., 1998. Bathurst 1:250 000 Geological Sheet SI/55-8: Explanatory Notes. Geological Survey of New South Wales, Sydney, xiv + 430 pp.
- Powell, C., M.C.A., 1984. 'Silurian to mid-Devonian - a dextral transtensional margin'. In: Veevers J. J. ed. *Phanerozoic Earth History of Australia*, pp. 309–329, Oxford Science Publications, Oxford.
- Raymond, O.L. and Pogson, D.J., et al, 1998. Bathurst 1:250 000 Geological Sheet SI/55-08, 2nd edition, *Geological Survey of New South Wales*, Sydney.
- Raymond, O.L., Sherwin, L., Wallace, D.A., Wyborn, D., Young, G.C. and Percival, I.G., 2000a, Parkes 1:100 000 Geological Sheet 8531, 1st edition. Geological Survey of New South Wales, Sydney & Geoscience Australia
- Raymond, O.L., Duggan, M.B., Lyons, P., Scott, M.M., Sherwin, L., Wallace, D.A., Krynen, J.P., Young, G.C., Wyborn, D., Glen, R.A., Percival, I.G. and Leys, M., 2000b. Forbes 1:250 000 Geological Sheet SI/55-07, 2nd edition, *Geological Survey of New South Wales*, Sydney.
- Reineck, H.E. & Singh, I.B., 1980. *Depositional sedimentary environments, with reference to terrigenous clastics* / H.-E. Reineck, I.B. Singh. 2nd, rev. and updated., Berlin; New York: Springer-Verlag.
- Ricci, J., Quidelleur, X., Pavlov, V., Orlov, S., Shatsillo, A. & Courtillot, V., 2013. New ⁴⁰Ar/³⁹Ar and K–Ar ages of the Viluy traps (Eastern Siberia): Further evidence for a relationship with the

- Frasnian–Famennian mass extinction. *Palaeogeography, Palaeoclimatology, Palaeoecology*, 386(C):531-540.
- Rosenbaum, G. 2018. The Tasmanides: Phanerozoic Tectonic Evolution of Eastern Australia. *Annual Review of Earth and Planetary Sciences*, 46:291-325.
- Sallan, L.C. & Coates., M.I., 2010. End-Devonian extinction and a bottleneck in the early evolution of modern jawed vertebrates. *Proceedings of the National Academy of Sciences*, 107(22):10131-10135.
- Thomson, K.S., 1973. Observations on a new rhipidistian fish from the Upper Devonian of Australia. *Palaeontographica* A143:209-220.
- VandenBerg, A.H.M., Willman, C.E., Maher, S., Simons, B.A., Cayley, R.A., Taylor, D.H., Morand, V.J., Moore, D.H. & Radojkovic, A., 2000. The Tasman Fold Belt System in Victoria. *Geological Survey of Victoria Special Publication*.
- Wallace, D.A. and Raymond, O.L. 2000. ‘Glenisla Volcanics’. In: Raymond, O.L., Duggan, M.B., Lyons, P., Scott, M.M., Sherwin, L., Wallace, D.A., Krynen, J.P., Young, G.C., Wyborn, D., Glen, R.A., Percival, I.G. and Leys, M., 2000. Forbes 1:250 000 Geological Sheet SI/55-07, 2nd edition, *Geological Survey of New South Wales*, Sydney.
- Warren, A. and Watkins, J.J., 1998. ‘Middle Devonian’. In: Pogson D.J. & Watkins J.J., 1998. Bathurst 1:250 000 Geological Sheet SI/55-8: Explanatory Notes. Geological Survey of New South Wales, Sydney, xiv + 430 pp.
- Webby, B., 1972. Devonian geological history of the Lachlan Geosyncline. *Journal of the Geological Society of Australia*, 19(1):99-123.
- Wiedenbeck, M., Allé, P., Corfu, F., Griffin, W.L., Meier, M., Oberli, F., Von Quadt, A., Roddick, J.C., Spiegel, W., 1995. Three natural zircon standards for U–Th–Pb, Lu–Hf, trace element and REE analyses. *Geostandards Newsletter*, 19:1–23.
- Young, G.C., 1999. Preliminary report on the biostratigraphy of new placoderm discoveries in the Hervey Group (Upper Devonian) of central New South Wales. *Records of the Western Australian Museum Supplement* 57:139-150.
- Young, G.C., 2000. ‘Mandagery Formation’. In: Lyons, P., Raymond, O.L. & Duggan, M.B., 2000. Forbes 1:250 000 Geological Sheet S155-7 (2nd edition) Explanatory Notes. *Australian Geological Survey Organisation Record*, 20:80-82.
- Young, G.C., 2006a. Biostratigraphic and biogeographic context for tetrapod origins during the Devonian: Australian evidence. *Alcheringa* Special Issue 1:409-428.
- Young, G.C., 2006b. Devonian fish remains, biostratigraphy and unconformities, Narromine 1:250000 map sheet area, central New South Wales (Lachlan Fold Belt). *Australian Journal of Earth Sciences* 53:605-615.
- Young, G., 2010. Placoderms (Armored Fish): Dominant Vertebrates of the Devonian Period. *Annual Review of Earth and Planetary Sciences*, 38:523-550.

Supplementary material

Table A1: Summary of collected samples

| SAMPLE | STRAT | LITHOLOGY | LONGITUDE (E.) | LATITUDE (S) | ELEVATION | LOCATION |
|--------|-----------------------------------|---------------------------------------------------------------|----------------|--------------|-----------|-------------------------------------------------------------------|
| TUFF | Mandagery Formation, Hervey Gp | 1.5cm thick layer, very fine-grained, tuffaceous looking | NA | NA | NA | Provided by Bruce Loomes/ Originally from Canowindra Fish site |
| AOFM1 | Mandagery Formation, Hervey Gp | Fine sandstone overlaid by thin very fine-grained white layer | NA | NA | NA | Age Of Fishes Museum/ Originally from Canowindra Fish site |
| AOFM2 | Mandagery Formation, Hervey Gp | Fine sandstone overlaid by thin very fine-grained white layer | NA | NA | NA | Age Of Fishes Museum/ Originally from Canowindra Fish site |
| AOFM3 | Mandagery Formation, Hervey Gp | Fine sandstone overlaid by thin very fine-grained white layer | NA | NA | NA | Age Of Fishes Museum/ Originally from Canowindra Fish site |
| AOFM4 | Mandagery Formation, Hervey Gp | Fine sandstone overlaid by thin very fine-grained white layer | NA | NA | NA | Age Of Fishes Museum/ Originally from Canowindra Fish site |
| AOFM5 | Mandagery Formation, Hervey Gp | Fine sandstone overlaid by thin very fine-grained white layer | NA | NA | NA | Age Of Fishes Museum/ Originally from Canowindra Fish site |
| AOFM6 | Mandagery Formation, Hervey Gp | Fine sandstone overlaid by thin very fine-grained white layer | NA | NA | NA | Age Of Fishes Museum/ Originally from Canowindra Fish site |
| AOFM7 | Mandagery Formation, Hervey Gp | Fine sandstone overlaid by thin very fine-grained white layer | NA | NA | NA | Age Of Fishes Museum/ Originally from Canowindra Fish site |
| AOFM8 | Mandagery Formation, Hervey Gp | Fine sandstone overlaid by thin very fine-grained white layer | NA | NA | NA | Age Of Fishes Museum/ Originally from Canowindra Fish site |
| CNO1.1 | Mandagery Formation, Hervey Gp | Fine sandstone | 148°33.974' | 33°35.951' | 286 m | Originally from Canowindra Fish site |
| CNO1.2 | Mandagery Formation, Hervey Gp | Sandstone, with small dark oval marks on top of the sample | 148°33.986' | 33°35.940' | 288 m | Canowindra fish site |
| CNO2.1 | Mandagery Formation, Hervey Gp | Coarser sandstone, rich in feldspar and quartz | 148°33.983' | 33°35.921' | 293 m | 10 metres above Age Of Fishes site |
| CNO2.2 | Mandagery Formation, Hervey Gp | Coarser sandstone, rich in feldspar and quartz | 148°33.983' | 33°35.921' | 293 m | 10 metres above Age Of Fishes site |
| CNO2.3 | Mandagery Formation, Hervey Gp | Coarser sandstone, rich in feldspar and quartz | 148°33.983' | 33°35.921' | 293 m | 10 metres above Age Of Fishes site |
| CNO2.4 | Mandagery Formation, Hervey Gp | Coarser sandstone, rich in feldspar and quartz | 148°33.983' | 33°35.921' | 293 m | 10 metres above Age Of Fishes site |
| CNO2.5 | Mandagery Formation, Hervey Gp | Coarser sandstone, rich in feldspar and quartz | 148°33.983' | 33°35.921' | 293 m | 10 metres above Age Of Fishes site |
| CNO3 | Mandagery Formation, Hervey Gp | Fine sandstone with worm burrows/bioturbation | 148°34.062' | 33°35.062' | 315 m | 10 metres above Age Of Fishes site |
| CNO4.1 | Merriganowry Beds, Rocky Ponds Gp | Volcanic ash, tuff | 148°32.325' | 33°41.632' | 288 m | Merriganowry quarry |
| CNO4.2 | Merriganowry Beds, Rocky Ponds Gp | Shale, fish fossils | 148°32.325' | 33°41.632' | 289 m | Merriganowry quarry |
| CNO5.1 | Mandagery Formation, Hervey Gp | Very fine grained tuff-like texture | 148°34.492' | 33°32.743' | 323 m | South side of Nangar Road |
| CNO5.2 | Mandagery Formation, Hervey Gp | Very fine grained tuff-like texture | 148°34.492' | 33°32.743' | 323 m | South side of Nangar Road |
| CNO5.3 | Mandagery Formation, Hervey Gp | Very fine grained tuff-like texture | 148°34.492' | 33°32.743' | 323 m | South side of Nangar Road |
| CNO5.4 | Mandagery Formation, Hervey Gp | Fine sandstone, no feldspars | 148°34.492' | 33°32.743' | 323 m | South side of Nangar Road |
| CNO5.5 | Mandagery Formation, Hervey Gp | Fine sandstone, no feldspars | 148°34.492' | 33°32.743' | 323 m | South side of Nangar Road |
| CNO5.6 | Mandagery Formation, Hervey Gp | Fine sandstone, no feldspars | 148°34.492' | 33°32.743' | 323 m | South side of Nangar Road |

Green: Sample “TUFF” analysed. **Orange:** Samples from fish bed (AOFM) separated into samples “AOFM-SD” and “AOFM-Tuff”. **Blue:** Samples used for “CN02” analysis.

Table A2: U/Pb age data of CN02. Red: rejected data.

| Analysis N | U-Pb RATIOS | | | | | | | | AGES (Ma) | | | | | | | |
|----------------|-----------------------------------|---------------|----------------------------------|---------------|----------------------------------|---------------|-----------------------------------|---------------|-----------------------------------|---------------|----------------------------------|---------------|----------------------------------|---------------|-----------------------------------|---------------|
| | $^{207}\text{Pb}/^{206}\text{Pb}$ | $\pm 2\sigma$ | $^{207}\text{Pb}/^{235}\text{U}$ | $\pm 2\sigma$ | $^{206}\text{Pb}/^{238}\text{U}$ | $\pm 2\sigma$ | $^{208}\text{Pb}/^{232}\text{Th}$ | $\pm 2\sigma$ | $^{207}\text{Pb}/^{206}\text{Pb}$ | $\pm 2\sigma$ | $^{207}\text{Pb}/^{235}\text{U}$ | $\pm 2\sigma$ | $^{206}\text{Pb}/^{238}\text{U}$ | $\pm 2\sigma$ | $^{208}\text{Pb}/^{232}\text{Th}$ | $\pm 2\sigma$ |
| CN02-57 | 0.11248 | 0.00326 | 0.61078 | 0.01706 | 0.03938 | 0.00060 | 0.01051 | 0.00054 | 1840 | 54 | 484 | 10 | 249 | 4 | 211 | 10 |
| CN02-05 | 0.0556 | 0.00194 | 0.45194 | 0.01514 | 0.05896 | 0.00088 | 0.01917 | 0.00072 | 436 | 80 | 379 | 10 | 369 | 6 | 384 | 14 |
| CN02-30 | 0.05331 | 0.00380 | 0.43871 | 0.03000 | 0.05969 | 0.00152 | 0.01693 | 0.00150 | 342 | 166 | 369 | 22 | 374 | 10 | 339 | 30 |
| CN02-53 | 0.05422 | 0.00198 | 0.44689 | 0.01582 | 0.05977 | 0.00096 | 0.01873 | 0.00082 | 380 | 84 | 375 | 12 | 374 | 6 | 375 | 16 |
| CN02-42 | 0.06023 | 0.00412 | 0.52564 | 0.03454 | 0.0633 | 0.00118 | 0.01954 | 0.00040 | 612 | 152 | 429 | 22 | 396 | 8 | 391 | 8 |
| CN02-48 | 0.06031 | 0.00268 | 0.5384 | 0.02272 | 0.06475 | 0.00114 | 0.01574 | 0.00112 | 615 | 98 | 437 | 14 | 404 | 6 | 316 | 22 |
| CN02-56 | 0.05492 | 0.00214 | 0.49148 | 0.01842 | 0.0649 | 0.00104 | 0.02084 | 0.00090 | 409 | 90 | 406 | 12 | 405 | 6 | 417 | 18 |
| CN02-22 | 0.05609 | 0.00174 | 0.50524 | 0.01488 | 0.06534 | 0.00090 | 0.01955 | 0.00106 | 456 | 70 | 415 | 10 | 408 | 6 | 391 | 22 |
| CN02-52 | 0.05612 | 0.00192 | 0.50609 | 0.01658 | 0.06541 | 0.00098 | 0.01968 | 0.00112 | 457 | 78 | 416 | 12 | 408 | 6 | 394 | 22 |
| CN02-11 | 0.05544 | 0.00126 | 0.50996 | 0.01122 | 0.06672 | 0.00082 | 0.01968 | 0.00076 | 430 | 52 | 418 | 8 | 416 | 4 | 394 | 16 |
| CN02-49 | 0.05635 | 0.00130 | 0.51964 | 0.01156 | 0.06689 | 0.00084 | 0.02089 | 0.00066 | 466 | 52 | 425 | 8 | 417 | 6 | 418 | 14 |
| CN02-58 | 0.0602 | 0.00244 | 0.55459 | 0.02176 | 0.06682 | 0.00118 | 0.01988 | 0.00140 | 611 | 90 | 448 | 14 | 417 | 8 | 398 | 28 |
| CN02-17 | 0.0582 | 0.00246 | 0.53802 | 0.02190 | 0.06705 | 0.00122 | 0.02669 | 0.00170 | 537 | 94 | 437 | 14 | 418 | 8 | 532 | 34 |
| CN02-02 | 0.05623 | 0.00116 | 0.52447 | 0.01062 | 0.06766 | 0.00082 | 0.02329 | 0.00072 | 461 | 46 | 428 | 8 | 422 | 4 | 465 | 14 |
| CN02-35 | 0.05617 | 0.00184 | 0.52335 | 0.01650 | 0.06758 | 0.00100 | 0.02033 | 0.00112 | 459 | 74 | 427 | 10 | 422 | 6 | 407 | 22 |
| CN02-21 | 0.05707 | 0.00238 | 0.53324 | 0.02144 | 0.06776 | 0.00120 | 0.01509 | 0.00102 | 494 | 94 | 434 | 14 | 423 | 8 | 303 | 20 |
| CN02-25 | 0.05564 | 0.00124 | 0.52047 | 0.01126 | 0.06786 | 0.00084 | 0.02129 | 0.00070 | 438 | 50 | 425 | 8 | 423 | 6 | 426 | 14 |
| CN02-38 | 0.05462 | 0.00184 | 0.51131 | 0.01658 | 0.0679 | 0.00102 | 0.02244 | 0.00122 | 397 | 78 | 419 | 12 | 423 | 6 | 449 | 24 |
| CN02-44 | 0.05572 | 0.00166 | 0.52111 | 0.01494 | 0.06783 | 0.00096 | 0.01834 | 0.00104 | 441 | 68 | 426 | 10 | 423 | 6 | 367 | 20 |
| CN02-32 | 0.05587 | 0.00136 | 0.52388 | 0.01222 | 0.06801 | 0.00084 | 0.02192 | 0.00076 | 447 | 56 | 428 | 8 | 424 | 6 | 438 | 16 |
| CN02-36 | 0.05622 | 0.00202 | 0.52924 | 0.01822 | 0.06828 | 0.00106 | 0.02124 | 0.00138 | 461 | 82 | 431 | 12 | 426 | 6 | 425 | 28 |
| CN02-59 | 0.05511 | 0.00322 | 0.51896 | 0.02900 | 0.06829 | 0.00148 | 0.01791 | 0.00194 | 417 | 134 | 424 | 20 | 426 | 8 | 359 | 38 |
| CN02-13 | 0.05551 | 0.00126 | 0.52372 | 0.01160 | 0.06843 | 0.00086 | 0.0183 | 0.00072 | 433 | 52 | 428 | 8 | 427 | 6 | 367 | 14 |
| CN02-31 | 0.05727 | 0.00144 | 0.54048 | 0.01320 | 0.06845 | 0.00090 | 0.01861 | 0.00076 | 502 | 56 | 439 | 8 | 427 | 6 | 373 | 16 |
| CN02-19 | 0.05595 | 0.00146 | 0.52937 | 0.01334 | 0.06863 | 0.00092 | 0.02124 | 0.00084 | 450 | 60 | 431 | 8 | 428 | 6 | 425 | 16 |
| CN02-40 | 0.05692 | 0.00186 | 0.53842 | 0.01708 | 0.0686 | 0.00104 | 0.02046 | 0.00112 | 488 | 74 | 437 | 12 | 428 | 6 | 409 | 22 |
| CN02-16 | 0.0576 | 0.00196 | 0.54649 | 0.01772 | 0.06881 | 0.00102 | 0.01582 | 0.00068 | 515 | 76 | 443 | 12 | 429 | 6 | 317 | 14 |
| CN02-29 | 0.05557 | 0.00140 | 0.52708 | 0.01282 | 0.0688 | 0.00088 | 0.02242 | 0.00098 | 435 | 58 | 430 | 8 | 429 | 6 | 448 | 20 |
| CN02-37 | 0.056 | 0.00146 | 0.53344 | 0.01352 | 0.06909 | 0.00092 | 0.02109 | 0.00088 | 452 | 60 | 434 | 8 | 431 | 6 | 422 | 18 |
| CN02-43 | 0.05694 | 0.00138 | 0.54274 | 0.01278 | 0.06914 | 0.00088 | 0.0197 | 0.00082 | 489 | 54 | 440 | 8 | 431 | 6 | 394 | 16 |
| CN02-20 | 0.05573 | 0.00146 | 0.53289 | 0.01336 | 0.06935 | 0.00090 | 0.02169 | 0.00092 | 442 | 60 | 434 | 8 | 432 | 6 | 434 | 18 |
| CN02-24 | 0.05528 | 0.00192 | 0.5277 | 0.01754 | 0.06924 | 0.00102 | 0.02255 | 0.00112 | 424 | 80 | 430 | 12 | 432 | 6 | 451 | 22 |
| CN02-27 | 0.05542 | 0.00140 | 0.52939 | 0.01312 | 0.06929 | 0.00092 | 0.02051 | 0.00088 | 429 | 58 | 431 | 8 | 432 | 6 | 410 | 18 |
| CN02-51 | 0.05666 | 0.00164 | 0.54116 | 0.01502 | 0.06928 | 0.00096 | 0.02073 | 0.00100 | 478 | 66 | 439 | 10 | 432 | 6 | 415 | 20 |
| CN02-55 | 0.05674 | 0.00136 | 0.54239 | 0.01246 | 0.06934 | 0.00086 | 0.02185 | 0.00082 | 481 | 54 | 440 | 8 | 432 | 6 | 437 | 16 |
| CN02-10 | 0.05587 | 0.00176 | 0.53595 | 0.01624 | 0.06958 | 0.00100 | 0.02225 | 0.00088 | 447 | 72 | 436 | 10 | 434 | 6 | 445 | 18 |
| CN02-45 | 0.05749 | 0.00376 | 0.55221 | 0.03486 | 0.06966 | 0.00118 | 0.02162 | 0.00044 | 511 | 148 | 446 | 22 | 434 | 8 | 432 | 8 |
| CN02-26 | 0.05527 | 0.00138 | 0.53427 | 0.01296 | 0.07012 | 0.00092 | 0.02112 | 0.00078 | 423 | 58 | 435 | 8 | 437 | 6 | 422 | 16 |
| CN02-15 | 0.05538 | 0.00140 | 0.53658 | 0.01320 | 0.07028 | 0.00092 | 0.02237 | 0.00098 | 428 | 58 | 436 | 8 | 438 | 6 | 447 | 20 |
| CN02-08 | 0.05621 | 0.00134 | 0.5466 | 0.01268 | 0.07054 | 0.00090 | 0.02226 | 0.00074 | 461 | 54 | 443 | 8 | 439 | 6 | 445 | 14 |
| CN02-03 | 0.05716 | 0.00162 | 0.5565 | 0.01532 | 0.07064 | 0.00098 | 0.02302 | 0.00104 | 498 | 64 | 449 | 10 | 440 | 6 | 460 | 20 |
| CN02-41 | 0.05616 | 0.00186 | 0.54977 | 0.01756 | 0.071 | 0.00106 | 0.0226 | 0.00116 | 459 | 76 | 445 | 12 | 442 | 6 | 452 | 22 |
| CN02-09 | 0.0568 | 0.00130 | 0.55669 | 0.01230 | 0.07109 | 0.00088 | 0.02232 | 0.00078 | 484 | 52 | 449 | 8 | 443 | 6 | 446 | 16 |
| CN02-61 | 0.05549 | 0.00194 | 0.54948 | 0.01842 | 0.07182 | 0.00112 | 0.02565 | 0.00148 | 432 | 80 | 445 | 12 | 447 | 6 | 512 | 30 |
| CN02-60 | 0.05674 | 0.00210 | 0.56787 | 0.02018 | 0.07259 | 0.00112 | 0.02281 | 0.00120 | 481 | 84 | 457 | 14 | 452 | 6 | 456 | 24 |
| CN02-54 | 0.05725 | 0.00176 | 0.5756 | 0.01690 | 0.07293 | 0.00102 | 0.02377 | 0.00112 | 501 | 70 | 462 | 10 | 454 | 6 | 475 | 22 |
| CN02-33 | 0.05826 | 0.00272 | 0.58826 | 0.02610 | 0.07327 | 0.00132 | 0.02095 | 0.00150 | 540 | 104 | 470 | 16 | 456 | 8 | 419 | 30 |
| CN02-34 | 0.05662 | 0.00152 | 0.57543 | 0.01488 | 0.07372 | 0.00096 | 0.02315 | 0.00090 | 477 | 60 | 462 | 10 | 459 | 6 | 463 | 18 |
| CN02-06 | 0.05772 | 0.00126 | 0.58955 | 0.01248 | 0.07409 | 0.00090 | 0.02349 | 0.00074 | 519 | 50 | 471 | 8 | 461 | 6 | 469 | 14 |
| CN02-18 | 0.05734 | 0.00128 | 0.59917 | 0.01300 | 0.0758 | 0.00094 | 0.02574 | 0.00082 | 505 | 50 | 477 | 8 | 471 | 6 | 514 | 16 |
| CN02-50 | 0.05883 | 0.00200 | 0.64163 | 0.02084 | 0.07911 | 0.00118 | 0.02204 | 0.00122 | 561 | 74 | 503 | 12 | 491 | 8 | 441 | 24 |
| CN02-47 | 0.05826 | 0.00150 | 0.63717 | 0.01562 | 0.07932 | 0.00100 | 0.02859 | 0.00124 | 540 | 58 | 501 | 10 | 492 | 6 | 570 | 24 |
| CN02-28 | 0.05836 | 0.00214 | 0.66034 | 0.02336 | 0.08207 | 0.00136 | 0.02562 | 0.00156 | 543 | 82 | 515 | 14 | 508 | 8 | 511 | 30 |
| CN02-46 | 0.0597 | 0.00170 | 0.70263 | 0.01926 | 0.08536 | 0.00118 | 0.03455 | 0.00162 | 593 | 64 | 540 | 12 | 528 | 8 | 687 | 32 |
| CN02-04 | 0.05849 | 0.00124 | 0.69289 | 0.01436 | 0.08593 | 0.00104 | 0.0269 | 0.00080 | 548 | 48 | 535 | 8 | 531 | 6 | 537 | 16 |
| CN02-39 | 0.06032 | 0.00226 | 0.74942 | 0.02706 | 0.0901 | 0.00150 | 0.02844 | 0.00164 | 615 | 82 | 568 | 16 | 556 | 8 | 567 | 32 |
| CN02-14 | 0.05943 | 0.00134 | 0.76146 | 0.01670 | 0.09293 | 0.00118 | 0.02887 | 0.00112 | 583 | 50 | 575 | 10 | 573 | 6 | 575 | 22 |
| CN02-07 | 0.06019 | 0.00120 | 0.8086 | 0.01558 | 0.09745 | 0.00116 | 0.03028 | 0.00096 | 610 | 44 | 602 | 8 | 599 | 6 | 603 | 18 |
| CN02-01 | 0.06363 | 0.00256 | 0.96506 | 0.03726 | 0.11004 | 0.00190 | 0.03563 | 0.00168 | 729 | 88 | 686 | 20 | 673 | 12 | 708 | 32 |
| CN02-23 | 0.08095 | 0.00180 | 2.30203 | 0.04966 | 0.20626 | 0.00264 | 0.06048 | 0.00204 | 1220 | 44 | 1213 | 16 | 1209 | 14 | 1187 | 38 |
| CN02-12 | 0.21594 | 0.00712 | 16.79507 | 0.52888 | 0.56413 | 0.00884 | 0.14172 | 0.00940 | 2951 | 54 | 2923 | 30 | 2884 | 36 | 2679 | 166 |

Table A3: U/Pb age data of sample AOFM-SD. Red: rejected data.

| Analysis N | U-Pb RATIOS | | | | | | | | AGES (Ma) | | | | | | | |
|------------|--------------------------------------|---------|-------------------------------------|---------|-------------------------------------|---------|--------------------------------------|---------|--------------------------------------|------|-------------------------------------|------|-------------------------------------|------|--------------------------------------|------|
| | ²⁰⁷ Pb/ ²⁰⁶ Pb | ± 2S | ²⁰⁷ Pb/ ²³⁵ U | ± 2S | ²⁰⁶ Pb/ ²³⁸ U | ± 2S | ²⁰⁸ Pb/ ²³² Th | ± 2S | ²⁰⁷ Pb/ ²⁰⁶ Pb | ± 2S | ²⁰⁷ Pb/ ²³⁵ U | ± 2S | ²⁰⁶ Pb/ ²³⁸ U | ± 2S | ²⁰⁸ Pb/ ²³² Th | ± 2S |
| AOFM-SD-39 | 0.12726 | 0.00794 | 1.00737 | 0.06028 | 0.05741 | 0.00100 | 0.01636 | 0.00028 | 2060 | 112 | 708 | 30 | 360 | 6 | 328 | 6 |
| AOFM-SD-31 | 0.05645 | 0.00160 | 0.44697 | 0.01230 | 0.05744 | 0.00080 | 0.01706 | 0.00066 | 470 | 64 | 375 | 8 | 360 | 4 | 342 | 14 |
| AOFM-SD-18 | 0.05493 | 0.00174 | 0.43643 | 0.01342 | 0.05763 | 0.00084 | 0.01682 | 0.00072 | 409 | 72 | 368 | 10 | 361 | 6 | 337 | 14 |
| AOFM-SD-13 | 0.05606 | 0.00290 | 0.44877 | 0.02224 | 0.05807 | 0.00114 | 0.01691 | 0.00142 | 455 | 118 | 376 | 16 | 364 | 6 | 339 | 28 |
| AOFM-SD-52 | 0.07341 | 0.00236 | 0.59499 | 0.01820 | 0.05893 | 0.00088 | 0.00932 | 0.00050 | 1025 | 66 | 474 | 12 | 369 | 6 | 188 | 10 |
| AOFM-SD-66 | 0.09168 | 0.00992 | 0.75284 | 0.08006 | 0.05956 | 0.00122 | 0.01755 | 0.00032 | 1461 | 212 | 570 | 46 | 373 | 8 | 352 | 6 |
| AOFM-SD-04 | 0.06304 | 0.00242 | 0.52148 | 0.01908 | 0.06 | 0.00096 | 0.01629 | 0.00096 | 710 | 84 | 426 | 12 | 376 | 6 | 327 | 20 |
| AOFM-SD-05 | 0.05798 | 0.00148 | 0.48357 | 0.01190 | 0.0605 | 0.00078 | 0.01475 | 0.00058 | 529 | 58 | 401 | 8 | 379 | 4 | 296 | 12 |
| AOFM-SD-12 | 0.05952 | 0.00258 | 0.49789 | 0.02058 | 0.06067 | 0.00108 | 0.01856 | 0.00124 | 586 | 96 | 410 | 14 | 380 | 6 | 372 | 24 |
| AOFM-SD-09 | 0.05884 | 0.00234 | 0.51172 | 0.01944 | 0.06309 | 0.00102 | 0.01964 | 0.00132 | 561 | 88 | 420 | 14 | 394 | 6 | 393 | 26 |
| AOFM-SD-57 | 0.06392 | 0.00622 | 0.55731 | 0.05298 | 0.06323 | 0.00134 | 0.01939 | 0.00046 | 739 | 212 | 450 | 34 | 395 | 8 | 388 | 10 |
| AOFM-SD-06 | 0.05691 | 0.00146 | 0.49763 | 0.01250 | 0.06343 | 0.00084 | 0.01697 | 0.00072 | 488 | 58 | 410 | 8 | 396 | 6 | 340 | 14 |
| AOFM-SD-25 | 0.06266 | 0.00292 | 0.5481 | 0.02434 | 0.06347 | 0.00120 | 0.01582 | 0.00118 | 697 | 102 | 444 | 16 | 397 | 8 | 317 | 24 |
| AOFM-SD-56 | 0.06105 | 0.00298 | 0.52633 | 0.02626 | 0.06361 | 0.00118 | 0.0173 | 0.00144 | 641 | 108 | 429 | 16 | 398 | 8 | 347 | 28 |
| AOFM-SD-55 | 0.06222 | 0.00430 | 0.54947 | 0.03624 | 0.06405 | 0.00130 | 0.0197 | 0.00044 | 682 | 150 | 445 | 24 | 400 | 8 | 394 | 8 |
| AOFM-SD-14 | 0.05686 | 0.00202 | 0.50284 | 0.01716 | 0.06415 | 0.00098 | 0.01965 | 0.00074 | 486 | 80 | 414 | 12 | 401 | 6 | 393 | 14 |
| AOFM-SD-08 | 0.05922 | 0.00172 | 0.52915 | 0.01478 | 0.06481 | 0.00090 | 0.01756 | 0.00080 | 575 | 64 | 431 | 10 | 405 | 6 | 352 | 16 |
| AOFM-SD-71 | 0.05914 | 0.00262 | 0.53006 | 0.02194 | 0.065 | 0.00102 | 0.02011 | 0.00034 | 572 | 98 | 432 | 14 | 406 | 6 | 402 | 6 |
| AOFM-SD-46 | 0.05744 | 0.00288 | 0.51478 | 0.02484 | 0.06501 | 0.00130 | 0.01483 | 0.00106 | 508 | 112 | 422 | 16 | 406 | 8 | 298 | 22 |
| AOFM-SD-01 | 0.06288 | 0.00628 | 0.56629 | 0.05576 | 0.06532 | 0.00110 | 0.02006 | 0.00030 | 704 | 218 | 456 | 36 | 408 | 6 | 402 | 6 |
| AOFM-SD-03 | 0.05862 | 0.00178 | 0.52947 | 0.01560 | 0.06551 | 0.00096 | 0.01618 | 0.00068 | 553 | 68 | 431 | 10 | 409 | 6 | 324 | 14 |
| AOFM-SD-51 | 0.05839 | 0.00208 | 0.52552 | 0.01772 | 0.06559 | 0.00102 | 0.01976 | 0.00124 | 544 | 80 | 429 | 12 | 410 | 6 | 395 | 24 |
| AOFM-SD-37 | 0.06201 | 0.00302 | 0.56166 | 0.02626 | 0.06571 | 0.00130 | 0.02014 | 0.00132 | 674 | 106 | 453 | 18 | 410 | 8 | 403 | 26 |
| AOFM-SD-32 | 0.0558 | 0.00142 | 0.50979 | 0.01264 | 0.06627 | 0.00088 | 0.01888 | 0.00076 | 444 | 58 | 418 | 8 | 414 | 6 | 378 | 16 |
| AOFM-SD-26 | 0.05794 | 0.00170 | 0.52949 | 0.01502 | 0.06628 | 0.00094 | 0.0184 | 0.00094 | 527 | 66 | 431 | 10 | 414 | 6 | 369 | 18 |
| AOFM-SD-19 | 0.06886 | 0.00296 | 0.62872 | 0.02588 | 0.06629 | 0.00122 | 0.02135 | 0.00160 | 895 | 90 | 495 | 16 | 414 | 8 | 427 | 32 |
| AOFM-SD-27 | 0.06044 | 0.00348 | 0.55256 | 0.03052 | 0.0663 | 0.00110 | 0.02046 | 0.00036 | 619 | 128 | 447 | 20 | 414 | 6 | 409 | 8 |
| AOFM-SD-21 | 0.06444 | 0.00190 | 0.59198 | 0.01682 | 0.06663 | 0.00096 | 0.01922 | 0.00096 | 756 | 64 | 472 | 10 | 416 | 6 | 385 | 20 |
| AOFM-SD-63 | 0.05748 | 0.00264 | 0.5282 | 0.02322 | 0.06665 | 0.00120 | 0.01757 | 0.00134 | 510 | 104 | 431 | 16 | 416 | 8 | 352 | 26 |
| AOFM-SD-15 | 0.05759 | 0.00288 | 0.53213 | 0.02502 | 0.06702 | 0.00112 | 0.0208 | 0.00038 | 514 | 112 | 433 | 16 | 418 | 6 | 416 | 8 |
| AOFM-SD-30 | 0.05663 | 0.00152 | 0.52637 | 0.01364 | 0.06742 | 0.00090 | 0.01912 | 0.00076 | 477 | 60 | 429 | 10 | 421 | 6 | 383 | 16 |
| AOFM-SD-34 | 0.10669 | 0.00706 | 0.99248 | 0.06358 | 0.06747 | 0.00114 | 0.01957 | 0.00030 | 1744 | 124 | 700 | 32 | 421 | 6 | 392 | 6 |
| AOFM-SD-58 | 0.0582 | 0.00224 | 0.54487 | 0.02010 | 0.06791 | 0.00110 | 0.02135 | 0.00142 | 537 | 86 | 442 | 14 | 424 | 6 | 427 | 28 |
| AOFM-SD-61 | 0.05748 | 0.00194 | 0.53905 | 0.01752 | 0.06802 | 0.00106 | 0.02094 | 0.00100 | 510 | 76 | 438 | 12 | 424 | 6 | 419 | 20 |
| AOFM-SD-50 | 0.05801 | 0.00186 | 0.54385 | 0.01666 | 0.06811 | 0.00100 | 0.01811 | 0.00090 | 530 | 72 | 441 | 10 | 425 | 6 | 363 | 18 |
| AOFM-SD-65 | 0.05468 | 0.00184 | 0.51416 | 0.01674 | 0.06821 | 0.00106 | 0.0211 | 0.00114 | 399 | 78 | 421 | 12 | 425 | 6 | 422 | 22 |
| AOFM-SD-64 | 0.05528 | 0.00166 | 0.52004 | 0.01514 | 0.06824 | 0.00098 | 0.02147 | 0.00090 | 424 | 68 | 425 | 10 | 426 | 6 | 429 | 18 |
| AOFM-SD-20 | 0.05622 | 0.00150 | 0.53189 | 0.01382 | 0.06863 | 0.00094 | 0.02275 | 0.00102 | 461 | 60 | 433 | 10 | 428 | 6 | 455 | 20 |
| AOFM-SD-67 | 0.0582 | 0.00354 | 0.55319 | 0.03216 | 0.06894 | 0.00126 | 0.02137 | 0.00044 | 537 | 136 | 447 | 22 | 430 | 8 | 427 | 8 |
| AOFM-SD-02 | 0.05619 | 0.00158 | 0.53499 | 0.01352 | 0.06905 | 0.00088 | 0.02149 | 0.00030 | 460 | 64 | 435 | 8 | 430 | 6 | 430 | 6 |
| AOFM-SD-28 | 0.05863 | 0.00160 | 0.55815 | 0.01476 | 0.06906 | 0.00094 | 0.02007 | 0.00094 | 553 | 60 | 450 | 10 | 430 | 6 | 402 | 18 |
| AOFM-SD-59 | 0.05575 | 0.00146 | 0.53318 | 0.01364 | 0.06937 | 0.00094 | 0.02103 | 0.00080 | 442 | 60 | 434 | 10 | 432 | 6 | 421 | 16 |
| AOFM-SD-68 | 0.0575 | 0.00190 | 0.55111 | 0.01758 | 0.06952 | 0.00108 | 0.02019 | 0.00110 | 511 | 74 | 446 | 12 | 433 | 6 | 404 | 26 |
| AOFM-SD-47 | 0.05802 | 0.00308 | 0.55716 | 0.02826 | 0.06966 | 0.00140 | 0.02226 | 0.00180 | 531 | 120 | 450 | 18 | 434 | 8 | 445 | 32 |
| AOFM-SD-49 | 0.05654 | 0.00192 | 0.54235 | 0.01772 | 0.06967 | 0.00104 | 0.02181 | 0.00100 | 474 | 76 | 440 | 12 | 434 | 6 | 436 | 20 |
| AOFM-SD-60 | 0.05631 | 0.00148 | 0.54476 | 0.01402 | 0.07017 | 0.00096 | 0.0222 | 0.00096 | 465 | 60 | 442 | 10 | 437 | 6 | 444 | 18 |
| AOFM-SD-41 | 0.05685 | 0.00144 | 0.55486 | 0.01374 | 0.07079 | 0.00094 | 0.01896 | 0.00086 | 486 | 58 | 448 | 8 | 441 | 6 | 380 | 18 |
| AOFM-SD-69 | 0.05941 | 0.00326 | 0.58457 | 0.03066 | 0.07138 | 0.00154 | 0.02412 | 0.00206 | 582 | 122 | 467 | 20 | 444 | 10 | 482 | 40 |
| AOFM-SD-07 | 0.05937 | 0.00128 | 0.58872 | 0.01244 | 0.07193 | 0.00090 | 0.02801 | 0.00098 | 581 | 48 | 470 | 8 | 448 | 6 | 558 | 20 |
| AOFM-SD-35 | 0.05621 | 0.00132 | 0.55822 | 0.01272 | 0.07204 | 0.00092 | 0.02299 | 0.00090 | 461 | 54 | 450 | 8 | 448 | 6 | 459 | 18 |
| AOFM-SD-70 | 0.05693 | 0.00222 | 0.56707 | 0.02132 | 0.07225 | 0.00122 | 0.0213 | 0.00124 | 489 | 88 | 456 | 14 | 450 | 8 | 426 | 24 |
| AOFM-SD-33 | 0.06573 | 0.00372 | 0.65602 | 0.03524 | 0.07241 | 0.00158 | 0.01639 | 0.00148 | 798 | 122 | 512 | 22 | 451 | 10 | 329 | 30 |
| AOFM-SD-62 | 0.05893 | 0.00228 | 0.59394 | 0.02206 | 0.07311 | 0.00124 | 0.02124 | 0.00116 | 565 | 86 | 473 | 14 | 455 | 8 | 425 | 22 |
| AOFM-SD-36 | 0.06199 | 0.00344 | 0.62852 | 0.03316 | 0.07355 | 0.00154 | 0.02877 | 0.00252 | 674 | 122 | 495 | 20 | 458 | 10 | 573 | 50 |
| AOFM-SD-43 | 0.06858 | 0.00376 | 0.70309 | 0.03700 | 0.07436 | 0.00164 | 0.01962 | 0.00186 | 886 | 116 | 541 | 22 | 462 | 10 | 393 | 36 |
| AOFM-SD-22 | 0.06275 | 0.00266 | 0.64432 | 0.02562 | 0.07447 | 0.00106 | 0.02288 | 0.00034 | 700 | 92 | 505 | 16 | 463 | 6 | 457 | 6 |
| AOFM-SD-42 | 0.0576 | 0.00238 | 0.59539 | 0.02364 | 0.07498 | 0.00126 | 0.02855 | 0.00216 | 515 | 92 | 474 | 16 | 466 | 8 | 569 | 42 |
| AOFM-SD-40 | 0.06099 | 0.00310 | 0.63587 | 0.03106 | 0.07562 | 0.00156 | 0.02346 | 0.00218 | 639 | 112 | 500 | 20 | 470 | 10 | 469 | 44 |
| AOFM-SD-24 | 0.06328 | 0.00178 | 0.66869 | 0.01822 | 0.07666 | 0.00106 | 0.0222 | 0.00098 | 718 | 62 | 520 | 12 | 476 | 6 | 444 | 20 |
| AOFM-SD-29 | 0.05789 | 0.00180 | 0.61429 | 0.01730 | 0.07696 | 0.00100 | 0.02387 | 0.00034 | 526 | 70 | 486 | 10 | 478 | 6 | 477 | 6 |
| AOFM-SD-45 | 0.05865 | 0.00168 | 0.62952 | 0.01738 | 0.07791 | 0.00110 | 0.02515 | 0.00114 | 554 | 64 | 496 | 10 | 484 | 6 | 502 | 22 |
| AOFM-SD-54 | 0.07026 | 0.00770 | 0.75975 | 0.08162 | 0.07843 | 0.00174 | 0.02379 | 0.00054 | 936 | 232 | 574 | 48 | 487 | 10 | 475 | 10 |
| AOFM-SD-44 | 0.05771 | 0.00158 | 0.62829 | 0.01670 | 0.07901 | 0.00110 | 0.02541 | 0.00112 | 519 | 62 | 495 | 10 | 490 | 6 | 507 | 22 |
| AOFM-SD-10 | 0.0577 | 0.00174 | 0.64021 | 0.01870 | 0.08047 | 0.00118 | 0.02374 | 0.00126 | 518 | 68 | 502 | 12 | 499 | 8 | 474 | 24 |
| AOFM-SD-38 | 0.06135 | 0.00282 | 0.71013 | 0.03138 | 0.08394 | 0.00160 | 0.02505 | 0.00202 | 652 | 100 | 545 | 18 | 520 | 10 | 500 | 40 |
| AOFM-SD-72 | 0.0593 | 0.00204 | 0.68818 | 0.02270 | 0.08418 | 0.00134 | 0.02517 | 0.00152 | 578 | 76 | 532 | 14 | 521 | 8 | 502 | 30 |
| AOFM-SD-16 | 0.06365 | 0.00130 | 0.81841 | 0.01644 | 0.09327 | 0.00114 | 0.02777 | 0.00086 | 730 | 44 | 607 | 10 | 575 | 6 | 554 | 16 |
| AOFM-SD-53 | 0.07128 | 0.00250 | 1.089 | 0.03612 | 0.11121 | 0.00176 | 0.04693 | 0.00268 | 965 | 74 | 748 | 18 | 680 | 10 | 927 | 52 |
| AOFM-SD-48 | 0.06927 | 0.00282 | 1.4107 | 0.05542 | 0.14772 | 0.00268 | 0.0528 | 0.00378 | 907 | 86 | 893 | 24 | 888 | 16 | 1040 | 72 |
| AOFM-SD-11 | 0.07479 | 0.00152 | 1.77615 | 0.03510 | 0.17226 | 0.00210 | 0.051 | | | | | | | | | |

Table A4: U/Pb age data of sample AOFM-Tuff1. Red: rejected data.

| Analysis N | U-Pb RATIOS | | | | | | | | AGES (Ma) | | | | | | | |
|---------------|-----------------------------------|---------------|----------------------------------|---------------|----------------------------------|---------------|-----------------------------------|---------------|-----------------------------------|---------------|----------------------------------|---------------|----------------------------------|---------------|-----------------------------------|---------------|
| | $^{207}\text{Pb}/^{206}\text{Pb}$ | $\pm 2\sigma$ | $^{207}\text{Pb}/^{235}\text{U}$ | $\pm 2\sigma$ | $^{206}\text{Pb}/^{238}\text{U}$ | $\pm 2\sigma$ | $^{208}\text{Pb}/^{232}\text{Th}$ | $\pm 2\sigma$ | $^{207}\text{Pb}/^{206}\text{Pb}$ | $\pm 2\sigma$ | $^{207}\text{Pb}/^{235}\text{U}$ | $\pm 2\sigma$ | $^{206}\text{Pb}/^{238}\text{U}$ | $\pm 2\sigma$ | $^{208}\text{Pb}/^{232}\text{Th}$ | $\pm 2\sigma$ |
| AOFM-Tuff1-44 | 0.05361 | 0.00198 | 0.42498 | 0.01524 | 0.05751 | 0.00094 | 0.01249 | 0.00060 | 355 | 86 | 360 | 10 | 360 | 6 | 251 | 12 |
| AOFM-Tuff1-06 | 0.05199 | 0.00300 | 0.43488 | 0.02422 | 0.06067 | 0.00118 | 0.0147 | 0.00084 | 285 | 136 | 367 | 18 | 380 | 8 | 295 | 16 |
| AOFM-Tuff1-09 | 0.05831 | 0.00466 | 0.49356 | 0.03772 | 0.0614 | 0.00170 | 0.01478 | 0.00128 | 541 | 180 | 407 | 26 | 384 | 10 | 297 | 26 |
| AOFM-Tuff1-02 | 0.0699 | 0.00212 | 0.60565 | 0.01772 | 0.06284 | 0.00094 | 0.0132 | 0.00066 | 925 | 64 | 481 | 12 | 393 | 6 | 265 | 14 |
| AOFM-Tuff1-07 | 0.05675 | 0.00220 | 0.49738 | 0.01862 | 0.06357 | 0.00106 | 0.01669 | 0.00100 | 482 | 88 | 410 | 12 | 397 | 6 | 335 | 20 |
| AOFM-Tuff1-26 | 0.05262 | 0.00200 | 0.46372 | 0.01710 | 0.06394 | 0.00106 | 0.0185 | 0.00102 | 312 | 88 | 387 | 12 | 400 | 6 | 371 | 20 |
| AOFM-Tuff1-51 | 0.06298 | 0.00470 | 0.55929 | 0.03966 | 0.06442 | 0.00174 | 0.01876 | 0.00236 | 708 | 162 | 451 | 26 | 402 | 10 | 376 | 46 |
| AOFM-Tuff1-48 | 0.05651 | 0.00220 | 0.50488 | 0.01916 | 0.06483 | 0.00112 | 0.01025 | 0.00046 | 472 | 88 | 415 | 12 | 405 | 6 | 206 | 10 |
| AOFM-Tuff1-35 | 0.06894 | 0.00324 | 0.61668 | 0.02764 | 0.06487 | 0.00130 | 0.01591 | 0.00104 | 897 | 100 | 488 | 18 | 405 | 8 | 319 | 20 |
| AOFM-Tuff1-45 | 0.0655 | 0.00330 | 0.59024 | 0.02838 | 0.06535 | 0.00100 | 0.01998 | 0.00034 | 791 | 108 | 471 | 18 | 408 | 6 | 400 | 6 |
| AOFM-Tuff1-24 | 0.05082 | 0.00216 | 0.46189 | 0.01874 | 0.06592 | 0.00120 | 0.01534 | 0.00110 | 233 | 100 | 386 | 14 | 412 | 8 | 308 | 22 |
| AOFM-Tuff1-49 | 0.06466 | 0.00362 | 0.59116 | 0.03162 | 0.0663 | 0.00142 | 0.02036 | 0.00194 | 763 | 120 | 472 | 20 | 414 | 8 | 407 | 38 |
| AOFM-Tuff1-04 | 0.06086 | 0.00266 | 0.55705 | 0.02332 | 0.06638 | 0.00114 | 0.01777 | 0.00154 | 634 | 96 | 450 | 16 | 414 | 6 | 356 | 30 |
| AOFM-Tuff1-42 | 0.05415 | 0.00216 | 0.4978 | 0.01914 | 0.06669 | 0.00112 | 0.02009 | 0.00132 | 377 | 92 | 410 | 12 | 416 | 6 | 402 | 26 |
| AOFM-Tuff1-34 | 0.0589 | 0.00204 | 0.54349 | 0.01824 | 0.06694 | 0.00108 | 0.01798 | 0.00106 | 563 | 78 | 441 | 12 | 418 | 6 | 360 | 22 |
| AOFM-Tuff1-36 | 0.05486 | 0.00196 | 0.507 | 0.01744 | 0.06704 | 0.00108 | 0.01699 | 0.00102 | 407 | 82 | 416 | 12 | 418 | 6 | 341 | 20 |
| AOFM-Tuff1-21 | 0.059 | 0.00268 | 0.54658 | 0.02384 | 0.0672 | 0.00128 | 0.01702 | 0.00146 | 567 | 102 | 443 | 16 | 419 | 8 | 341 | 30 |
| AOFM-Tuff1-47 | 0.06124 | 0.00188 | 0.56988 | 0.01696 | 0.0675 | 0.00100 | 0.01526 | 0.00074 | 648 | 68 | 458 | 10 | 421 | 6 | 306 | 14 |
| AOFM-Tuff1-50 | 0.06172 | 0.00198 | 0.57501 | 0.01806 | 0.06757 | 0.00104 | 0.01318 | 0.00056 | 664 | 70 | 461 | 12 | 421 | 6 | 265 | 12 |
| AOFM-Tuff1-38 | 0.06289 | 0.00324 | 0.58836 | 0.02904 | 0.06786 | 0.00136 | 0.02056 | 0.00208 | 705 | 112 | 470 | 18 | 423 | 8 | 411 | 42 |
| AOFM-Tuff1-40 | 0.05718 | 0.00236 | 0.53569 | 0.02128 | 0.06796 | 0.00120 | 0.01824 | 0.00124 | 498 | 94 | 436 | 14 | 424 | 8 | 365 | 24 |
| AOFM-Tuff1-32 | 0.06849 | 0.00478 | 0.64305 | 0.04244 | 0.06811 | 0.00176 | 0.01494 | 0.00158 | 883 | 148 | 504 | 26 | 425 | 10 | 300 | 32 |
| AOFM-Tuff1-30 | 0.05564 | 0.00150 | 0.52362 | 0.01372 | 0.06826 | 0.00092 | 0.02202 | 0.00112 | 438 | 62 | 428 | 10 | 426 | 6 | 440 | 22 |
| AOFM-Tuff1-28 | 0.05999 | 0.00232 | 0.56577 | 0.02106 | 0.06841 | 0.00116 | 0.02179 | 0.00146 | 603 | 86 | 455 | 14 | 427 | 6 | 436 | 28 |
| AOFM-Tuff1-17 | 0.05697 | 0.00244 | 0.53784 | 0.02224 | 0.06848 | 0.00120 | 0.0204 | 0.00130 | 490 | 96 | 437 | 14 | 427 | 8 | 408 | 26 |
| AOFM-Tuff1-03 | 0.05764 | 0.00218 | 0.54463 | 0.01982 | 0.06853 | 0.00114 | 0.01847 | 0.00112 | 516 | 84 | 441 | 14 | 427 | 6 | 370 | 22 |
| AOFM-Tuff1-20 | 0.06136 | 0.00228 | 0.57978 | 0.02082 | 0.06854 | 0.00114 | 0.01871 | 0.00140 | 652 | 82 | 464 | 14 | 427 | 6 | 375 | 28 |
| AOFM-Tuff1-31 | 0.05544 | 0.00202 | 0.5254 | 0.01860 | 0.06873 | 0.00110 | 0.0217 | 0.00140 | 430 | 84 | 429 | 12 | 428 | 6 | 434 | 28 |
| AOFM-Tuff1-37 | 0.05639 | 0.00224 | 0.53922 | 0.02064 | 0.06935 | 0.00116 | 0.01772 | 0.00126 | 468 | 90 | 438 | 14 | 432 | 6 | 355 | 26 |
| AOFM-Tuff1-43 | 0.05701 | 0.00202 | 0.54554 | 0.01880 | 0.06943 | 0.00114 | 0.01469 | 0.00072 | 492 | 80 | 442 | 12 | 433 | 6 | 295 | 14 |
| AOFM-Tuff1-39 | 0.06122 | 0.00244 | 0.58871 | 0.02264 | 0.06975 | 0.00116 | 0.02183 | 0.00172 | 647 | 88 | 470 | 14 | 435 | 6 | 436 | 34 |
| AOFM-Tuff1-05 | 0.06377 | 0.00310 | 0.61347 | 0.02856 | 0.06977 | 0.00130 | 0.01938 | 0.00180 | 734 | 106 | 486 | 18 | 435 | 8 | 388 | 36 |
| AOFM-Tuff1-22 | 0.06491 | 0.00340 | 0.62878 | 0.03156 | 0.07027 | 0.00150 | 0.01922 | 0.00216 | 771 | 112 | 495 | 20 | 438 | 10 | 385 | 42 |
| AOFM-Tuff1-46 | 0.05569 | 0.00220 | 0.54318 | 0.02062 | 0.07076 | 0.00116 | 0.0225 | 0.00154 | 440 | 90 | 441 | 14 | 441 | 6 | 450 | 30 |
| AOFM-Tuff1-16 | 0.0556 | 0.00156 | 0.5425 | 0.01470 | 0.07077 | 0.00096 | 0.02168 | 0.00106 | 436 | 64 | 440 | 10 | 441 | 6 | 434 | 20 |
| AOFM-Tuff1-19 | 0.0548 | 0.00262 | 0.53628 | 0.02466 | 0.071 | 0.00132 | 0.0212 | 0.00172 | 404 | 110 | 436 | 16 | 442 | 8 | 424 | 34 |
| AOFM-Tuff1-15 | 0.0591 | 0.00300 | 0.5915 | 0.02882 | 0.07259 | 0.00146 | 0.0177 | 0.00118 | 571 | 114 | 472 | 18 | 452 | 8 | 355 | 24 |
| AOFM-Tuff1-08 | 0.06022 | 0.00364 | 0.61256 | 0.03538 | 0.07377 | 0.00172 | 0.01483 | 0.00122 | 611 | 134 | 485 | 22 | 459 | 10 | 298 | 24 |
| AOFM-Tuff1-23 | 0.05846 | 0.00208 | 0.59861 | 0.02042 | 0.07428 | 0.00116 | 0.02293 | 0.00128 | 547 | 80 | 476 | 12 | 462 | 6 | 458 | 26 |
| AOFM-Tuff1-01 | 0.05954 | 0.00250 | 0.63342 | 0.02548 | 0.07715 | 0.00136 | 0.0181 | 0.00100 | 587 | 94 | 498 | 16 | 479 | 8 | 363 | 20 |
| AOFM-Tuff1-27 | 0.06124 | 0.00218 | 0.71067 | 0.02434 | 0.08416 | 0.00132 | 0.02578 | 0.00170 | 648 | 78 | 545 | 14 | 521 | 8 | 514 | 34 |
| AOFM-Tuff1-11 | 0.06237 | 0.00358 | 0.7243 | 0.03958 | 0.0842 | 0.00182 | 0.02374 | 0.00216 | 687 | 126 | 553 | 24 | 521 | 10 | 474 | 42 |
| AOFM-Tuff1-10 | 0.06124 | 0.00174 | 0.72816 | 0.02010 | 0.08624 | 0.00122 | 0.02279 | 0.00140 | 648 | 62 | 555 | 12 | 533 | 8 | 455 | 28 |
| AOFM-Tuff1-41 | 0.05905 | 0.00160 | 0.73015 | 0.01918 | 0.08968 | 0.00122 | 0.02824 | 0.00134 | 569 | 60 | 557 | 12 | 554 | 8 | 563 | 26 |
| AOFM-Tuff1-13 | 0.07127 | 0.00156 | 1.60354 | 0.03446 | 0.16319 | 0.00208 | 0.04042 | 0.00166 | 965 | 46 | 972 | 14 | 974 | 12 | 801 | 32 |
| AOFM-Tuff1-25 | 0.06533 | 0.00326 | 1.48889 | 0.07070 | 0.16533 | 0.00346 | 0.03855 | 0.00298 | 785 | 108 | 926 | 28 | 986 | 20 | 765 | 58 |
| AOFM-Tuff1-33 | 0.13116 | 0.00408 | 4.73207 | 0.14198 | 0.26168 | 0.00412 | 0.04507 | 0.00284 | 2114 | 56 | 1773 | 26 | 1498 | 22 | 891 | 54 |
| AOFM-Tuff1-18 | 0.10844 | 0.00430 | 4.88177 | 0.18570 | 0.32653 | 0.00604 | 0.07699 | 0.00588 | 1773 | 74 | 1799 | 32 | 1822 | 30 | 1499 | 110 |
| AOFM-Tuff1-12 | 0.11682 | 0.00242 | 5.44724 | 0.11056 | 0.33821 | 0.00430 | 0.08379 | 0.00336 | 1908 | 38 | 1892 | 18 | 1878 | 20 | 1626 | 62 |
| AOFM-Tuff1-14 | 0.14872 | 0.00522 | 8.59526 | 0.29062 | 0.41928 | 0.00712 | 0.06476 | 0.00408 | 2331 | 62 | 2296 | 30 | 2257 | 32 | 1268 | 78 |
| AOFM-Tuff1-29 | 0.18445 | 0.00536 | 13.24448 | 0.37406 | 0.52087 | 0.00792 | 0.13509 | 0.00822 | 2693 | 50 | 2697 | 26 | 2703 | 34 | 2561 | 146 |

Table A5: U/Pb age data of sample AOFM-Tuff2. Red: rejected data.

| Analysis N | U-Pb RATIOS | | | | | | | | AGES (Ma) | | | | | | | |
|---------------|--------------------------------------|---------|-------------------------------------|---------|-------------------------------------|---------|--------------------------------------|---------|--------------------------------------|------|-------------------------------------|------|-------------------------------------|------|--------------------------------------|------|
| | ²⁰⁷ Pb/ ²⁰⁶ Pb | ± 2S | ²⁰⁷ Pb/ ²³⁵ U | ± 2S | ²⁰⁶ Pb/ ²³⁸ U | ± 2S | ²⁰⁸ Pb/ ²³² Th | ± 2S | ²⁰⁷ Pb/ ²⁰⁶ Pb | ± 2S | ²⁰⁷ Pb/ ²³⁵ U | ± 2S | ²⁰⁶ Pb/ ²³⁸ U | ± 2S | ²⁰⁸ Pb/ ²³² Th | ± 2S |
| AOFM-Tuff2-50 | 0.0545 | 0.00328 | 0.43572 | 0.02518 | 0.05798 | 0.00130 | 0.0168 | 0.00094 | 392 | 138 | 367 | 18 | 363 | 8 | 337 | 18 |
| AOFM-Tuff2-03 | 0.0551 | 0.00166 | 0.44132 | 0.01282 | 0.05811 | 0.00084 | 0.01643 | 0.00062 | 416 | 68 | 371 | 10 | 364 | 6 | 329 | 12 |
| AOFM-Tuff2-42 | 0.05511 | 0.00188 | 0.44231 | 0.01456 | 0.05821 | 0.00090 | 0.01894 | 0.00098 | 417 | 78 | 372 | 10 | 365 | 6 | 379 | 20 |
| AOFM-Tuff2-51 | 0.06479 | 0.00416 | 0.52308 | 0.03260 | 0.05856 | 0.00092 | 0.01793 | 0.00058 | 767 | 138 | 427 | 22 | 367 | 6 | 359 | 12 |
| AOFM-Tuff2-27 | 0.06459 | 0.00356 | 0.52327 | 0.02756 | 0.05878 | 0.00128 | 0.01809 | 0.00158 | 761 | 118 | 427 | 18 | 368 | 8 | 362 | 32 |
| AOFM-Tuff2-34 | 0.05595 | 0.00274 | 0.45405 | 0.02142 | 0.05887 | 0.00112 | 0.01846 | 0.00084 | 450 | 112 | 380 | 14 | 369 | 6 | 370 | 16 |
| AOFM-Tuff2-12 | 0.08111 | 0.00834 | 0.6767 | 0.06856 | 0.06051 | 0.00110 | 0.01807 | 0.00044 | 1224 | 208 | 525 | 42 | 379 | 6 | 362 | 8 |
| AOFM-Tuff2-23 | 0.0578 | 0.00316 | 0.49875 | 0.02616 | 0.0626 | 0.00132 | 0.02083 | 0.00144 | 522 | 122 | 411 | 18 | 391 | 8 | 417 | 28 |
| AOFM-Tuff2-36 | 0.06125 | 0.00268 | 0.53121 | 0.02224 | 0.06291 | 0.00114 | 0.0148 | 0.00094 | 648 | 96 | 433 | 14 | 393 | 6 | 297 | 18 |
| AOFM-Tuff2-22 | 0.05512 | 0.00124 | 0.48087 | 0.01052 | 0.06329 | 0.00080 | 0.02089 | 0.00076 | 417 | 52 | 399 | 8 | 396 | 4 | 418 | 16 |
| AOFM-Tuff2-01 | 0.05878 | 0.00160 | 0.5145 | 0.01242 | 0.06349 | 0.00078 | 0.01965 | 0.00026 | 559 | 60 | 421 | 8 | 397 | 4 | 393 | 6 |
| AOFM-Tuff2-26 | 0.05736 | 0.00180 | 0.50593 | 0.01546 | 0.06399 | 0.00096 | 0.0202 | 0.00114 | 505 | 70 | 416 | 10 | 400 | 6 | 404 | 22 |
| AOFM-Tuff2-33 | 0.05794 | 0.00154 | 0.51125 | 0.01324 | 0.06401 | 0.00088 | 0.02113 | 0.00072 | 527 | 60 | 419 | 8 | 400 | 6 | 423 | 14 |
| AOFM-Tuff2-48 | 0.06009 | 0.00194 | 0.53133 | 0.01650 | 0.06413 | 0.00096 | 0.02053 | 0.00112 | 607 | 72 | 433 | 10 | 401 | 6 | 411 | 22 |
| AOFM-Tuff2-54 | 0.0595 | 0.00136 | 0.52662 | 0.01182 | 0.06421 | 0.00084 | 0.01663 | 0.00062 | 585 | 50 | 430 | 8 | 401 | 6 | 333 | 12 |
| AOFM-Tuff2-60 | 0.05862 | 0.00196 | 0.5203 | 0.01670 | 0.06439 | 0.00098 | 0.01842 | 0.00098 | 553 | 74 | 425 | 12 | 402 | 6 | 369 | 20 |
| AOFM-Tuff2-06 | 0.05328 | 0.00214 | 0.47414 | 0.01828 | 0.06455 | 0.00108 | 0.02291 | 0.00122 | 341 | 94 | 394 | 12 | 403 | 6 | 458 | 24 |
| AOFM-Tuff2-31 | 0.05965 | 0.00180 | 0.53267 | 0.01542 | 0.06478 | 0.00092 | 0.02089 | 0.00104 | 591 | 66 | 434 | 10 | 405 | 6 | 418 | 20 |
| AOFM-Tuff2-04 | 0.08285 | 0.00360 | 0.74668 | 0.03036 | 0.06536 | 0.00100 | 0.01947 | 0.00032 | 1266 | 86 | 566 | 18 | 408 | 6 | 390 | 6 |
| AOFM-Tuff2-15 | 0.0547 | 0.00292 | 0.49286 | 0.02524 | 0.06535 | 0.00098 | 0.0204 | 0.00036 | 400 | 122 | 407 | 18 | 408 | 6 | 408 | 6 |
| AOFM-Tuff2-30 | 0.08173 | 0.00366 | 0.73559 | 0.03174 | 0.06531 | 0.00128 | 0.02032 | 0.00158 | 1239 | 90 | 560 | 18 | 408 | 8 | 407 | 32 |
| AOFM-Tuff2-39 | 0.0574 | 0.00186 | 0.51653 | 0.01620 | 0.06528 | 0.00100 | 0.02001 | 0.00108 | 507 | 72 | 423 | 10 | 408 | 6 | 400 | 22 |
| AOFM-Tuff2-28 | 0.05985 | 0.00290 | 0.54146 | 0.02498 | 0.06562 | 0.00100 | 0.02027 | 0.00034 | 598 | 108 | 439 | 16 | 410 | 6 | 406 | 6 |
| AOFM-Tuff2-37 | 0.06003 | 0.00242 | 0.54666 | 0.02126 | 0.06605 | 0.00116 | 0.02122 | 0.00152 | 605 | 90 | 443 | 14 | 412 | 8 | 424 | 30 |
| AOFM-Tuff2-07 | 0.06474 | 0.00188 | 0.59109 | 0.01668 | 0.06622 | 0.00096 | 0.01717 | 0.00082 | 766 | 62 | 472 | 10 | 413 | 6 | 344 | 16 |
| AOFM-Tuff2-08 | 0.05675 | 0.00148 | 0.51851 | 0.01316 | 0.06628 | 0.00088 | 0.01907 | 0.00086 | 482 | 58 | 424 | 8 | 414 | 6 | 382 | 18 |
| AOFM-Tuff2-18 | 0.06079 | 0.00252 | 0.55604 | 0.02218 | 0.06636 | 0.00118 | 0.0217 | 0.00130 | 632 | 92 | 449 | 14 | 414 | 8 | 434 | 26 |
| AOFM-Tuff2-47 | 0.0568 | 0.00182 | 0.51938 | 0.01604 | 0.06632 | 0.00100 | 0.0191 | 0.00084 | 484 | 72 | 425 | 10 | 414 | 6 | 382 | 16 |
| AOFM-Tuff2-52 | 0.06673 | 0.00274 | 0.60962 | 0.02392 | 0.06626 | 0.00118 | 0.01632 | 0.00094 | 829 | 88 | 483 | 16 | 414 | 8 | 327 | 18 |
| AOFM-Tuff2-20 | 0.0562 | 0.00146 | 0.51552 | 0.01302 | 0.06655 | 0.00090 | 0.02042 | 0.00092 | 460 | 58 | 422 | 8 | 415 | 6 | 409 | 18 |
| AOFM-Tuff2-35 | 0.05508 | 0.00128 | 0.50465 | 0.01156 | 0.06647 | 0.00088 | 0.02147 | 0.00084 | 415 | 54 | 415 | 8 | 415 | 6 | 429 | 16 |
| AOFM-Tuff2-40 | 0.05584 | 0.00178 | 0.51162 | 0.01570 | 0.06645 | 0.00098 | 0.02013 | 0.00098 | 446 | 72 | 420 | 10 | 415 | 6 | 403 | 20 |
| AOFM-Tuff2-45 | 0.05573 | 0.00242 | 0.51075 | 0.02134 | 0.06647 | 0.00120 | 0.02129 | 0.00156 | 442 | 98 | 419 | 14 | 415 | 8 | 426 | 30 |
| AOFM-Tuff2-29 | 0.06253 | 0.00242 | 0.57621 | 0.02160 | 0.06685 | 0.00114 | 0.02027 | 0.00138 | 692 | 84 | 462 | 14 | 417 | 6 | 406 | 28 |
| AOFM-Tuff2-09 | 0.0574 | 0.00200 | 0.52957 | 0.01782 | 0.06692 | 0.00104 | 0.02189 | 0.00118 | 507 | 78 | 432 | 12 | 418 | 6 | 438 | 24 |
| AOFM-Tuff2-21 | 0.05837 | 0.00170 | 0.54366 | 0.01534 | 0.06757 | 0.00098 | 0.0231 | 0.00106 | 544 | 66 | 441 | 10 | 421 | 6 | 462 | 20 |
| AOFM-Tuff2-10 | 0.05618 | 0.00234 | 0.52757 | 0.02058 | 0.0681 | 0.00100 | 0.0212 | 0.00034 | 460 | 94 | 430 | 14 | 425 | 6 | 424 | 6 |
| AOFM-Tuff2-11 | 0.05565 | 0.00120 | 0.52289 | 0.01088 | 0.06815 | 0.00082 | 0.02175 | 0.00084 | 438 | 50 | 427 | 8 | 425 | 4 | 435 | 16 |
| AOFM-Tuff2-59 | 0.05667 | 0.00218 | 0.53219 | 0.01962 | 0.06813 | 0.00112 | 0.02199 | 0.00150 | 479 | 86 | 433 | 14 | 425 | 6 | 440 | 30 |
| AOFM-Tuff2-41 | 0.05665 | 0.00170 | 0.53956 | 0.01566 | 0.06908 | 0.00102 | 0.0216 | 0.00110 | 478 | 68 | 438 | 10 | 431 | 6 | 432 | 22 |
| AOFM-Tuff2-17 | 0.05604 | 0.00156 | 0.53485 | 0.01436 | 0.06924 | 0.00096 | 0.02546 | 0.00110 | 454 | 64 | 435 | 10 | 432 | 6 | 508 | 22 |
| AOFM-Tuff2-13 | 0.05689 | 0.00152 | 0.54849 | 0.01426 | 0.06993 | 0.00096 | 0.02225 | 0.00108 | 487 | 60 | 444 | 10 | 436 | 6 | 445 | 22 |
| AOFM-Tuff2-14 | 0.06748 | 0.00256 | 0.65062 | 0.02352 | 0.06994 | 0.00114 | 0.02036 | 0.00136 | 853 | 80 | 509 | 14 | 436 | 6 | 407 | 26 |
| AOFM-Tuff2-49 | 0.05723 | 0.00168 | 0.55338 | 0.01566 | 0.07013 | 0.00098 | 0.0245 | 0.00116 | 500 | 66 | 447 | 10 | 437 | 6 | 489 | 22 |
| AOFM-Tuff2-25 | 0.05854 | 0.00166 | 0.56903 | 0.01566 | 0.07052 | 0.00100 | 0.02573 | 0.00128 | 550 | 64 | 457 | 10 | 439 | 6 | 513 | 26 |
| AOFM-Tuff2-53 | 0.08482 | 0.00290 | 0.8538 | 0.02798 | 0.073 | 0.00120 | 0.01812 | 0.00096 | 1311 | 68 | 627 | 16 | 454 | 8 | 363 | 20 |
| AOFM-Tuff2-61 | 0.06155 | 0.00414 | 0.62435 | 0.03996 | 0.07358 | 0.00186 | 0.01581 | 0.00110 | 659 | 148 | 493 | 24 | 458 | 12 | 317 | 22 |
| AOFM-Tuff2-19 | 0.05798 | 0.00256 | 0.63667 | 0.02710 | 0.07966 | 0.00146 | 0.02875 | 0.00190 | 529 | 98 | 500 | 16 | 494 | 8 | 573 | 38 |
| AOFM-Tuff2-55 | 0.05978 | 0.00154 | 0.70485 | 0.01766 | 0.08553 | 0.00116 | 0.02394 | 0.00098 | 596 | 58 | 542 | 10 | 529 | 6 | 478 | 20 |
| AOFM-Tuff2-44 | 0.05737 | 0.00500 | 0.70727 | 0.05948 | 0.08941 | 0.00206 | 0.02776 | 0.00072 | 506 | 196 | 543 | 36 | 552 | 12 | 553 | 14 |
| AOFM-Tuff2-56 | 0.06618 | 0.00276 | 0.84571 | 0.03282 | 0.09268 | 0.00140 | 0.0283 | 0.00048 | 812 | 90 | 622 | 18 | 571 | 8 | 564 | 10 |
| AOFM-Tuff2-58 | 0.06291 | 0.00442 | 0.83184 | 0.05566 | 0.09592 | 0.00252 | 0.02666 | 0.00206 | 705 | 154 | 615 | 30 | 590 | 14 | 532 | 40 |
| AOFM-Tuff2-16 | 0.06547 | 0.00266 | 0.97472 | 0.03690 | 0.10798 | 0.00156 | 0.03301 | 0.00052 | 789 | 88 | 691 | 18 | 661 | 10 | 656 | 10 |
| AOFM-Tuff2-38 | 0.06769 | 0.00216 | 1.26855 | 0.03916 | 0.13594 | 0.00210 | 0.04028 | 0.00210 | 859 | 68 | 832 | 18 | 822 | 12 | 798 | 40 |
| AOFM-Tuff2-24 | 0.07203 | 0.00170 | 1.57879 | 0.03614 | 0.15901 | 0.00208 | 0.05182 | 0.00216 | 987 | 50 | 962 | 14 | 951 | 12 | 1021 | 42 |
| AOFM-Tuff2-02 | 0.07589 | 0.00440 | 1.9594 | 0.10820 | 0.1873 | 0.00458 | 0.04781 | 0.00270 | 1092 | 118 | 1102 | 38 | 1107 | 24 | 944 | 52 |
| AOFM-Tuff2-05 | 0.09515 | 0.00232 | 3.32501 | 0.07886 | 0.25347 | 0.00350 | 0.08003 | 0.00322 | 1531 | 46 | 1487 | 18 | 1456 | 18 | 1556 | 60 |

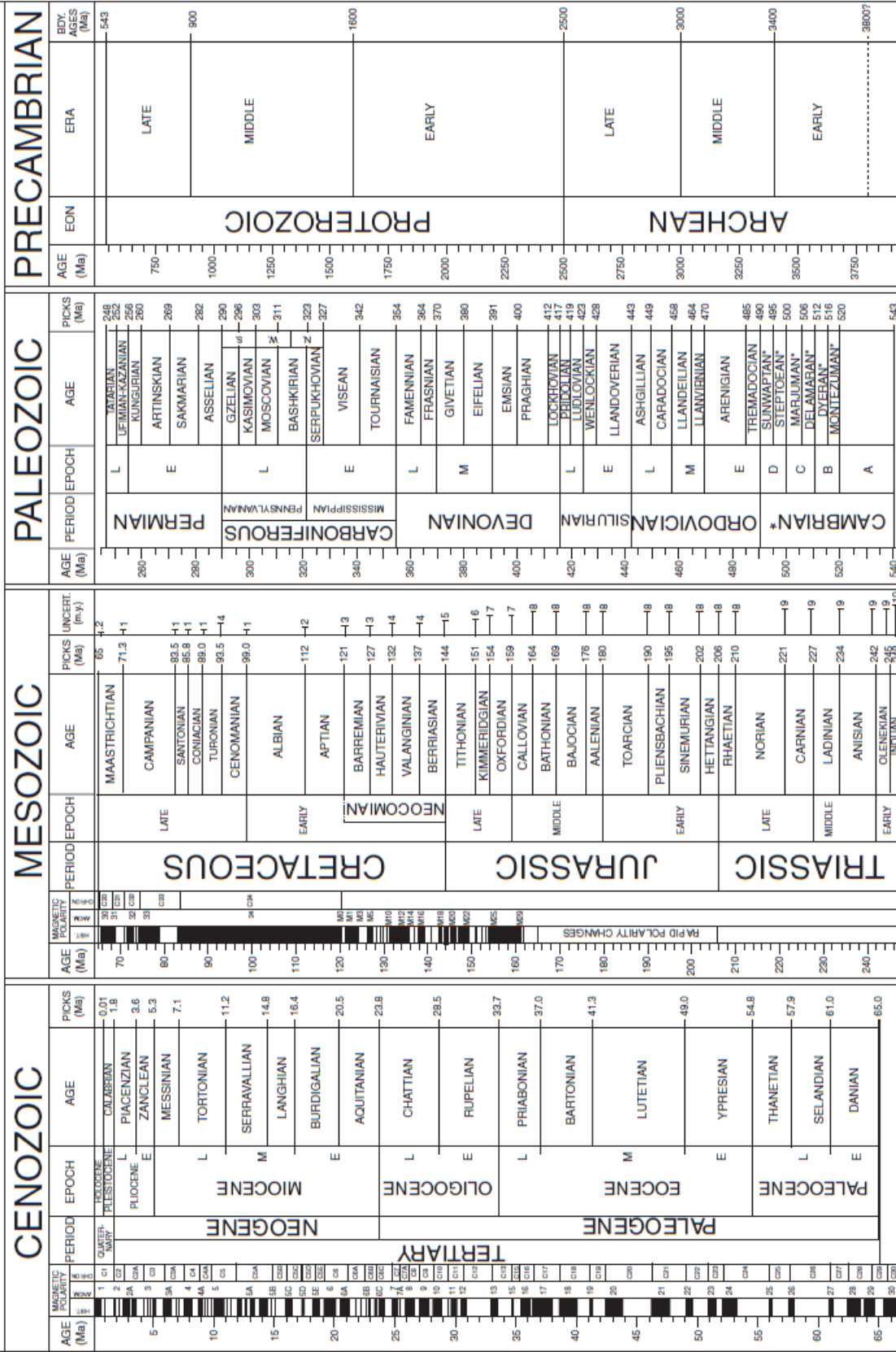
Table A6: LA-ICPMS trace-element data (ppm) of sample CN02, AOFM-SD, AOFM-Tuff1 & AOFM-Tuff2.
 Red: rejected data.

| Analysis N | P | Ti | Y | Nb | La | Ce | Pr | Nd | Sm | Eu | Gd | Dy | Ho | Er | Yb | Lu | Hf | Ta | Th | U |
|---------------|--------|-------|--------|-----|-----|------|-----|------|------|------|-------|-------|-------|-------|--------|---------|---------|------|-------|-------|
| CN02-05 | 259.1 | 11.3 | 627.6 | 1.7 | 0.0 | 2.1 | 0.0 | 0.6 | 1.7 | 0.2 | 10.6 | 52.8 | 20.9 | 97.3 | 184.9 | 37.7 | 10160.4 | 0.6 | 39.2 | 147.5 |
| CN02-30 | 385.7 | 9.0 | 1156.5 | 1.9 | 0.0 | 3.5 | 0.1 | 1.2 | 3.3 | 0.2 | 20.5 | 101.3 | 38.6 | 175.7 | 315.6 | 61.5 | 10762.9 | 0.8 | 78.0 | 161.0 |
| CN02-53 | 426.2 | 27.9 | 1233.9 | 2.0 | 0.1 | 3.7 | 0.3 | 4.2 | 8.2 | 0.7 | 37.5 | 125.1 | 40.9 | 160.9 | 241.7 | 43.4 | 10357.4 | 0.7 | 81.0 | 144.8 |
| CN02-22 | 1076.9 | 2.8 | 2433.4 | 1.7 | 0.3 | 6.1 | 0.3 | 2.3 | 3.3 | 0.7 | 23.0 | 180.3 | 79.4 | 404.4 | 871.3 | 171.9 | 12662.7 | 1.3 | 72.8 | 524.9 |
| CN02-52 | 1103.5 | 9.5 | 2478.7 | 1.9 | 0.1 | 2.6 | 0.1 | 1.0 | 2.8 | 0.3 | 24.6 | 184.8 | 79.9 | 402.7 | 815.6 | 158.9 | 12198.0 | 1.0 | 64.2 | 370.7 |
| CN02-56 | 178.6 | 15.3 | 602.3 | 1.7 | 1.4 | 0.0 | 0.9 | 1.8 | 0.3 | 12.0 | 54.6 | 20.3 | 92.7 | 177.1 | 34.2 | 9246.3 | 0.6 | 41.9 | 106.9 | |
| CN02-11 | 1186.2 | 5.3 | 3082.3 | 2.0 | 0.0 | 1.8 | 0.1 | 0.9 | 3.6 | 0.2 | 31.3 | 235.3 | 99.4 | 491.6 | 1022.5 | 188.8 | 11761.9 | 1.3 | 71.2 | 476.3 |
| CN02-17 | 307.0 | 7.6 | 746.6 | 4.0 | 0.0 | 17.0 | 0.1 | 1.0 | 2.2 | 0.4 | 13.3 | 58.2 | 22.9 | 105.5 | 206.5 | 41.5 | 11175.8 | 1.6 | 144.7 | 93.3 |
| CN02-49 | 347.1 | 6.4 | 989.4 | 2.0 | 0.1 | 6.3 | 0.1 | 1.0 | 1.8 | 0.2 | 14.7 | 78.7 | 32.0 | 156.1 | 321.3 | 64.2 | 10829.6 | 0.9 | 106.4 | 236.9 |
| CN02-13 | 979.9 | 6.4 | 2415.4 | 1.8 | 0.4 | 7.2 | 0.4 | 3.4 | 4.9 | 0.7 | 26.7 | 189.7 | 77.8 | 391.4 | 795.5 | 154.9 | 12085.4 | 1.0 | 97.3 | 396.5 |
| CN02-29 | 1042.9 | 4.3 | 2659.9 | 1.8 | 1.1 | 0.0 | 0.6 | 2.8 | 0.2 | 25.6 | 197.3 | 84.3 | 431.6 | 934.1 | 172.6 | 11795.5 | 1.2 | 57.4 | 438.9 | |
| CN02-38 | 779.6 | 6.0 | 1875.4 | 1.5 | 0.0 | 1.1 | 0.0 | 0.6 | 2.4 | 0.1 | 19.9 | 142.4 | 59.8 | 299.6 | 636.3 | 119.2 | 11786.4 | 0.9 | 46.2 | 320.8 |
| CN02-59 | 762.7 | 6.9 | 1940.7 | 2.1 | 0.0 | 2.4 | 0.1 | 0.9 | 2.9 | 0.2 | 23.9 | 149.2 | 63.3 | 308.3 | 631.2 | 121.0 | 11712.6 | 1.2 | 70.1 | 345.1 |
| CN02-10 | 155.7 | 9.0 | 890.3 | 1.4 | 0.1 | 7.5 | 0.2 | 2.3 | 3.8 | 0.8 | 18.3 | 72.5 | 28.5 | 136.5 | 284.3 | 57.4 | 9558.1 | 0.7 | 94.5 | 141.5 |
| CN02-20 | 717.0 | 4.7 | 1777.9 | 1.8 | 0.5 | 4.7 | 0.2 | 1.4 | 3.0 | 0.4 | 20.6 | 137.3 | 57.7 | 294.2 | 631.1 | 124.0 | 11928.6 | 1.2 | 83.1 | 315.8 |
| CN02-24 | 454.0 | 5.4 | 1345.2 | 2.2 | 0.4 | 7.1 | 0.1 | 0.9 | 2.7 | 0.4 | 19.0 | 107.1 | 43.9 | 213.7 | 451.1 | 87.2 | 10557.7 | 1.1 | 108.0 | 259.0 |
| CN02-27 | 937.0 | 5.2 | 2409.8 | 2.0 | 0.4 | 13.5 | 0.6 | 4.7 | 5.7 | 1.0 | 29.8 | 192.2 | 76.6 | 381.7 | 836.8 | 143.9 | 11599.1 | 1.3 | 103.5 | 362.6 |
| CN02-09 | 620.3 | 6.2 | 1549.6 | 1.5 | 0.0 | 1.5 | 0.0 | 1.0 | 2.5 | 0.1 | 18.8 | 119.8 | 50.4 | 248.6 | 507.8 | 98.0 | 12013.6 | 0.9 | 64.7 | 325.6 |
| CN02-41 | 992.4 | 4.8 | 2646.7 | 2.0 | 0.0 | 2.2 | 0.1 | 0.8 | 3.4 | 0.2 | 28.2 | 200.6 | 85.3 | 426.8 | 896.3 | 166.3 | 11529.0 | 1.4 | 84.1 | 477.4 |
| AOFM-SD-04 | 1385.6 | 12.9 | 3520.5 | 4.3 | 0.5 | 17.4 | 1.4 | 10.8 | 10.2 | 1.7 | 49.9 | 274.0 | 112.0 | 535.9 | 1017.4 | 200.8 | 11537.4 | 1.4 | 218.7 | 555.8 |
| AOFM-SD-05 | 402.5 | 4.3 | 1140.3 | 4.1 | 0.1 | 5.0 | 0.1 | 1.6 | 2.6 | 0.4 | 17.0 | 85.9 | 34.4 | 175.6 | 408.1 | 88.8 | 11322.8 | 2.0 | 144.5 | 426.5 |
| AOFM-SD-09 | 815.9 | 6.2 | 2029.6 | 2.8 | 0.1 | 3.4 | 0.1 | 2.1 | 4.1 | 0.2 | 28.8 | 165.4 | 66.7 | 320.0 | 632.9 | 120.2 | 12489.7 | 1.1 | 107.5 | 314.3 |
| AOFM-SD-18 | 493.2 | 7.1 | 1265.7 | 2.6 | 0.0 | 2.5 | 0.1 | 2.1 | 5.1 | 0.5 | 33.3 | 130.9 | 42.1 | 166.5 | 265.5 | 47.8 | 11998.4 | 0.8 | 72.2 | 210.9 |
| AOFM-SD-25 | 1024.8 | 8.5 | 3167.8 | 3.1 | 0.2 | 4.3 | 0.4 | 3.6 | 4.9 | 0.4 | 38.5 | 249.4 | 100.0 | 477.2 | 942.9 | 173.2 | 12313.2 | 1.3 | 112.8 | 500.1 |
| AOFM-SD-31 | 891.5 | 15.2 | 2694.0 | 2.4 | 0.1 | 2.7 | 0.3 | 3.5 | 7.6 | 0.5 | 48.3 | 235.5 | 89.1 | 380.7 | 631.8 | 113.4 | 11238.9 | 0.8 | 111.0 | 208.0 |
| AOFM-SD-08 | 1184.2 | 5.7 | 2945.6 | 2.1 | 0.0 | 2.6 | 0.1 | 1.3 | 4.4 | 0.5 | 37.1 | 230.7 | 78.8 | 455.2 | 901.9 | 169.9 | 11389.7 | 1.1 | 86.0 | 382.6 |
| AOFM-SD-14 | 669.1 | 13.4 | 1780.6 | 1.2 | 0.0 | 1.1 | 0.1 | 2.5 | 6.6 | 0.4 | 37.5 | 172.1 | 61.7 | 265.9 | 535.6 | 86.1 | 10329.5 | 0.5 | 52.9 | 141.8 |
| AOFM-SD-37 | 682.5 | 9.5 | 1715.0 | 1.4 | 0.1 | 4.1 | 0.1 | 1.6 | 4.2 | 0.5 | 27.4 | 142.7 | 56.7 | 264.2 | 522.2 | 94.7 | 11222.7 | 0.6 | 59.1 | 143.3 |
| AOFM-SD-51 | 754.9 | 6.4 | 1934.1 | 2.0 | 0.2 | 3.9 | 0.3 | 2.1 | 3.3 | 0.3 | 21.6 | 144.1 | 60.4 | 309.5 | 687.5 | 136.9 | 12456.3 | 1.5 | 80.5 | 558.8 |
| AOFM-SD-57 | 962.4 | 8.9 | 2728.9 | 2.1 | 0.2 | 4.7 | 0.4 | 2.5 | 4.7 | 0.6 | 34.9 | 216.4 | 86.1 | 400.0 | 830.4 | 130.6 | 11505.1 | 0.9 | 84.1 | 381.9 |
| AOFM-SD-27 | 742.6 | 10.5 | 1955.2 | 2.2 | 1.2 | 21.8 | 2.7 | 17.1 | 9.8 | 2.2 | 32.4 | 162.4 | 42.6 | 296.6 | 627.8 | 112.6 | 11982.9 | 0.9 | 87.5 | 417.1 |
| AOFM-SD-63 | 546.6 | 11.3 | 1397.9 | 2.1 | 0.7 | 22.9 | 1.5 | 9.0 | 7.3 | 1.6 | 23.3 | 116.0 | 44.6 | 211.4 | 439.7 | 82.8 | 10429.2 | 1.1 | 92.2 | 284.6 |
| AOFM-SD-61 | 621.4 | 15.4 | 2080.7 | 3.0 | 1.4 | 34.5 | 2.9 | 20.8 | 14.3 | 3.6 | 48.1 | 190.7 | 67.5 | 296.9 | 532.2 | 100.5 | 10092.1 | 1.2 | 325.2 | 346.0 |
| AOFM-SD-64 | 505.1 | 6.1 | 1055.1 | 1.5 | 0.0 | 4.6 | 0.0 | 1.0 | 2.9 | 0.3 | 17.5 | 87.9 | 34.8 | 161.3 | 332.2 | 64.2 | 11706.9 | 1.0 | 59.0 | 201.2 |
| AOFM-SD-65 | 890.7 | 7.8 | 2483.7 | 2.1 | 0.2 | 5.8 | 0.4 | 3.6 | 4.6 | 0.6 | 28.4 | 186.2 | 78.9 | 385.9 | 807.9 | 151.3 | 11509.1 | 1.1 | 110.5 | 388.2 |
| AOFM-SD-02 | 613.6 | 5.8 | 1443.1 | 2.5 | 0.1 | 4.6 | 0.3 | 2.1 | 2.7 | 0.3 | 17.0 | 111.3 | 44.3 | 210.5 | 453.5 | 86.8 | 11940.5 | 1.8 | 66.2 | 498.6 |
| AOFM-SD-59 | 958.6 | 12.0 | 2563.3 | 2.3 | 2.9 | 35.0 | 4.8 | 29.5 | 18.8 | 5.0 | 52.3 | 214.2 | 78.8 | 368.4 | 740.3 | 136.4 | 11409.9 | 1.8 | 159.7 | 448.3 |
| AOFM-SD-35 | 932.0 | 5.3 | 2326.9 | 1.8 | 0.1 | 2.2 | 0.3 | 1.4 | 3.4 | 0.2 | 24.5 | 175.0 | 74.7 | 375.5 | 816.2 | 153.3 | 11866.8 | 1.3 | 70.0 | 481.7 |
| AOFM-SD-41 | 1170.1 | 5.3 | 2832.1 | 1.8 | 0.1 | 2.5 | 0.2 | 1.6 | 3.8 | 0.4 | 31.2 | 211.1 | 89.1 | 449.2 | 912.9 | 178.4 | 11381.7 | 1.3 | 72.7 | 392.2 |
| AOFM-SD-49 | 166.2 | 8.3 | 1248.0 | 1.3 | 0.2 | 7.5 | 0.5 | 3.9 | 5.3 | 1.3 | 26.3 | 103.3 | 39.4 | 184.0 | 396.9 | 74.3 | 8451.2 | 0.4 | 172.1 | 306.9 |
| AOFM-SD-70 | 584.7 | 12.6 | 1359.8 | 1.8 | 0.2 | 10.8 | 0.5 | 4.9 | 7.2 | 1.4 | 34.3 | 133.1 | 43.6 | 178.2 | 320.2 | 56.6 | 11555.7 | 0.9 | 101.5 | 272.0 |
| AOFM-SD-23 | 706.3 | 4.6 | 1753.7 | 1.7 | 0.0 | 3.5 | 0.1 | 0.8 | 2.5 | 0.3 | 19.3 | 133.4 | 56.5 | 283.0 | 638.1 | 112.9 | 11325.6 | 1.3 | 68.1 | 353.4 |
| AOFM-Tuff1-06 | 251.6 | 17.1 | 1332.2 | 4.4 | 0.3 | 14.4 | 0.4 | 3.8 | 7.5 | 3.8 | 34.0 | 126.2 | 45.6 | 200.0 | 346.3 | 70.2 | 7450.2 | 0.7 | 55.7 | 70.4 |
| AOFM-Tuff1-09 | 314.5 | 21.4 | 1154.6 | 4.1 | 0.4 | 22.5 | 0.4 | 3.7 | 4.8 | 1.2 | 22.0 | 94.3 | 36.3 | 163.4 | 309.8 | 62.9 | 8429.1 | 0.8 | 75.6 | 90.0 |
| AOFM-Tuff1-44 | 591.1 | 5.4 | 1725.2 | 4.7 | 0.5 | 21.4 | 0.7 | 8.2 | 10.3 | 2.2 | 50.7 | 172.0 | 52.2 | 185.4 | 253.9 | 45.5 | 12125.3 | 1.4 | 106.0 | 378.3 |
| AOFM-Tuff1-26 | 309.7 | 6.6 | 1829.2 | 3.6 | 1.0 | 26.5 | 0.6 | 5.1 | 5.7 | 1.1 | 34.0 | 159.6 | 59.8 | 278.5 | 536.2 | 97.2 | 10516.2 | 1.6 | 235.9 | 353.5 |
| AOFM-Tuff1-35 | 578.1 | 7.0 | 1494.0 | 5.0 | 0.4 | 22.9 | 0.6 | 4.9 | 5.3 | 1.8 | 28.7 | 126.2 | 47.7 | 230.7 | 455.0 | 97.7 | 12002.7 | 2.4 | 114.8 | 292.9 |
| AOFM-Tuff1-48 | 799.0 | 11.4 | 2630.0 | 3.4 | 1.9 | 58.8 | 3.0 | 18.4 | 15.0 | 3.3 | 55.4 | 247.8 | 88.7 | 376.0 | 718.2 | 117.1 | 10091.7 | 1.4 | 250.9 | 624.2 |
| AOFM-Tuff1-51 | 930.3 | 11.8 | 2295.9 | 2.0 | 0.8 | 37.8 | 0.8 | 5.9 | 6.0 | 1.0 | 31.0 | 181.6 | 74.9 | 367.5 | 759.8 | 135.0 | 11176.4 | 0.9 | 89.5 | 308.4 |
| AOFM-Tuff1-34 | 1342.5 | 54.5 | 3658.7 | 1.6 | 0.2 | 6.3 | 0.6 | 4.4 | 7.9 | 0.7 | 48.3 | 286.5 | 114.0 | 527.5 | 1050.6 | 176.2 | 10660.2 | 0.9 | 101.3 | 414.0 |
| AOFM-Tuff1-36 | 1675.6 | 18.9 | 4857.4 | 2.9 | 1.6 | 66.1 | 2.4 | 15.4 | 15.2 | 3.8 | 72.5 | 375.9 | 144.7 | 674.7 | 1241.4 | 235.7 | 11232.6 | 1.5 | 229.4 | 586.5 |
| AOFM-Tuff1-42 | 182.7 | 9.3 | 1293.7 | 2.1 | 0.1 | 9.9 | 0.3 | 4.4 | 8.5 | 2.4 | 34.8 | 129.4 | 44.4 | 192.9 | 388.6 | 64.3 | 9028.4 | 0.7 | 189.3 | 328.5 |
| AOFM-Tuff1-17 | 650.6 | 139.9 | 1838.5 | 2.2 | 0.2 | 7.7 | 0.2 | 2.4 | 4.9 | 0.6 | 29.1 | 153.2 | 59.8 | 279.3 | 542.7 | 97.3 | 10903.5 | 0.8 | 97.7 | 209.3 |
| AOFM-Tuff1-30 | 1652.2 | 8.0 | 3417.7 | 2.5 | 0.2 | 10.0 | 0.2 | 2.9 | 4.8 | 0.5 | 39.1 | 256.7 | 106.3 | 516.8 | 997.0 | 188.8 | 10877.3 | 1.4 | 135.4 | 395.0 |
| AOFM-Tuff1-40 | 445.3 | 6.7 | 2919.3 | 2.8 | 0.3 | 19.1 | 0.6 | 8.0 | 13.2 | 3.1 | 63.2 | 260.2 | 97.1 | 442.2 | 942.7 | 155.0 | 9068.0 | 0.9 | 341.1 | 412.0 |
| AOFM-Tuff1-37 | 663.1 | 32.9 | 1951.3 | 5.0 | 1.6 | 73.7 | 2.7 | 16.5 | 14.1 | 3.5 | 44.2 | 192.9 | 68.3 | 311.7 | 623.4 | 98.6 | 9243.0 | 2.3 | 312.4 | 842.1 |
| AOFM-Tuff1-43 | 1146.9 | 11.6 | 3127.0 | 2.4 | 0.2 | 7.9 | 0.3 | 2.5 | 4.7 | 0.6 | 34.1 | 230.2 | 97.5 | 484.3 | 996.2 | 187.4 | 11555.2 | 1.3 | 111.8 | 492.3 |
| AOFM-Tuff1-16 | 812.0 | 5.3 | 2057.0 | 2.0 | 0.0 | 3.3 | 0.0 | 0.8 | 3.1 | 0.4 | 25.5 | 156.8 | 66.1 | 330.7 | 665.7 | 127.7 | 11010.2 | 1.0 | 88.0 | 314.4 |
| AOFM-Tuff1-46 | 968.9 | 12.7 | 2675.7 | 2.2 | 0.3 | 42.7 | 0.4 | 5.3 | 8.8 | 1.6 | 51.0 | 228.9 | 85.7 | 385.5 | 691.2 | 132.1 | 10440.9 | 1.0 | 156.9 | 297.2 |
| AOFM-Tuff1-18 | 430.2 | 12.5 | 1140.0 | 2.0 | 0.2 | 15.9 | 0.4 | 2.7 | 4.0 | 0.6 | 20.5 | 97.7 | 37.5 | 174.3 | 348.6 | 65.2 | 10456.9 | 0.9 | 100.1 | 176.3 |
| AOFM-Tuff2-05 | 1171.2 | 12.6 | 3647.2 | 2.2 | 0.2 | 12.4 | 0.4 | 4.8 | 10.2 | 0.9 | 62.8 | 3 | | | | | | | | |

Table A7: LAM-ICPMS Lu-Hf isotope data of sample CN02, AOFM-SD, AOFM-Tuff1 & AOFM-Tuff2.
Red: rejected data.

| Analysis N | Lu-Hf RATIOS | | | | Hf _{initial} | εHf(T) | ± SE | T _{DM} (Ga) | T _{DM} ^{Crustal} (Ga) |
|----------------------|--------------------------------------|----------|--------------------------------------|--------------------------------------|-----------------------|--------|------|----------------------|-----------------------------------------|
| | ¹⁷⁶ Hf/ ¹⁷⁷ Hf | ± SE | ¹⁷⁶ Lu/ ¹⁷⁷ Hf | ¹⁷⁶ Yb/ ¹⁷⁷ Hf | | | | | |
| CN02-05 | 0.282455 | 0.000015 | 0.000685 | 0.029993 | 0.282451 | -3.8 | 0.5 | 1.12 | 1.59 |
| CN02-30 | 0.282456 | 0.000010 | 0.000825 | 0.028201 | 0.282450 | -3.8 | 0.4 | 1.12 | 1.59 |
| CN02-53 | 0.282320 | 0.000010 | 0.000742 | 0.029942 | 0.282315 | -8.6 | 0.4 | 1.31 | 1.89 |
| AOFM-SD-13 | 0.282617 | 0.000021 | 0.001698 | 0.050461 | 0.282605 | 1.6 | 0.7 | 0.92 | 1.24 |
| AOFM-SD-18 | 0.282383 | 0.000025 | 0.001054 | 0.030041 | 0.282376 | -6.5 | 0.9 | 1.23 | 1.75 |
| AOFM-SD-31 | 0.282452 | 0.000017 | 0.001675 | 0.050699 | 0.282440 | -4.2 | 0.6 | 1.15 | 1.61 |
| AOFM-Tuff1-44 | 0.282483 | 0.000012 | 0.000608 | 0.020726 | 0.282479 | -2.8 | 0.4 | 1.08 | 1.52 |
| AOFM-Tuff2-03 | 0.282575 | 0.000012 | 0.003260 | 0.104101 | 0.282553 | -0.2 | 0.4 | 1.02 | 1.36 |
| AOFM-Tuff2-42 | 0.282502 | 0.000008 | 0.001209 | 0.048838 | 0.282493 | -2.3 | 0.3 | 1.07 | 1.49 |
| AOFM-Tuff2-50 | 0.282686 | 0.000019 | 0.003566 | 0.108520 | 0.282662 | 3.7 | 0.7 | 0.86 | 1.11 |

1999 GEOLOGIC TIME SCALE



GEOLOGICAL SOCIETY OF AMERICA

© 1999, The Geological Society of America. Product code CTS004. Compilers: A. R. Palmer, John Geissman

*International ages have not been established. These are regional (Laurentian) only. Boundary Picks were based on dating techniques and fossil records as of 1999. Paleomagnetic attributions have errors. Please ignore the paleomagnetic scale.

Sources for nomenclature and ages: Primarily from Gradstein, F., and Ogg, J., 1996, *Episodes*, v. 19, nos. 1 & 2; Gradstein, F., et al., 1995, *SEPM Special Pub. 54*, p. 95-128; Berggren, W. A., et al., 1995, *SEPM Special Pub. 54*, p. 129-212; Cambrian and basal Ordovician ages adapted from Landing, E., 1998, *Canadian Journal of Earth Sciences*, v. 35, p. 329-338; and Davidek, K., et al., 1998, *Geological Magazine*, v. 135, p. 305-309. Cambrian age names from Palmer, A. R., 1998, *Canadian Journal of Earth Sciences*, v. 35, p. 323-328.

Figure A1: 1999 Geologic timescale (GSA, 1999)



INTERNATIONAL CHRONOSTRATIGRAPHIC CHART

v 2019/05

International Commission on Stratigraphy

www.stratigraphy.org

